A thermo-electro-chemo-mechanical model for phase transition of physical hydrogel between solution and gel phases identified by crosslink density

Wu, Tao

2016

Wu, T. (2016). A thermo-electro-chemo-mechanical model for phase transition of physical hydrogel between solution and gel phases identified by crosslink density. Doctoral thesis, Nanyang Technological University, Singapore.

https://hdl.handle.net/10356/67011

https://doi.org/10.32657/10356/67011

A THERMO-ELECTRO-CHEMO-MECHANICAL MODEL FOR PHASE TRANSITION OF PHYSICAL HYDROGEL BETWEEN SOLUTION AND GEL PHASES IDENTIFIED BY CROSSLINK DENSITY WU TAO 2016

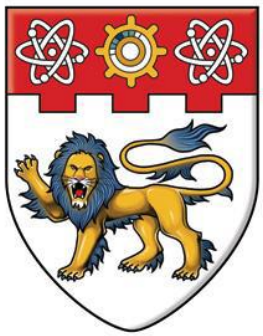

NANYANG TECHNOLOGICAL UNIVERSITY

A THERMO-ELECTRO-CHEMO-MECHANICAL MODEL FOR PHASE TRANSITION OF PHYSICAL HYDROGEL BETWEEN SOLUTION AND GEL PHASES IDENTIFIED BY CROSSLINK DENSITY

WU TAO

SCHOOL OF MECHANICAL AND AEROSPACE ENGINEERING

2016

A THERMO-ELECTRO-CHEMO-MECHANICAL MODEL FOR PHASE TRANSITION OF PHYSICAL HYDROGEL BETWEEN SOLUTION AND GEL PHASES IDENTIFIED BY CROSSLINK DENSITY

WU TAO

SCHOOL OF MECHANICAL AND AEROSPACE ENGINEERING

A THESIS SUBMITTED TO THE NANYANG TECHNOLOGICAL UNIVERSITY IN PARTIAL FULFILLMENT OF THE REQUIREMENT FOR THE DEGREE OF DOCTOR OF PHILOSOPHY

2016

Acknowledgements

I would like to express my sincere gratitude to my supervisor, Assoc Prof Li Hua, for the opportunity to do research in hydrogel phase transition. During the past four years, he has taught me how to express ideas in a clear and simple way for both writing scientific paper and oral presentation. I am grateful for all his contributions of time, constructive suggestions, and effort to make this Ph.D program fruitful.

I wish to extend my appreciation to my friends, Dr. Tong Shanshan, Dr. He Zhongjie, Dr. Zou Hua, Mr. Yang Songyuan, Mr. Hong Jiahua, Dr. Wang Zhiyong, Prof. Yan Xihong, Dr. Li Yong, Ms. Xie Hanlin, Mr. Liu Ning, Mr. Ji Dongxu, Mr. Gao Xiang, Ms. Li Yangyang, Ms. Ma Yue, Dr. Yu Bin, and Dr. Sun Baichuan. I am sincerely grateful for their support and friendship that made my study in NTU enjoyable and memorable.

Last but not least, I owe special thanks to my beloved family for their unselfish support, love and encouragement.

Table of contents

Summary

In general, hydrogel is a class of hydrophilic crosslinked polymeric network, consisting of the network matrix and interstitial fluid. Literature search reveals that the previously published studies focused on the bulk (single) phase behavior or the gel-gel phase transition.

In this thesis, a thermo-electro-chemo-mechanical model is developed mathematically for simulation of the solution-gel phase transition of physical hydrogels. By coupling the multiphysics effects together, the presently developed model consists of the governing equations for the equilibrium of forces, and the conservations of mass and energy. The constitutive equations are formulated by the second law of thermodynamics, which can reduce to the corresponding constitutive equations based on the non-equilibrium thermodynamic theory developed by Suo's group (Hong, Zhao et al. 2008, Hong, Liu et al. 2009, Hong, Zhao et al. 2010), if the interface is ignored when only a single bulk phase exists, i.e. no phase transition occurs. Therefore, as the first academic contribution, the presently developed constitutive equations generally accounts for both the bulk phase and interface behavior. In other words, the non-equilibrium model proposed by Suo's group (Hong, Zhao et al. 2008, Hong, Liu et al. 2009, Hong, Zhao et al. 2010) is just a special case of the present model, when the present two-phase control volume reduces to a single-phase one, in which only the gel phase with constant crosslink density exists in the hydrogel system.

As the second contribution, the density of crosslinks is used to identify the phases for the present domain covering the gel and solution states, which are considered as two distinct

phases, and an interface between them. The crosslink density is a much more accurate parameter for characterizing the phases, compared with the other options in the previously published studies, such as the volume fraction, temperature, or a simple numerical parameter, since the phase transition of the physical hydrogel between solid and liquid states is directly associated with the forming or breaking of the crosslinks subject to environmental stimuli. As a result, the solution phase is identified as the state when the crosslink density is small, while the gel as the state if the crosslink density becomes large. The interface is treated by two different methods, the sharp interface/configurational forces and the diffuse interface approaches, and an additional kinetic equation is imposed on the interface for its evolution during the phase transition.

As the third contribution, a novel Ginzburg-Landau type of free energy is proposed to model the solution-gel phase transition, which accounts for the effects of crosslink density, and consists of the elastic, mixing, binding, polarization and interface contributions. The free energy is in a double-well profile with respect to the crosslink density. As mentioned above, there exist the solution and gel phases and the interface between the two phases, which are identified by the crosslink density ρ. In other words, of the two wells within the free energy density, the one with the smaller crosslink density ρ corresponds to the solution phase, and the other with the larger ρ to the gel phase.

Finally, several case studies are conducted for analysis of the effect of chemical potential, pressure, surface tension and other parameters on the phase transition. After the reduction of the presently developed three-dimensional theoretical model to one-dimensional formulation, a MATLAB source code is developed, and then a spherically symmetrical

solution-gel phase transition is numerically simulated both in water and in ionic solution for analysis of the thermal, electrical, chemical and mechanical influences on the solution-gel phase transition.

List of figures

Glossary

Φ	Bulk Helmholtz free energy density
Ψ	Bulk free energy
α	Number of monomers in a Kuhn monomer
ε	Permittivity
η	Entropy densities in the bulk phases
$\eta^{\mathcal{S}}$	Entropy densities on the interface
λ	Principal stretches
μ_a	Electrochemical potential of species a
ξ	Constant coefficient of the crosslink density gradient
ρ	Crosslink density
σ	Surface tension
τ	Rate of relaxation to equilibrium
φ	Interfacial Helmholtz free energy density
χ	Dimensionless interaction parameter
φ	Interfacial Helmholtz free energy density
ψ	Interfacial free energy
ϕ	Electric potential
ϑ	Volume fraction of polymer
a	Species a
b	Kuhn length

$\boldsymbol{b}$ External body force

$\boldsymbol{b}^{\mathscr{S}}$ External interfacial force

c_a Number concentration of particles of species a in the bulk phase

$c_a^{\mathscr{S}}$ Number concentration of particles of species a on the interface

c_a^{o} Reference concentration of species a

C_v Specific heat capacity

$\boldsymbol{C}$ Bulk configurational stress

$\boldsymbol{C}^{\mathscr{S}}$ Interfacial configurational stress

D Diffusion coefficient

D_r Scalar electric displacement

$\boldsymbol{D}$ Electric displacement

$\boldsymbol{d}$ Normal part of tensor $\boldsymbol{C}^{\mathscr{S}} + \langle \boldsymbol{F} \rangle^T \boldsymbol{S}^{\mathscr{S}}$

E Internal energy densities in the bulk phases

$E^{\mathscr{S}}$ Internal energy densities on the interface

E_a Activation energy required to break a crosslink

E_r Scalar electric field

$\boldsymbol{E}$ Electric field

e Elementary charge

$\boldsymbol{F}$ Bulk deformation gradient

$\boldsymbol{F}^{\mathscr{S}}$ Interfacial deformation gradient

$\boldsymbol{g}$ Body configurational force density

$\boldsymbol{g}^{\mathscr{S}}$ Interfacial configurational force density

H Configurational heating the bulk phases

h Configurational heating on the interface

$\boldsymbol{h}$ Heat flux

J_a Configurational mass supplies of species a in the bulk phases

j_a Configurational mass supplies of species a on the interface

$\boldsymbol{j}_a$ Bulk mass flux supplies of species a

K Total curvature

$\boldsymbol{L}$ Curvature tensor

$\mathscr{I}$ Interception $\mathscr{I} = P \bigcap \mathscr{S}$ between the control volume P and the interface $\mathscr{S}(t)$

m Kinetic modulus

$\boldsymbol{m}$ Unit normal vector pointing from the phase α to phase β

N Average number of Kuhn monomers associated with each chain between two crosslinks

n Number density of the polymeric segments between neighboring crosslinks

$\boldsymbol{n}$ Unit normal vector to the boundary surface ∂P

$\boldsymbol{n}^{\mathscr{S}}$ Projection of $\boldsymbol{n}$ onto the interface

$P(t)$ Control volume

P Hydrostatic stress

$\boldsymbol{P}$ Superficial projection

Q Total electric charge density

q Bulk heat supply density

$q^{\mathscr{S}}$ Interfacial heat supply density

$\boldsymbol{q}$ Velocity of the boundary surface ∂P

R_0 Distance between the neighboring crosslinks at dry state

R Length of the one-dimensional domain, i.e., the radius of the spherical symmetrical system

r_a^b External mass supply in the bulk phases

$r_a^{\mathscr{S}}$ External mass supply on the interface

r_m^* Non-dimensional coordinate of the interface middle

$\mathscr{S}(t)$ Interface

S Scalar stress

$\boldsymbol{S}$ Bulk deformation stress

$\boldsymbol{S}^{\mathscr{S}}$ Interfacial deformation stress

T Temperature

T_M Reference temperature

t Time

U_a Electrochemical potential of species a on the boundary

u_a Electrochemical potential of species a on the interface

$V_{\partial P}$ Normal velocity of the boundary surface ∂P

V Normal component of the interface velocity v

$V_{\partial\mathscr{S}}$ Normal component of the boundary curve velocity $\boldsymbol{w}$

v Specific volume of a monomer unit

v Interface velocity

W Working of the system

w Coordinate of the interface in the radial direction

$\boldsymbol{w}$ Velocity of the boundary curve of the interception $\mathscr{S} = P \bigcap \mathscr{S}$

$\boldsymbol{X}$ Reference coordinate

$\boldsymbol{y}$ Current coordinate

$\boldsymbol{Z}$ Trajectory

z_a Valence of species a

Chapter 1. Introduction

1.1. Background

When hydrophilic polymer chains form the crosslinks of a network in a designed water, the resulting material is called hydrogel, in which the polymer chains are crosslinked by chemical bonds, such as covalent bonds (Rubinstein and Colby 2003), or by weaker physical bonds, for instance, hydrogen bonding, van der Waals interactions or entanglements (Kamath and Park 1993, Peppas, Bures et al. 2000, Rubinstein and Colby 2003). These elastic networks furnish the hydrogel structural and physical integrity, which guarantees the hydrogels exhibiting a thermodynamic compatibility with external solvent and allows them to swell/deswell in aqueous media (Flory and Rehner 1943, Flory and Rehner 1943). The characteristics of a solvent in the hydrogel determine the overall permeation of substance into and out of the hydrogels (Hoffman 2002). Due to the special network structure, hydrogels possess both the properties of solid and liquid, and are able to imbibe a large amount of water or other biological fluid, while maintaining the structure (Tanaka 1981, Osada and Gong 1993).

1.1.1. Physical hydrogel

There are several classifications of hydrogels, depending on their properties. For example, hydrogels may be affine or phantom according to the mechanical and structural characteristics of the network (Rubinstein and Colby 2003). They may also be classified into neutral or ionic hydrogels, based on the pendant groups bounded to the polymeric network. Furthermore, the type of bond forming the network of hydrogel may be used to

label the material as a chemical or physical hydrogel. Physical hydrogels are those whose polymer chains are cross-linked by weaker physical bonds, such as van der Waals interactions and hydrogen bonding (Qiu and Park 2001, Rubinstein and Colby 2003, Lee, West et al. 2006, An, Solis et al. 2010). They are different from chemical hydrogels, in which the polymer chains are cross-linked by chemical bonds, such as covalent bond.

1.1.2. Solution-gel phase transition

As mentioned above, the polymeric chains in the physical and chemical hydrogels are crosslinked by different types of bonds, while the different microscopic behaviors of chemical and physical crosslinks result in various macroscopic properties of chemical and physical hydrogels (Flory 1953, Rubinstein and Colby 2003). Since the covalent bonds in the chemical hydrogel prevent the chemical hydrogel from dissolving in the environmental solvent, the chemical hydrogel behaves mostly like solids. However, the weaker physical bonds are found capable of being dynamically created and dissolved in physical hydrogels. This property enables the physical hydrogels to exhibit phase transition between gel and solution phases, when the cross-links are formed and broken dynamically subject to environmental effects (Rubinstein and Colby 2003, An, Solis et al. 2010). At short time scales, the cross-links do not have time to dissolve against quick deformation, such that the physical hydrogel shares the same solid-like behavior of chemical gels. However, at long time scales, the physical hydrogel may adapt to the presence of environmental stimuli in a similar way as a liquid to release all shear of anisotropic stress via bond dissolution. In other words, the physical hydrogels may transit from the gel phase to solution phase. On the contrary, when the gel phase is more

favorable under certain environmental stimuli, the physical hydrogel may transit phases inversely from solution to gel.

Due to the unique properties, including swelling/shrinking behavior, significant liquid content, interesting mechanical properties, permeability, thermoreversibility and surface properties, physical hydrogels are used in diverse applications, and possess a lot of potential applications in both industry (cosmetics, food processing, pharmaceutics, etc.) and fundamental research (targeted drug delivery, biotechnology, etc.). For instance, physical hydrogels may be used for drug delivery system (Kim, Bae et al. 1992, Qiu and Park 2001, Huang, Yu et al. 2007, Hoare and Kohane 2008), tissue engineering (Lee and Mooney 2001, Biancamaria 2007, Studenovská, Šlouf et al. 2008, Putz and Burghelea 2009), artificial organ (Peppas 1987, Li, H. et al. 2006, Sawa, Tatsumi et al. 2008), wound dressing (Jones and Vaughan 2005, Snyders, Shingel et al. 2007, Yoo and Kim 2008), medical implants, tissue regeneration, and noninvasive intervertebral disc repair (Langer and Vacanti 1993, Hou, De Bank et al. 2004, Putz and Burghelea 2009).

1.2. Motivation, objective and scope

Based on the literature review conducted in the next chapter, it is noted that the bulk behavior of hydrogels is simulated due to different stimuli, such as mechanical loading, temperature, chemical potential, ionic concentration and electric field etc., by taking the hydrogel as a single-phase body, and applying the stimuli as boundary conditions. It is also known that the effects of the interface characteristics on the behavior of hydrogels, such as the surface tension and the kinetics related to the interface, were considered in the two-body hydrogel model for the interfacial behavior between phases. However, only the

gel-gel phase transition was modeled in the previous works, and the deformation was coupled with either temperature or diffusion only. On the other hand, the solution-gel phase transition may be modeled by the theory of configurational force, since it is independent of the specific constitutive theory, although it was proposed to describe coherent two-phase elastic solids and most of its use was linked to solids. Moreover, the theory may be improved to couple the thermal, electrical, chemical and mechanical effects together. In addition, the diffuse interface technique may also be used to model the solution-gel phase transition of hydrogels to obtain a deeper understanding of fundamental mechanism of phase transition and key material properties of hydrogels.

Therefore, the objective of this thesis is to develop a thermo-electro-chemo-mechanical model for simulation of the solution-gel phase transition of physical hydrogels. The scope of this objective is detailed as follows.

- Development of the mathematical model. The theoretical multiphysics models are developed for simulation of the solution-gel phase transition, in which the solution and gel states are considered as two distinct phases, with both sharp and diffuse interface approaches. The present governing equations account for the equilibrium of forces, the conservations of mass and energy, and an additional kinetic equation imposed for phase transition. Based on the second law of thermodynamics, the constitutive equations are formulated. The presently developed model couples the effects of thermal, electrical, chemical and mechanical fields together. It reduces to the non-equilibrium thermodynamic

theory, if the interface is ignored when only a single bulk phase exists, i.e. no phase transition occurs.

- Comparison of the present constitutive equations with those derived by a different approach. The present constitutive equations are compared with those derived by a different approach, called the non-equilibrium thermodynamic theory. The present constitutive equations reduce to the non-equilibrium thermodynamic theory, if the interface is ignored when only a single bulk phase exists, i.e. no phase transition occurs.
- Formulation of a novel free energy density. A novel free energy density is proposed, in which the gel and solution states are indicated by the density of crosslinks, in such a way that the solution phase is identified as a state when the crosslink density is small, while the gel is identified as another state with the large crosslink density. Therefore, a novel formulation of the free energy is presented, which accounts for the elasticity, mixing, polarization and bonding contributions with the effect of crosslink density.
- Numerical case studies. Based on the presently developed governing equations and boundary conditions, a MATLAB source code is developed to analyze the behavior of the bulk phases and the evolution of their interface for phase transition between the solution and gel states. Different pressures P, chemical potentials μ, electrical potentials ϕ and other boundary conditions are imposed for investigation of their effects on the phase transition. As case studies, the spherically symmetrical solution-gel phase transitions of hydrogel in water and in

ionic solution are numerically simulated for analysis of the effect of diffusion coefficient, surface tension and other parameters on the interface behavior.

All the four objectives mentioned above are motivated by different aspects of interests and applications, and they are achieved in this thesis.

1.3. Outline of thesis

This thesis is composed of five chapters, and each of them consists of several sections to make it well organized.

Chapter 1 introduces the background of the physical hydrogel and phase transition, states the motivation to develop a thermo-electro-chemo-mechanical model for phase transition of physical hydrogel between solution and gel phases identified by crosslink density, and then elaborates the objectives of the present research work, followed by the outline of this thesis.

Chapter 2 reviews the published research works on the phase transition of hydrogel, regarding the bulk behavior of single-phase hydrogel, two-phase hydrogels with phase transition, and phase transition of hydrogel with sharp and diffuse interfaces, respectively.

Chapter 3 develops a thermos-electro-chemo-mechanical model for hydrogel phase transition with sharp interface/configurational forces in three-dimensional domain. Apart from the classical governing equations for mass and energy conservations, and the force equilibrium in the two bulk phases and on their interface, an additional equilibrium equation for a so-called configurational force is imposed in the two bulk phases and on

their interface for the effect of the solution-gel phase transition. After the reduced one-dimension form is presented, the numerical case studies are conducted and then discussions on the interface characteristics are made in this chapter.

Chapter 4 formulates a three-dimensional multiphysics model for hydrogel phase transition with diffuse interface, in which the crosslink density is defined as a novel thermodynamically-consistent order parameter, and a novel Ginzburg-Landau type of free energy is proposed. The reduced one-dimensional model is also given in this chapter for numerical simulation of spherically symmetrically evolving interface of the hydrogel during the solution-gel phase transition.

Chapter 5 summarizes the present research work, and recommends the possible future work.

Chapter 2. Literature review: Theories of phase transition of hydrogel

This chapter concentrates literature review on the theoretical studies for phase transition of hydrogel, including the bulk behavior of single-phase hydrogel, the two-phase hydrogels with phase transition, and the phase transition of hydrogel with sharp interface and diffuse interface, respectively.

2.1. Single-phase hydrogels without phase transition

Based on the second law of thermodynamics, a large amount of works were done to simulate the performance and property of hydrogels, where a hydrogel was considered as a single-phase body characterized by free energy as a function of the concentration and the deformation gradient, with an overall integration of the mechanical and chemical processes. One of popularly cited woks was carried out by Suo's group (Hong, Zhao et al. 2008), who accounted for the coupling between the deformation of the network and the migration of the solvent. By invoking the procedure of non-equilibrium thermodynamics, the swelling of hydrogels was numerically simulated. Two ways were assumed for doing work, namely the mechanical work done by a weight and the work due to injection of small molecules with chemical potential. The constitutive equations and kinetic law were given based on the second law of thermodynamics, and an incompressibility condition was introduced to couple diffusion and large deformation. The free energy was specified by a sum of the contributions of stretching and mixing (Hong, Zhao et al. 2008). Based on Hong's work (Hong, Zhao et al. 2008), Zhao *et al.* formulated a theory of the hydrogel subject to electromechanical loads (Zhao, Hong et al. 2008, Zhao and Suo 2008). In addition to the mechanical and chemical work, a third way of doing work, the electrical

work, was considered. The free energy was thus modified by including the contribution of polarizing. This model was used to couple the quasilinear dielectric behavior and nonlinear elastic behavior for dielectric hydrogels, where the behavior of the hydrogel was significantly affected by mechanical constraints. Another field theory was also given by coupling large deformation and electrochemistry (Hong, Zhao et al. 2010).

Different from the integration of the mechanical and chemical processes by an overall deformation gradient, a multiplicative decomposition of deformation gradient into mechanical and chemical parts was introduced by Duda *et al.* (Duda, Souza et al. 2010), by assuming that the mechanical deformation was isochoric and the volume change was solely due to the fluid-induced deformation, which was function of fluid content per unit reference volume. This model was used to study the influence of mechanical and chemical interactions on equilibrium state and diffusive dynamical process. Similar work was done by Chester *et al.* (Chester and Anand 2010, Chester and Anand 2011), in which a mechanical continuum theory was formulated and the multiplicative decomposition was also used to decompose the deformation gradient into elastic and swelling parts. A Flory-Huggins model was used for the free energy change due to mixing of the fluid with the polymer network, and a non-Gaussian statistical mechanical model was proposed for large effective stretch (Chester and Anand 2010, Chester and Anand 2011). Several case studies were conducted using this model, such as three-dimensional swelling equilibrium, one-dimensional free swelling and pressure-difference-driven diffusion of solvent across elastomeric membranes (Chester and Anand 2010). This model was also numerically implemented through a finite element program to simulate swelling, squeezing of fluid by

mechanical forces, and thermally responsive swelling/deswelling of hydrogels (Chester and Anand 2011).

Although the deformation gradient was considered in the integrated or decomposed form for the hydrogels as a homogeneous body, inhomogeneity phenomenon may exist in the concentration of the solvent and the deformation of the network, even though the chemical potential of the solvent molecules is homogeneous when the polymeric network equilibrates with a solvent and mechanical load. Studies on inhomogeneity of hydrogels were done by Zhao *et al.* (Zhao, Hong et al. 2008) and Hong *et al.* (Hong, Liu et al. 2009). Using a Legendre transformation, the free energy was transformed as function of chemical potential and deformation gradient, and then the inhomogeneity of hydrogels was studied.

The instability of hydrogels also attracted attention from various researchers. Cai *et al.* studied the collapse of a void in an elastomer caused by osmosis (Cai, Bertoldi et al. 2010), in which a phenomenon called breathing at low tension was investigated. Besides, two types of instabilities caused by high tension were studied, namely buckling and creasing. The formation of creasing was also investigated by Hong (Hong, Zhao et al. 2009), in which critical conditions for creasing were calculated, and comparisons were made between the theoretical results and experimental observations.

When the amount of surrounding fluid is limited, increasing loading may reach a critical level, at which no additional fluid is available to uptake into the hydrogel, resulting in the loss of saturation. Loss or gain of fluid in the mixture may be caused by change in the mechanical loading, since the swelling of hydrogel is influenced by surrounding solvent

and mechanical load. Deng thus discussed a continuum model and distinguished between liquid-saturated and non-liquid-saturated systems, such that the effect of loss of saturation was investigated (Deng and Pence 2010, Deng and Pence 2010).

Instead of developing the governing and constitutive equations from the second law of thermodynamics, a multiphysics model of hydrogels was proposed for simulation of swelling equilibrium of ionized temperature sensitive hydrogels (Li, Wang et al. 2005), which consisted of the steady-state Nernst-Planck equation, Poisson equation and governing equation for swelling equilibrium. This model was used to study the influence of the salt concentration and initial fixed-charge density, and the volume phase transition (Li, Wang et al. 2005). Further modification was made to simulate the responsive behavior of hydrogels due to temperature (Li, Wang et al. 2005) electrical stimuli (Lam, Li et al. 2006), pH coupled with electrical voltage (Li, Luo et al. 2007), and ionic strength (Li, Luo et al. 2007, Lai, Li et al. 2010, Lai and Li 2011), in which the chemo-electro-mechanical coupling effects were considered for simulation of the swelling and shrinking behaviors.

In order to investigate the effect of glucose oxidation reaction catalyzed by enzyme, a multi-effect-coupling glucose-stimulus (MECglu) model was developed for the simulation of swelling behavior of hydrogels responding to changes in the environmental glucose concentration (Li, Luo et al. 2009). This model was composed of the Nernst–Planck equation, the Poisson equation, and a nonlinear mechanical equation for the large deformations of the hydrogel due to the conversion of chemical energy to mechanical one.

The impact of various solvent parameters was investigated on the responsive swelling behavior of the hydrogel by steady-state simulations.

From the viewpoint of classical continuum mechanics, Wu and Kirchner developed a second-order nonlinear elastic model for hydrogels (Wu and Kirchner 2010, Wu and Kirchner 2011). The elastic constants were estimated from the free energy densities. Several phenomena were studied, such as the stiffening of a biogel under tension, and a contraction under torsion (Wu and Kirchner 2010). The problem of a spherically symmetric dilatation in a spherical hydrogel was also solved by this model, and then an analytical solution was given by perturbation method (Wu and Kirchner 2011) .

2.2. Two-phase hydrogels with phase transition

Apart from taking the hydrogel as a single-phase body for the bulk behavior, the hydrogel may undergo phase transition due to change in temperature and other environmental conditions, because the amount of water in the hydrogel at equilibrium changes with such conditions discontinuously. The phase transition was also affected by the nonhydrostatic stress. By adopting the Flory-Rehner model, the problems associated with the phase transition were analyzed (Cai and Suo 2011), such as specifically coexistent phases in a rod, and coexistent phases undergoing inhomogeneous deformation. Another work was done by Li *et al.* (Li, Wang et al. 2005) who developed a chemo-electro-thermo-mechanical multiphysics model, by the Poisson-Nernst-Planck nonlinear system and Flory-based swelling equilibrium equation, with the capability of quantitatively simulating the volume phase transition of the ionized thermal-stimulus responsive hydrogels immersed in bathing solution with temperature change.

A Flory-type mean field theory and the mode coupling theory were also used to study the phase transitions of both crosslinked gels and single chains (Tanaka 1979), where the phase diagram and the swelling curve of the gel were calculated. The critical divergence and slowing-down of concentration fluctuations were also numerically described.

When polymer networks are charged, they are capable of undergoing large swelling transitions in response to the competition among the mechanical, chemical, and electric energies. This phenomenon was examined as a function of relative charge composition, bath salt concentration, and solvent quality (English, Tanaka et al. 1996). Based on a modified Flory–Huggins model, English et al. (1996) studied the nonlinear instabilities of hydrogels in swelling transitions over a restricted range of solvent and bath salt concentrations.

The equilibrium and non-equilibrium phase transitions in copolymer polyelectrolyte hydrogels were also investigated (English, Tanaka et al. 1997). In their work, a continuum model of polyelectrolyte hydrogel phase transitions were developed based on a concise thermodynamic and geometric foundation, and used to analyze the swelling pattern of hydrogels.

For investigation of the surface instability and phase coexistence, a macroscopic static theory was developed for gels upon swelling or volume phase transition (Sekimoto and Kawasaki 1989), which demonstrated that the surface modulational instability occurred as the result of softening of generalized Raylelgh surface waves. The stability criteria was derived for uniaxially strained bulk gels, and a three-dimensional model was also developed for phase coexistence of gels exhibiting a volume phase transition. In addition,

a two-dimensional model was also given for volumetric phase separation between the swollen and shrunken phases of gels (Sekimoto, Suematsu et al. 1989), where a peculiar percolating (spongelike) structure of the shrunken phase domain was found and qualitatively analyzed.

The change of temperature may also induce discontinuous shrinkage of hydrogels, which is theoretically analyzed by accounting for hydrophobic interaction (Otake, Inomata et al. 1989), where the free energy of a hydrogel is composed of the elastic, osmotic, mixing and hydrophobic parts. This model was able to explain the thermally induced shrinkage of gels, and the "convexo"-type volume phase transition.

Compared with chemical hydrogel, less attention was paid to physical hydrogels which may exhibit phase transition between hydrogel and solution phases, when the cross-links were formed or broken dynamically under environmental effects. An *et al.* developed a thermodynamic model for physical hydrogels (An, Solis et al. 2010), which was capable of predicting the static thermodynamic properties of physical hydrogels. The crosslink's reformation was captured by a connectivity tensor at a microscopic level, and the macroscopic quantities were defined as statistic averaging. Energy functional was constructed based on several averaged variables. The solution or gel state was indicated by S, the number of monomers between two cross-links, in such a way that large S denotes solution and finite S is for gel state. This theory was used to examine the un-constrained swelling or swelling under imposed stress conditions of physical hydrogels. Besides, the properties of the solution-gel transitions were studied, and critical stress and concentration were investigated for phase transition.

2.3. Sharp interface for phase transition

Thermoelastic solid may undergo phase transition between solid phases, when some quantities suffer a jump on an interface. In order to discuss the phase transition of thermoelastic solid, a mechanical continuum theory was developed for stress-induced solid-solid phase transition of tensile bars at stable equilibrium, on the basis of the one-dimensional theory of nonlinear elasticity using a non-monotonic relation between the longitudinal strain and the stress in the bar (Ericksen 1975). Afterwards, Abeyaratne and Knowles developed a continuum model (Abeyaratne and Knowles 1993). A Helmholtz free energy, a kinetic relation and a nucleation criterion were constructed for a one-dimensional thermoelastic solid, which was capable of undergoing either mechanically- or thermally-induced phase transition (Abeyaratne and Knowles 1993).

A non-equilibrium thermo-mechanics of two-phase continua was developed by allowing a sharp phase-interface endowed with energy and entropy (Gurtin 1988), in which an additional balance law, or called the balance of capillary forces, was imposed on the interface. This model took into consideration of both the interaction between the interface and the bulk material, and the micro-forces imposed across the boundary curve of the interface. According to the second law of thermodynamics, power due to the forces and energy inflow resulting from diffusion were used to characterize the evolution of the phase interface. Another model was given for the phase transition of perfect conductors (Angenent and Gurtin 1989), in which the constitutive equations subject to thermodynamic restrictions were derived by invoking the balance of capillary forces and a mechanical version of the second law of thermodynamics. A theory was also developed

for the dynamics of an interface in a two-phase elastic solid with kinetics driven by mass transport and stress (Gurtin and Voorhees 1993). The bulk regions were separated by a sharp interface, and the mass transport resulted from the bulk diffusion of a single independent species. The field equations and free-boundary conditions were expressed in terms of chemical potential and its time derivatives. This model was capable of describing the equilibrium shapes of misfitting particles and possible microstructures of the solid. However, only infinitesimal deformations were considered. By extending the concept of interfacial accretive forces to the bulk phases, the model was modified by including the bulk configurational force, but the thermal and compositional effects were neglected (Gurtin 1995). The configurational forces were systematically studied as a basic concept in continuum physics (Gurtin 2000), and found to coincide with the Eshelby tensor (Eshelby 1951, Eshelby 1956), which gave an insight into the relation among the bulk configurational forces, the bulk free energy, the standard bulk deformational stress, and the deformation gradient.

Due to the environmental stimuli, the hydrogel may swell or shrink by absorbing the small molecules from the surrounding solvent, or by expelling them from the hydrogel. Generally, there is an interface inside the hydrogel, which separates the hydrogel into two phases, namely the collapsed and the swelled phases. A sharp interface approach dealing with the gel-gel transition of hydrogels was developed by allowing for finite strain (Dolbow, Fried et al. 2004, Dolbow, Fried et al. 2005), in which the balance of configurational forces played a key role in coupling the mechanical and chemical effects. The swelling of a spherical specimen was studied by assuming the constant concentration in each phase, and the linear free energy with chemical potential (Dolbow, Fried et al.

2004). Various features of stimulus-responsive hydrogels were also investigated, such as the regimes of unstable and stable phase transitions, surface pattern formation, and bulk phase separation (Dolbow, Fried et al. 2005). The volume transitions in stimulus-responsive hydrogels induced by temperature was also studied by imposing an interfacial normal configurational force balance, in addition to standard bulk and interfacial force and energy balances (Ji, Mourad et al. 2006). This model was also used to examine the stability of the interface evolution.

2.4. Diffuse interface for phase transition

In order to study the interfacial structure in the case of dendritic growth, in which the properties of sharp interface approach may be quite subtle, the notion of a diffuse interface was introduced, of which the underlying idea was that the extensive quantities, e.g. the mass density, vary smoothly between two coexisting phases from their values in one phase to the other. The diffuse interface technique was first used as a numerical technique (Emmerich 2011), in order to overcome the necessity for solving the precise location of the interface by introducing one or several additional phase-field variables, which were continuous fields as functions of space and time. In this way, the diffuse interface method is also called phase-field method. With the development of understanding of the interface, an asymptotic analysis was conducted and demonstrated that the diffuse interface model may be reduced to the sharp interface formulation, when the width of the interface goes to zero, if a thermodynamically consistent phase-field model was assumed. Therefore, this method gains more and more attention for numerical efficiency and physical consistency.

The diffuse interface method, or called the phase-field method, was widely used to simulate the alloy solidification. One of the most cited works in this area was done by Wheeler *et al*. (Wheeler, Boettinger et al. 1992, McFadden, Wheeler et al. 1993, Wheeler, Boettinger et al. 1993), which was called the WBM model. The interfacial region was assumed to be a mixture of solid and liquid with the same composition, but the chemical potentials were different. The phase transition in binary alloys was simulated by relating the parameters in the phase-field model to material and growth parameters in real systems. In addition, an asymptotic analysis was conducted as the gradient energy coefficient of the phase field became small, showing that the classical sharp interface models were recovered when the interfacial layers were thin. Similar model was proposed by Caginalp and Xie (Caginalp and Xie 1993). Another model was developed by Tiaden *et al.* (Tiaden, Nestler et al. 1998), in which the compositions of solid and liquid of the mixture were different in the interfacial region, but the constant ratio was assumed. A mathematical method was presented for modeling and simulation of phase transitions in multiphase systems controlled by solute diffusion. In order to overcome the limit for the interface thickness in the WBM model (Wheeler, Boettinger et al. 1992, McFadden, Wheeler et al. 1993, Wheeler, Boettinger et al. 1993), Kim *et al.* proposed a model by assuming the mixture of liquid and solid in the interfacial region with the same chemical potential but different compositions (Kim, Kim et al. 1999).

In order to describe the evolution of multiphase boundaries, a phase field model for multiphase systems was developed (Steinbach, Pezzolla et al. 1996, Steinbach, Zhang et al. 2012), in which each phase is identified with an individual phase field and the transformation between all pairs of phases is treated with its own characteristics, and the

number of the order parameters has to be determined according to the number of phases. The multiphase-field model was used for numerical calculations of the peritectic reaction and transformation for Fe-C alloy system (Tiaden, Nestler et al. 1998), and was compared with the WBM model (Wheeler, Boettinger et al. 1992, McFadden, Wheeler et al. 1993, Wheeler, Boettinger et al. 1993) in a limited case.

In the area of modeling of dendritic crystal growth, Kobayashi (Kobayashi 1993) developed a phase field model for one-component melt growth by considering Ginzburg-Landau type free energy with a phase-field variable. Relations were discussed between the shape of crystals and some physical parameters, and the crucial influence of noises was revealed on the side branch structure. This model was also used to simulate the three-dimensional dendritic solidification (Kobayashi 1994).

In order to study the spinodal decomposition in gel, a Ginzburg-Landau model was developed for gels undergoing spinodal decomposition, in terms of the polymer volume fraction and a deformation tensor (Onuki and Puri 1999), which demonstrated that the domain growth is extremely slowed down in late stages, and that the surface tension force, which drives the coarsening in usual fluids, is cancelled by the elastic force.

For the effect of mechanics, Levitas *et al*. developed a model to resolve some contradictions of melting problems (Levitas and Samani 2011). Recently, the phase-field method was used to model the phase transition of polymeric gels on the basis of Cahn-Hilliard equation, which coupled large deformation with mass transport (Hong and Wang 2013).

2.5. Remarks

Based on the above literature review, it is known that the single-phase models were used to simulate the bulk behavior of hydrogels subject to different stimuli, such as mechanical loading, temperature, chemical potential, ionic concentration and electric field etc., by taking the hydrogel as a single-phase body, and applying the stimuli as boundary conditions. It is also noted that the effects of the interface characteristics on the behavior of hydrogels, such as the surface tension and the kinetics related to the interface, were considered in the two-body hydrogel model for the behavior of interface between phases.

However, the sharp interface approach was used to study the gel-gel phase transition, and the deformation is coupled with either temperature or diffusion only. On the other hand, the mathematical theory of configurational force may be extended to model solution-gel phase transition, since it is independent of the specific constitutive theory, although it was proposed to describe coherent two-phase elastic solids and most of its use was for solids. By taking the gel and the solution as two distinct phases and allowing a sharp interface separating the solution and gel phases, it is reasonable to extend the concept of configurational force, which is related to phase transitions, for modeling of the solution-gel phase transition of physical hydrogels. Moreover, the theory may be improved to couple the thermal, electrical, chemical and mechanical effects together. The behavior of the bulk phases and the evolution of their interface may thus be simulated for phase transition between solution and gel states. In addition, the diffuse interface technique may be extended for modeling the solution-gel phase transition of hydrogels as well, by taking the crosslink density as a novel thermodynamically-consistent order parameter, which is

homogeneous in each distinct phase with smooth variation over the interface from one phase to another, in order to obtain a deeper understanding of fundamental mechanism of phase transition and key material properties of hydrogels.

Chapter 3. Development of a multiphysics model for hydrogel phase transition with sharp interface/configurational forces

This chapter develops a mathematic model for simulation of the solution-gel phase transition of physical hydrogels with sharp interface/configurational forces, which couples the thermal, electrical, chemical and mechanical effects together. The chapter is organized as follows. After an introduction in Section 3.1, the three-dimensional model is formulated in Section 3.2, in which the conservation laws are employed, the constitutive equations are formulated and a novel formulation of free energy density is proposed. Section 3.3 reduces the model into one-dimensional domain, and then corresponding numerical analysis is conducted in Section 3.4 for investigation of the behavior of the bulk phases and the evolution of their interface during solution-gel phase transition. Finally, several remarks are given in Section 0, including a review comment on the present sharp interface model for a further development of the model with diffuse interface.

3.1. Introduction and assumptions

In this chapter, a multiphysics model is developed for simulation of the interface behavior of hydrogel during solution-gel phase transition, in which the solution and gel states are considered as two distinct phases and separated by a sharp interface technique. Apart from the classical governing equations for mass and energy conservations, and the force equilibrium in the two bulk phases and on their interface, an additional equilibrium equation for a so-called configurational force is imposed in the two bulk phases and on their interface for modeling of the solution-gel phase transition (Gurtin and Voorhees 1993, Gurtin 1995, Gurtin 2000). Correspondingly, the configurational heating and mass

supply are proposed to account for entropy change due to the migration of the control volume. By the second law of thermodynamics, the constitutive equations are formulated, including an evolution equation for the interface. In order to simulate the solution-gel phase transition of the physical hydrogel, a novel formulation of the free energy is proposed, which considers the effects of the crosslink density in such a way that the solution phase is identified as the state when the crosslink density is small, while the gel is identified as the state with the large crosslink density. The presently developed model couples the thermal, electrical, chemical and mechanical effects together. It can reduce to the non-equilibrium thermodynamic model (Hong, Zhao et al. 2008, Hong, Liu et al. 2009, Hong, Zhao et al. 2010), if the interface is ignored when only a single bulk phase exists, namely when no phase transition occurs. For case studies, the spherically symmetrical solution-gel phase transitions in water and in ionic solution are simulated numerically for analysis of the kinetic effects of diffusion coefficient, surface tension and other parameters on the interface behavior.

In order to develop the mathematic model for simulation of the solution-gel phase transition of physical hydrogels with sharp interface/configurational forces, the assumptions are made below.

- The chemical potential is continuous across the interface, namely $[\mu_a]=0$.
- The electrical potential is continuous across the interface, namely $[\phi]=0$.
- The motion is coherent, namely $[\boldsymbol{y}]=\boldsymbol{0}$.
- The permittivity ε is constant.
- The surface tension is constant, namely $\sigma = const$.

- No heat supply exists.
- No chemical reaction occurs.
- No mass supply exists.
- The diffusion is much faster than the interface evolution.
- The mobility is isotropic and homogeneous, namely $\boldsymbol{M}_a = M_a \boldsymbol{I}$.
- The crosslinks are isotropically distributed in a diamond lattice at equilibrium state.
- All crosslinks are assumed in the same structure.
- The specific volume of a monomer unit is as the same as that of the solvent and the mobile ions.
- The specific heat capacity C_v is constant and independent of temperature.

3.2. Formulation of three-dimensional model

By modifying the theory conducted by Gurtin *et al.* (Gurtin and Voorhees 1993, Gurtin 1995, Gurtin 2000), a three-dimensional multiphysics model is developed in this section via coupling the thermal, chemical, electrical, and mechanical effects together, in which large deformation is allowed.

3.2.1. Kinematics

Let us consider a two-phase control volume $P(t)$, as shown in Fig. 3.1, which migrates with time and is separated by the interface $\mathscr{S}(t)$ into two phases α and β. In the

present work, the phase α represents the gel, and the phase β the solution. The normal component of the velocity of ∂P as the boundary surface of P is constrained by

$$\boldsymbol{q} \cdot \boldsymbol{n} = V_{\partial P} \tag{3.1}$$

where $\boldsymbol{q}$ is the velocity of the boundary surface ∂P, $\boldsymbol{n}$ is the unit normal vector to the boundary surface ∂P pointing outward from P, and $V_{\partial P}$ is the normal velocity of the boundary surface ∂P.

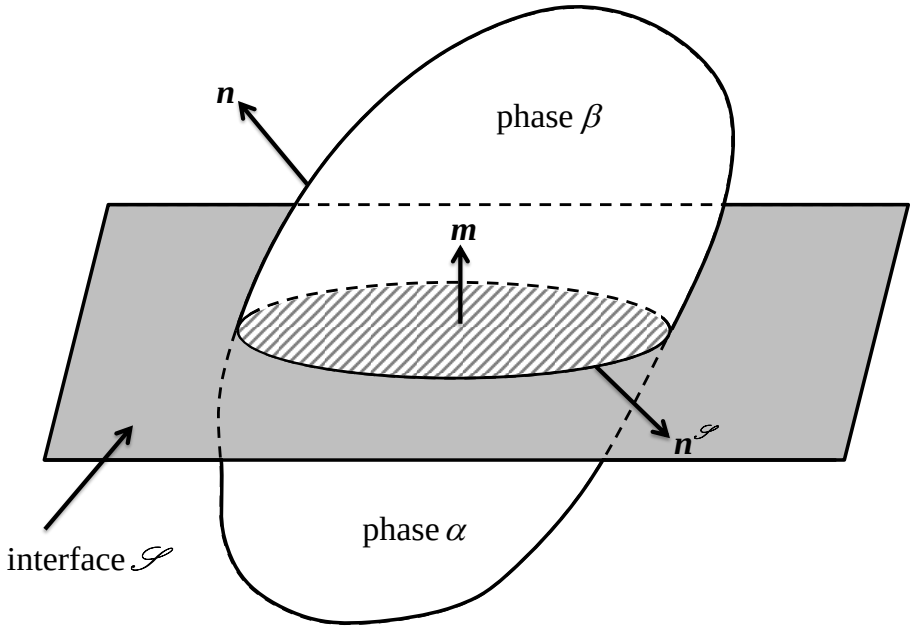

Fig. 3.1. Migrating control volume.

The interface $\mathscr{S}(t)$ is assumed as a smoothly evolving surface with the unit normal vector $\boldsymbol{m}(\boldsymbol{X})$ pointing from the phase α to phase β. The normal component of the interface velocity $\boldsymbol{v}$ is constrained by

$$\boldsymbol{v} \cdot \boldsymbol{m} = V \tag{3.2}$$

A similar constraint given by Equation (3.3) is imposed on the velocity $\boldsymbol{w}$ for the boundary curve of the interception $\mathscr{I} = P \bigcap \mathscr{S}$ between the control volume P and the interface $\mathscr{S}(t)$,

$$\boldsymbol{w} \cdot \boldsymbol{m} = V, \qquad \boldsymbol{w} \cdot \boldsymbol{n}^{\mathscr{I}} = V_{\partial \mathscr{I}} \tag{3.3}$$

where $\boldsymbol{n}^{\mathscr{I}}$ is the projection of $\boldsymbol{n}$ onto the interface.

By nonlinear deformation theory, if a material point at a place with coordinate $\boldsymbol{X} \in P$ moves to a new place $\boldsymbol{y} = \boldsymbol{y}(\boldsymbol{X}, t)$ at time t, the deformation gradient is defined as

$$\boldsymbol{F} = \nabla \boldsymbol{y} = \frac{\partial \boldsymbol{y}(\boldsymbol{X}, t)}{\partial \boldsymbol{X}} \tag{3.4}$$

Similarly, the interfacial deformation gradient is defined as

$$\boldsymbol{F}^{\mathscr{I}} = \nabla_{\mathscr{I}} \boldsymbol{y} = \langle \boldsymbol{F} \rangle \boldsymbol{P} \tag{3.5}$$

where $\nabla_{\mathscr{I}} \boldsymbol{y}$ is the surface gradient of $\boldsymbol{y}$, $\boldsymbol{P} = \boldsymbol{I} - \boldsymbol{m} \otimes \boldsymbol{m}$ is the superficial projection and $\langle \Phi \rangle$ is the average value of a bulk field Φ across the interface. Here Φ is assumed to be smooth up to $\mathscr{S}$ in each phase. The jump of Φ across the interface is denoted as $[\Phi]$, i.e.

$$\langle \Phi \rangle = \frac{1}{2}(\Phi^{+} + \Phi^{-}), \; [\Phi] = \Phi^{+} - \Phi^{-} \quad \text{with} \quad \Phi^{\pm}(\boldsymbol{X}, t) = \Phi(\boldsymbol{X} \pm 0\boldsymbol{m}(\boldsymbol{X}, t), t) \tag{3.6}$$

As well known, the trajectory $\boldsymbol{Z}(\tau)$ of a particle passing through $\boldsymbol{X} \in \partial P(t)$ at time t is the unique solution of the following equation,

$$\frac{d\boldsymbol{Z}(\tau)}{d\tau} = \boldsymbol{q}\big(\boldsymbol{Z}(\tau), \tau\big), \quad \boldsymbol{Z}(t) = \boldsymbol{X} \tag{3.7}$$

As such, the time derivative of a field $\boldsymbol{\Phi}(\boldsymbol{X}, t)$ following ∂P is the time derivative along such trajectories and is given as

$$\overset{\circ}{\boldsymbol{\Phi}}\big(\boldsymbol{X}, \mathrm{t}\big) = \frac{d}{d\tau}\boldsymbol{\Phi}\big(\boldsymbol{Z}(\tau), \tau\big)\Big|_{\tau = t} \tag{3.8}$$

In a similar way, the time derivatives of a field $\boldsymbol{\Phi}(\boldsymbol{X}, t)$ following the interface $\mathscr{S}$ and the boundary curve $\partial\mathscr{S}$ are denoted as $\overset{\square}{\boldsymbol{\Phi}}$ and $\overset{\triangle}{\boldsymbol{\Phi}}$, respectively (Gurtin 2000, Dolbow, Fried et al. 2005).

The velocity following ∂P is thus related to the material velocity $\dot{\boldsymbol{y}}$ by

$$\overset{\circ}{\boldsymbol{y}} = \dot{\boldsymbol{y}} + \boldsymbol{F}\boldsymbol{q} \tag{3.9}$$

As a result, the velocity field following interface $\mathscr{S}$ is given as

$$\overset{\square}{\boldsymbol{y}} = \langle \dot{\boldsymbol{y}} \rangle + \langle \boldsymbol{F} \rangle \boldsymbol{v} \tag{3.10}$$

Another velocity field, the velocity following the boundary curve $\partial\mathscr{S}$, is given in a similar form as

$$\overset{\vartriangle}{\boldsymbol{y}} = \langle \dot{\boldsymbol{y}} \rangle + \langle \boldsymbol{F} \rangle \boldsymbol{w} \tag{3.11}$$

If the motion is coherent, i.e. $[\boldsymbol{y}] = \boldsymbol{0}$, the compatibility conditions is given as

$$[\boldsymbol{F}]\boldsymbol{P} = \boldsymbol{0}, \quad \text{and} \quad [\dot{\boldsymbol{y}}] + [\boldsymbol{F}]\boldsymbol{v} = \boldsymbol{0} \tag{3.12}$$

In general, a tangential vector $\boldsymbol{t}$ on the interface $\mathscr{S}$ is perpendicular to $\boldsymbol{m}(\boldsymbol{X})$ at $\boldsymbol{X} \in \mathscr{S}(t)$, i.e. $\boldsymbol{t} \cdot \boldsymbol{m} = \boldsymbol{0}$. The projection of $\mathfrak{n}$ onto the interface is denoted as $\boldsymbol{n}^{\mathscr{S}}$, and it is tangent to $\mathscr{S}$ but normal to $\partial\mathscr{S}$. A superficial tensor field $\boldsymbol{T}^{\mathscr{S}}$ on $\mathscr{S}$ is thus required to satisfy

$$\boldsymbol{T}^{\mathscr{S}} \boldsymbol{m} = \boldsymbol{0} \tag{3.13}$$

All superficial tensor fields may be decomposed into tangential and normal parts as

$$\boldsymbol{T}^{\mathscr{S}} = \boldsymbol{T}^{\mathscr{S}}_{\tan} + \boldsymbol{m} \otimes \boldsymbol{t} \tag{3.14}$$

in which $\boldsymbol{T}^{\mathscr{S}}_{\tan} = \boldsymbol{P}\boldsymbol{T}^{\mathscr{S}}$, $\boldsymbol{t} = \boldsymbol{T}^{\mathscr{S}} \boldsymbol{m}$.

Additionally, the curvature tensor $\boldsymbol{L}$ and total curvature K are defined as

$$\boldsymbol{L} = -\nabla_{\mathscr{S}} \boldsymbol{m} \tag{3.15}$$

and

$$K = tr\boldsymbol{L} = \boldsymbol{P} \cdot \boldsymbol{L} = -Div_{\mathscr{S}} \boldsymbol{m} \tag{3.16}$$

The total curvature K, the superficial projection $\boldsymbol{P}$ and the unit normal vector $\boldsymbol{m}$ follow the relations below,

$$Div_{\mathscr{S}} \boldsymbol{P} = K\boldsymbol{m} \tag{3.17}$$

and

$$\overset{\square}{\boldsymbol{m}} = -\nabla_{\mathscr{S}} V = -\boldsymbol{P}\nabla V \tag{3.18}$$

In addition, the two useful identities are given below for the formulation in the subsections 3.2.3 to 3.2.5.

$$\frac{d}{dt}\{\int_P \Psi dv\} = \int_P \dot{\Psi} dv + \int_{\partial P} \Psi V_{\partial P} da - \int_{\mathscr{S}} [\Psi] V da \tag{3.19}$$

$$\frac{d}{dt}\{\int_{\mathscr{S}} \psi da\} = \int_{\mathscr{S}} (\overset{\square}{\psi} - \psi K V) da + \int_{\partial \mathscr{S}} \psi V_{\partial \mathscr{S}} ds \tag{3.20}$$

3.2.2. Balance of force

In the present model, two force systems are considered: a standard force system for deformation and a configurational force system for phase transition (Gurtin and Voorhees 1993, Gurtin 1995). All force fields in each system are assumed to comply with their equilibrium laws.

3.2.2.1. Standard force

The standard force system generally consists of the bulk deformation stress $\boldsymbol{S}$, the interfacial deformation stress $\boldsymbol{S}^{\mathscr{S}}$, the external body force $\boldsymbol{b}$, and the external interfacial force $\boldsymbol{b}^{\mathscr{S}}$. The balance of force and momentum requires

$$\int_{\partial P} \boldsymbol{S}\boldsymbol{n}da + \int_{P} \boldsymbol{b}dv + \int_{\partial \mathscr{S}} \boldsymbol{S}^{\mathscr{S}}\boldsymbol{n}^{\mathscr{S}}ds + \int_{\mathscr{S}} \boldsymbol{b}^{\mathscr{S}}da = \boldsymbol{0} \tag{3.21}$$

and

$$\int_{\partial P} \boldsymbol{y}\times\boldsymbol{S}\boldsymbol{n}da + \int_{P} \boldsymbol{y}\times\boldsymbol{b}dv + \int_{\partial \mathscr{S}} \boldsymbol{y}\times\boldsymbol{S}^{\mathscr{S}}\boldsymbol{n}^{\mathscr{S}}ds + \int_{\mathscr{S}} \boldsymbol{y}\times\boldsymbol{b}^{\mathscr{S}}da = \boldsymbol{0} \tag{3.22}$$

Applying the bulk and surface divergence theorem gives the local bulk force balance as

$$Div\boldsymbol{S} + \boldsymbol{b} = \boldsymbol{0} \quad \text{and} \quad \boldsymbol{S}\boldsymbol{F}^{T} = \boldsymbol{F}\boldsymbol{S}^{T} \tag{3.23}$$

and the interfacial equation in the form of

$$[\boldsymbol{S}]\boldsymbol{m} + Div_{\mathscr{S}}\boldsymbol{S}^{\mathscr{S}} + \boldsymbol{b}^{\mathscr{S}} = \boldsymbol{0} \quad \text{and} \quad \boldsymbol{S}^{\mathscr{S}}(\boldsymbol{F}^{\mathscr{S}})^{T} = \boldsymbol{F}^{\mathscr{S}}(\boldsymbol{S}^{\mathscr{S}})^{T} \tag{3.24}$$

3.2.2.2. Configurational force

Apart from the standard force system, a configurational force is required to characterize the material structure and phase interface (Gurtin and Voorhees 1993, Gurtin 1995, Gurtin 2000). The configurational force system consists of the bulk configurational stress $\boldsymbol{C}$, the interfacial configurational stress $\boldsymbol{C}^{\mathscr{S}}$, the body configurational force density $\boldsymbol{g}$,

and the interfacial configurational force density $\boldsymbol{g}^{\mathscr{S}}$. The configurational force balance thus requires

$$\int_{\partial P} \boldsymbol{C}\boldsymbol{n}da + \int_{P} \boldsymbol{g}dv + \int_{\partial\mathscr{S}} \boldsymbol{C}^{\mathscr{S}}\boldsymbol{n}^{\mathscr{S}}ds + \int_{\mathscr{S}} \boldsymbol{g}^{\mathscr{S}}da = \boldsymbol{0} \tag{3.25}$$

Using the bulk and surface divergence theorem gives the bulk equation as

$$Div\boldsymbol{C} + \boldsymbol{g} = \boldsymbol{0} \tag{3.26}$$

and the interface equation in the form of

$$[\boldsymbol{C}]\boldsymbol{m} + Div_{\mathscr{S}}\boldsymbol{C}^{\mathscr{S}} + \boldsymbol{g}^{\mathscr{S}} = \boldsymbol{0} \tag{3.27}$$

3.2.3. Conservation of mass

As well known, hydrogel is a mixture of polymeric network matrix and interstitial fluid. Here the number concentrations of particles of species a in the bulk phase and on the interface are denoted by c_a and $c_a^{\mathscr{S}}$, the bulk mass flux by $\boldsymbol{j}_a$, and the external mass supply by r_a^b in the bulk phases and $r_a^{\mathscr{S}}$ on the interface. In order to account for the bulk and interface mass flux due to the migration of the control volume P, the configurational mass fluxes of species a are required in the bulk phases and on the interface, and denoted as J_a and j_a. If no chemical reaction occurs, the conservation of mass for all P at any time requires

$$\frac{d}{dt}\{\int_{P} c_a dv + \int_{\mathscr{S}} c_a^{\mathscr{S}} da\} = -\int_{\partial P} \boldsymbol{j}_a \cdot \boldsymbol{n}da + \int_{P} r_a^b dv + \int_{\mathscr{S}} r_a^{\mathscr{S}} da + \int_{\partial P} J_a V_{\partial P} da + \int_{\partial\mathscr{S}} j_a V_{\partial\mathscr{S}} ds \tag{3.28}$$

resulting in the bulk diffusion equation in the form of

$$\dot{c}_a = -Div\boldsymbol{j}_a + r_a^b \tag{3.29}$$

and the interfacial diffusion equation as

$$\overset{\square}{c}_a^{\mathscr{S}} - c_a^{\mathscr{S}} KV - [c_a]V = -[\boldsymbol{j}_a]\cdot\boldsymbol{m} + r_a^{\mathscr{S}} \tag{3.30}$$

as well as the following relations

$$J_a = c_a, \qquad j_a = c_a^{\mathscr{S}} \tag{3.31}$$

which demonstrates the coincidence between the concentration and the configurational mass flux due to the migration of the control volume.

3.2.4. Conservation of energy

In the present model, the conservation of energy is included in the system, which is formulated in this subsection.

3.2.4.1. Internal energy

The internal energy densities in the bulk phases and on the interface are denoted as E and $E^{\mathscr{S}}$, respectively. The total internal energy of P is given as

$$\int_P E dv + \int_{\mathscr{S}} E^{\mathscr{S}} da \tag{3.32}$$

3.2.4.2. Heating

Heating is a main contribution to the change of internal energy. Similarly, the bulk heat supply density, interfacial heat supply density and heat flux are denoted by q, $q^{\mathscr{S}}$, and $\boldsymbol{h}$ for the control volume P. In order to account for the bulk and interfacial heat transfer into the control volume P, the configurational heating is required in the bulk phases and on the interface, and denoted by H and h. Therefore, the overall heating is given as

$$-\int_{\partial P}\boldsymbol{h}\cdot\boldsymbol{n}da+\int_{P}qdv+\int_{\partial P}HV_{\partial P}da+\int_{\mathscr{S}}q^{\mathscr{S}}da+\int_{\partial\mathscr{S}}hV_{\partial\mathscr{S}}ds \tag{3.33}$$

By the divergence law in the bulk and on the surface, Equation (3.33) is rewritten as

$$-\int_{P}Div\boldsymbol{h}dv-\int_{\mathscr{S}}\boldsymbol{h}\cdot\boldsymbol{m}da+\int_{P}qdv+\int_{\partial P}HV_{\partial P}da+\int_{\mathscr{S}}q^{\mathscr{S}}da+\int_{\partial\mathscr{S}}hV_{\partial\mathscr{S}}ds \tag{3.34}$$

3.2.4.3. Working

As mentioned before, the two force systems are included in the present model, such that the working of both the standard and configurational forces is required. According to classical mechanics, the standard traction $\boldsymbol{Sn}$ is work-conjugate to the velocity $\dot{\boldsymbol{y}}$ when the control volume remains unchanged. However, it is appropriate to use $\overset{\circ}{\boldsymbol{y}}$ as the work-conjugate velocity for $\boldsymbol{Sn}$ in a migrating control volume, when the material is added and removed continuously. Similarly, $\boldsymbol{b}^{\mathscr{S}}$ and $\boldsymbol{S}^{\mathscr{S}}\boldsymbol{n}^{\mathscr{S}}$ are work-conjugate to $\overset{\square}{\boldsymbol{y}}$ and $\overset{\wedge}{\boldsymbol{y}}$ respectively. On the other hand, the configurational force accounts for the change in the material structure and evolution of phase interface, such that $\boldsymbol{Cn}$ and $\boldsymbol{C}^{\mathscr{S}}\boldsymbol{n}^{\mathscr{S}}$ are work-

conjugate to $\boldsymbol{q}$ and $\boldsymbol{w}$. Since the material points are fixed at the reference body, no work is done by $\boldsymbol{g}$ and $\boldsymbol{g}^{\mathscr{S}}$. Therefore, the working of the system is given as

$$W(P)=\int_{\partial P}(\boldsymbol{C}\boldsymbol{n}\cdot\boldsymbol{q}+\boldsymbol{S}\boldsymbol{n}\cdot\overset{\circ}{\boldsymbol{y}})da+\int_{P}\boldsymbol{b}\cdot\dot{\boldsymbol{y}}dv+\int_{\partial\mathscr{S}}(\boldsymbol{C}^{\mathscr{S}}\boldsymbol{n}^{\mathscr{S}}\cdot\boldsymbol{w}+\boldsymbol{S}^{\mathscr{S}}\boldsymbol{n}^{\mathscr{S}}\cdot\overset{\triangle}{\boldsymbol{y}})ds+\int_{\mathscr{S}}\boldsymbol{b}^{\mathscr{S}}\cdot\overset{\square}{\boldsymbol{y}}da \quad (3.35)$$

By Equations (3.23) and (3.24), applying the divergence theorem gives

$$\begin{aligned}W(P)=&\int_{\partial P}(\boldsymbol{C}\boldsymbol{n}+\boldsymbol{F}^{T}\boldsymbol{S}\boldsymbol{n})\cdot\boldsymbol{q}da+\int_{P}\boldsymbol{S}\cdot\dot{\boldsymbol{F}}dv+\int_{\mathscr{S}}-\boldsymbol{m}\cdot[\boldsymbol{F}^{T}\boldsymbol{S}]\boldsymbol{m}Vda\\&+\int_{\partial\mathscr{S}}(\boldsymbol{C}^{\mathscr{S}}\boldsymbol{n}^{\mathscr{S}}\cdot\boldsymbol{w}+\boldsymbol{S}^{\mathscr{S}}\boldsymbol{n}^{\mathscr{S}}\cdot\overset{\triangle}{\boldsymbol{y}})ds\end{aligned} \quad (3.36)$$

By the constraint (3.1) on the normal component of the velocity $\boldsymbol{q}$, it is required that the integrand in the first term has to be in the form of

$$\boldsymbol{C}+\boldsymbol{F}^{T}\boldsymbol{S}=\pi\boldsymbol{I} \quad (3.37)$$

which is an explicit expression for the bulk configurational stress $\boldsymbol{C}$.

According to Equation (3.14), the superficial tensor $\boldsymbol{C}^{\mathscr{S}}+\langle\boldsymbol{F}\rangle^{T}\boldsymbol{S}^{\mathscr{S}}$ is decomposed into the following form as

$$\boldsymbol{C}^{\mathscr{S}}+\langle\boldsymbol{F}\rangle^{T}\boldsymbol{S}^{\mathscr{S}}=\sigma\boldsymbol{P}+\boldsymbol{m}\otimes\boldsymbol{d} \quad (3.38)$$

where $\boldsymbol{d}$ is the normal part of tensor $\boldsymbol{C}^{\mathscr{S}}+\langle\boldsymbol{F}\rangle^{T}\boldsymbol{S}^{\mathscr{S}}$.

As a result, the tangent part of $\boldsymbol{C}^{\mathscr{S}}$ is presented by

$$\boldsymbol{C}_{\tan}^{\mathscr{S}} = \sigma \boldsymbol{P} - \left\langle \boldsymbol{F}^{\mathscr{S}} \right\rangle^{T} \boldsymbol{S}^{\mathscr{S}} \tag{3.39}$$

where σ is surface tension.

Inserting Equations (3.37) and (3.38) into Equation (3.36), and applying the surface divergence law give

$$\begin{aligned} W(P) = & \int_{\partial P} \pi V_{\partial P} da + \int_{P} \boldsymbol{S} \cdot \dot{\boldsymbol{F}} dv + \int_{\mathscr{S}} (-\boldsymbol{m} \cdot [\boldsymbol{F}^{T} \boldsymbol{S}] \boldsymbol{m} + \boldsymbol{m} \cdot Div_{\mathscr{S}} \boldsymbol{C}^{\mathscr{S}}) V da \\ & + \int_{\mathscr{S}} (\boldsymbol{S}^{\mathscr{S}} \cdot \left\langle \overset{\square}{\boldsymbol{F}} \right\rangle - \sigma K V - \boldsymbol{d} \cdot \overset{\square}{\boldsymbol{m}}) da + \int_{\partial \mathscr{S}} \sigma V_{\partial \mathscr{S}} ds \end{aligned} \tag{3.40}$$

3.2.4.4. Formulation for energy conservation

According to the conservation of energy, it is required that the change of internal energy is equal to the sum of the heating and working, given by

$$\begin{aligned} & \frac{d}{dt} \{ \int_{P} E dv + \int_{\mathscr{S}} E^{\mathscr{S}} da \} \\ & = - \int_{P} Div \boldsymbol{h} dv - \int_{\mathscr{S}} [\boldsymbol{h}] \cdot \boldsymbol{m} da + \int_{P} q dv + \int_{\partial P} H V_{\partial P} da + \int_{\mathscr{S}} q^{\mathscr{S}} da + \int_{\partial \mathscr{S}} h V_{\partial \mathscr{S}} ds + W(P) \end{aligned} \tag{3.41}$$

Substituting Equation (3.40) into (3.41) gives the bulk conservation law as

$$\dot{E} = -Div \boldsymbol{h} + q + \boldsymbol{S} \cdot \dot{\boldsymbol{F}} \tag{3.42}$$

and the interfacial conservation law in the form of

$$\begin{aligned} & \overset{\square}{E}^{\mathscr{S}} - E^{\mathscr{S}} K V - [E] V \\ & = -[\boldsymbol{h}] \cdot \boldsymbol{m} + q^{\mathscr{S}} - (\boldsymbol{m} \cdot [\boldsymbol{F}^{T} \boldsymbol{S}] \boldsymbol{m} - \boldsymbol{m} \cdot Div_{\mathscr{S}} \boldsymbol{C}^{\mathscr{S}}) V + \boldsymbol{S}^{\mathscr{S}} \cdot \left\langle \overset{\square}{\boldsymbol{F}} \right\rangle - \sigma K V - \boldsymbol{d} \cdot \overset{\square}{\boldsymbol{m}} \end{aligned} \tag{3.43}$$

as well as the following two relations

$$E = \pi + H, \quad \text{and} \quad E^{\mathscr{S}} = \sigma + h \tag{3.44}$$

3.2.5. Entropy subject to the second law of thermodynamics

In this subsection, the entropies subject to the second law of thermodynamics are formulated for the system.

3.2.5.1. Heating

The entropy change due to heating is given as

$$-\int_{\partial P} \frac{\boldsymbol{h}}{T} \cdot \boldsymbol{n} da + \int_{P} \frac{q}{T} dv + \int_{\partial P} \frac{H}{T} V_{\partial P} da + \int_{\mathscr{S}} \frac{q^{\mathscr{S}}}{T} da + \int_{\partial \mathscr{S}} \frac{h}{T} V_{\partial \mathscr{S}} ds \tag{3.45}$$

where T is the temperature.

By the divergence law in the bulk and on the surface, Equation (3.45) is rewritten as

$$-\int_{P} \frac{Div\boldsymbol{h}}{T} dv - \int_{\mathscr{S}} [\frac{\boldsymbol{h}}{T}] \cdot \boldsymbol{m} da + \int_{P} \frac{\boldsymbol{h} \cdot \nabla T}{T^2} dv + \int_{P} \frac{q}{T} dv + \int_{\partial P} \frac{H}{T} V_{\partial P} da + \int_{\mathscr{S}} \frac{q^{\mathscr{S}}}{T} da + \int_{\partial \mathscr{S}} \frac{h}{T} V_{\partial \mathscr{S}} ds \tag{3.46}$$

3.2.5.2. Diffusion

The diffusion of mass into and out of P also contributes to the change in entropy. The electrochemical potential of species a, denoted by μ_a, is required to account for the entropy change due to diffusion. In such a way, the entropy change resulting from diffusion of species a is given as

$$\int_{\partial P}\frac{\mu_a \boldsymbol{j}_a}{T}\cdot\boldsymbol{n}da-\int_{P}\frac{\mu_a r_a^b}{T}dv-\int_{\partial P}\frac{\mu_a J_a}{T}V_{\partial P}da-\int_{\mathscr{S}}\frac{\mu_a r_a^{\mathscr{S}}}{T}da-\int_{\partial\mathscr{S}}\frac{\mu_a j_a}{T}V_{\partial\mathscr{S}}ds \tag{3.47}$$

where the continuity across the interface is assumed for the chemical potential, i.e.

$$[\mu_a]=0 \tag{3.48}$$

By the divergence theorem and Equation (3.31), Equation (3.47) is written as

$$\begin{aligned}&\int_{P}\frac{\mu_a Div\boldsymbol{j}_a}{T}dv+\int_{P}\frac{\boldsymbol{j}_a\cdot\nabla\mu_a}{T}dv+\int_{\mathscr{S}}\mu_a[\frac{\boldsymbol{j}_a}{T}]\cdot\boldsymbol{m}da-\int_{P}\frac{\mu_a\boldsymbol{j}_a\cdot\nabla T}{T^2}dv\\&-\int_{P}\frac{\mu_a r_a^b}{T}dv-\int_{\partial P}\frac{\mu_a c_a}{T}V_{\partial P}da-\int_{\mathscr{S}}\frac{\mu_a r_a^{\mathscr{S}}}{T}da-\int_{\partial\mathscr{S}}\frac{\mu_a c_a^{\mathscr{S}}}{T}V_{\partial\mathscr{S}}ds\end{aligned} \tag{3.49}$$

3.2.5.3. Electricity

If the valence of each species a is z_a, and the electric potential relative to the ground is $\phi=\phi(\boldsymbol{X},t)$, the contribution of the electric field to the entropy change for species a is given as

$$-\int_{\partial P}\frac{\phi e z_a\boldsymbol{j}_a}{T}\cdot\boldsymbol{n}da+\int_{P}\frac{\phi e z_a r_a^b}{T}dv+\int_{\partial P}\frac{\phi e z_a J_a}{T}V_{\partial P}da+\int_{\mathscr{S}}\frac{\phi e z_a r_a^{\mathscr{S}}}{T}da+\int_{\partial\mathscr{S}}\frac{\phi e z_a j_a}{T}V_{\partial\mathscr{S}}ds \tag{3.50}$$

where e is the elementary charge.

By the divergence theorem and Equation (3.31), Equation (3.50) is written as

$$-\int_P \frac{ez_a \nabla\phi \cdot \boldsymbol{j}_a}{T} dv - \int_P \frac{ez_a \phi Div \boldsymbol{j}_a}{T} dv + \int_P \frac{ez_a \phi \nabla T \cdot \boldsymbol{j}_a}{T^2} dv - \int_{\mathscr{S}} \phi ez_a [\frac{\boldsymbol{j}_a}{T}] \cdot \boldsymbol{m} da$$
$$+\int_P \frac{\phi ez_a r_a^b}{T} dv + \int_{\partial P} \frac{\phi ez_a c_a}{T} V_{\partial P} da + \int_{\mathscr{S}} \frac{\phi ez_a r_a^{\mathscr{S}}}{T} da + \int_{\partial \mathscr{S}} \frac{\phi ez_a c_a^{\mathscr{S}}}{T} V_{\partial \mathscr{S}} ds \tag{3.51}$$

where the continuity across the interface is assumed for the electric potential, i.e.

$$[\phi] = 0 \tag{3.52}$$

According to electrostatics, Maxwell's equation with neglecting magnetic effects reduces to (Wang, Wang et al. 1997)

$$\sum_a ez_a \boldsymbol{j}_a + \dot{\boldsymbol{D}} = 0 \tag{3.53}$$

where $\boldsymbol{D}$ is the electric displacement and is associated with the electric field $\boldsymbol{E} = -\nabla\phi$ via

$$\boldsymbol{D} = \varepsilon \boldsymbol{E} = -\varepsilon \nabla \phi \tag{3.54}$$

where ε is the permittivity and is assumed to be constant in the whole system.

Therefore, the Gauss' law is formulated as

$$Div\boldsymbol{D} = Div(\varepsilon \boldsymbol{E}) = Q = \sum_a ez_a c_a \tag{3.55}$$

where Q is the total electric charge density.

3.2.5.4. Application of the second law of thermodynamics

According to the second law of thermodynamics, the entropy of the whole system must not decrease i.e.

$$\begin{aligned}
&\frac{d}{dt}\{\int_P \eta dv + \int_{\mathscr{S}} \eta^{\mathscr{S}} da\} \\
&\geq -\int_P \frac{Div\boldsymbol{h}}{T} dv + \int_P \frac{\boldsymbol{h}\cdot\nabla T}{T^2} dv - \int_{\mathscr{S}} [\frac{\boldsymbol{h}}{T}]\cdot\boldsymbol{m} da + \int_P \frac{q}{T} dv + \int_{\partial P} \frac{H}{T} V_{\partial P} da + \int_{\mathscr{S}} \frac{q^{\mathscr{S}}}{T} da + \int_{\partial\mathscr{S}} \frac{h}{T} V_{\partial\mathscr{S}} ds \\
&\quad + \sum_a (\int_P \frac{\mu_a Div\boldsymbol{j}_a}{T} dv + \int_P \frac{\boldsymbol{j}_a\cdot\nabla\mu_a}{T} dv + \int_{\mathscr{S}} \mu_a [\frac{\boldsymbol{j}_a}{T}]\cdot\boldsymbol{m} da - \int_P \frac{\mu_a \boldsymbol{j}_a\cdot\nabla T}{T^2} dv) \\
&\quad + \sum_a (-\int_P \frac{\mu_a r_a^b}{T} dv - \int_{\partial P} \frac{\mu_a c_a}{T} V_{\partial P} da - \int_{\mathscr{S}} \frac{\mu_a r_a^{\mathscr{S}}}{T} da - \int_{\partial\mathscr{S}} \frac{\mu_a c_a^{\mathscr{S}}}{T} V_{\partial\mathscr{S}} da) \\
&\quad + \sum_a (-\int_P \frac{ez_a\nabla\phi\cdot\boldsymbol{j}_a}{T} dv - \int_P \frac{ez_a\phi Div\boldsymbol{j}_a}{T} dv + \int_P \frac{ez_a\phi\nabla T\cdot\boldsymbol{j}_a}{T^2} dv - \int_{\mathscr{S}} [\frac{\phi ez_a \boldsymbol{j}_a}{T}]\cdot\boldsymbol{m} da) \\
&\quad + \sum_a (\int_P \frac{\phi ez_a r_a^b}{T} dv + \int_{\partial P} \frac{\phi ez_a c_a}{T} V_{\partial P} da + \int_{\mathscr{S}} \frac{\phi ez_a r_a^{\mathscr{S}}}{T} da + \int_{\partial\mathscr{S}} \frac{\phi ez_a c_a^{\mathscr{S}}}{T} V_{\partial\mathscr{S}} ds)
\end{aligned} \tag{3.56}$$

where η and $\eta^{\mathscr{S}}$ are the entropy densities in the bulk phases and on the interface, respectively.

As a result, the bulk inequality is in the form of

$$\begin{aligned}
T\dot{\eta} \geq & -Div\boldsymbol{h} + \frac{1}{T}\boldsymbol{h}\cdot\nabla T + q + \sum_a (\mu_a Div\boldsymbol{j}_a + \boldsymbol{j}_a\cdot\nabla\mu_a - \frac{1}{T}\mu_a\boldsymbol{j}_a\cdot\nabla T - \mu_a r_a^b) \\
& + \sum_a (-ez_a\nabla\phi\cdot\boldsymbol{j}_a - ez_a\phi Div\boldsymbol{j}_a + \frac{1}{T} ez_a\phi\nabla T\cdot\boldsymbol{j}_a + \phi ez_a r_a^b)
\end{aligned} \tag{3.57}$$

and the interfacial inequality in the form of

$$\dot{\eta}^{\mathscr{S}} - \eta^{\mathscr{S}} KV - [\eta]V \geq -[\frac{\boldsymbol{h}}{T}] \cdot \boldsymbol{m} + \frac{q^{\mathscr{S}}}{T} + \sum_a (\mu_a [\frac{\boldsymbol{j}_a}{T}] \cdot \boldsymbol{m} - \frac{\mu_a r_a^{\mathscr{S}}}{T}) + \sum_a (-\phi ez_a [\frac{\boldsymbol{j}_a}{T}] \cdot \boldsymbol{m} + \phi ez_a \frac{r_a^{\mathscr{S}}}{T}) \tag{3.58}$$

as well as the following two relations among the entropy densities η for the bulk phases and $\eta^{\mathscr{S}}$ for the interface, and the configurational heatings H for the bulk phases and h for the interface as

$$\eta = \frac{H - \sum_a \mu_a J_a + \sum_a \phi ez_a c_a}{T} \qquad \eta^{\mathscr{S}} = \frac{h - \sum_a \mu_a c_a^{\mathscr{S}} + \sum_a \phi ez_a c_a^{\mathscr{S}}}{T} \tag{3.59}$$

Substituting Equation (3.59) into Equation (3.44), and using Equation (3.31), we have

$$\pi = E - \eta T - \sum_a \mu_a c_a + \sum_a \phi ez_a c_a = E - \eta T - \sum_a (\mu_a - \phi ez_a) c_a \tag{3.60}$$

$$\sigma = E^{\mathscr{S}} - \eta^{\mathscr{S}} T - \sum_a \mu_a c_a^{\mathscr{S}} + \sum_a \phi ez_a c_a^{\mathscr{S}} = E^{\mathscr{S}} - \eta^{\mathscr{S}} T - \sum_a (\mu_a - \phi ez_a) c_a^{\mathscr{S}} \tag{3.61}$$

3.2.6. Constitutive equations

In this subsection, the constitutive equations are formulated based on the second law of thermodynamics in the bulk phases and on the interface.

3.2.6.1. Bulk constitutive equations

According to thermodynamics, Helmholtz free energy density is given by $\Phi = E - \eta T$. By Equations (3.29), (3.42) (3.53) and (3.57), the inequality in the bulk phases is given in the form of

$$\dot{\Phi} \le \boldsymbol{S}\cdot\dot{\boldsymbol{F}} - \eta\dot{T} - \nabla\phi\cdot\dot{\boldsymbol{D}} + \sum_a(\mu_a - ez_a\phi)\dot{c}_a - \frac{1}{T}\boldsymbol{h}\cdot\nabla T - \sum_a \boldsymbol{j}_a\cdot\nabla\mu_a + \sum_a\left(\frac{\mu_a - \phi ez_a}{T}\boldsymbol{j}_a\cdot\nabla T\right) \tag{3.62}$$

If $\Phi = \Phi(\boldsymbol{F}, c_a, T, \rho)$ is a function of c_a, T, $\boldsymbol{D}$, $\boldsymbol{F}$ and ρ, the bulk constitutive equations in the bulk phases are given as follows,

$$\mu_a - ez_a\varphi = \frac{\partial\Phi}{\partial c_a}, \qquad \eta = -\frac{\partial\Phi}{\partial T}, \qquad -\nabla\phi = \frac{\partial\Phi}{\partial\boldsymbol{D}}, \quad \boldsymbol{S} = \frac{\partial\Phi}{\partial\boldsymbol{F}} \tag{3.63}$$

$$\boldsymbol{j}_a = -\boldsymbol{M}_a\nabla\mu_a, \qquad \boldsymbol{h} = -\boldsymbol{K}\nabla T \tag{3.64}$$

where $\boldsymbol{M}_a$ and $\boldsymbol{K}$ are the mobility and thermal conductivity, and both are positive-definite tensors.

Meanwhile, we also have the following relation for an equilibrium state,

$$\frac{\partial\Phi}{\partial\rho} = 0 \tag{3.65}$$

In addition, a sufficient and necessary condition required by the second law of thermodynamics is imposed on the scalar thermal conductivity K, and scalar motility M_a as (Caginalp and Jones 1995)

$$KT - \frac{M_a}{4}(\mu_a - \phi ez_a)^2 \ge 0 \tag{3.66}$$

which is automatically satisfied when $\mu_a - \phi ez_a$ is sufficiently small.

By applying the Legendre transformation, the free energy densities are presented in the new form of $\Psi = \Phi - \sum_a \frac{\partial \Phi}{\partial c_a} c_a = \Phi - \sum_a (\mu_a - \phi ez_a) c_a$ in the bulk phases (Gurtin and Voorhees 1993). Equation (3.61) shows the coincidence between the surface free energy and surface tension, and Equation (3.60) demonstrates the classical Eshelby relation (Eshelby 1951) as

$$\boldsymbol{C} = \pi \boldsymbol{I} - \boldsymbol{F}^T \boldsymbol{S} = \left\{ \Phi - \sum_a (\mu_a - \varphi ez_a) c_a \right\} \boldsymbol{I} - \boldsymbol{F}^T \boldsymbol{S} = \Psi \boldsymbol{I} - \boldsymbol{F}^T \boldsymbol{S} \tag{3.67}$$

Consequently, by using the new free energy density $\Psi = \Phi - \sum_a (\mu_a - \varphi ez_a) c_a$, the inequality in the bulk phases, Equation (3.62), is refined in the following form as

$$\begin{aligned} \dot{\Psi} \le \boldsymbol{S} \cdot \dot{\boldsymbol{F}} - \eta \dot{T} - \sum_a (\dot{\mu}_a - \dot{\phi} ez_a) c_a - \nabla \phi \cdot \dot{\boldsymbol{D}} - \frac{1}{T} \boldsymbol{h} \cdot \nabla T - \sum_a (\boldsymbol{j}_a \cdot \nabla \mu_a) \\ + \sum_a \left(\frac{\mu_a - \phi ez_a}{T} \boldsymbol{j}_a \cdot \nabla T \right) \end{aligned} \tag{3.68}$$

If Ψ is a function of $\mu_a^c = \mu_a - \phi ez_a$, T , $\boldsymbol{D}$ and $\boldsymbol{F}$, the bulk constitutive equations (3.63) in the bulk phases are refined as follows,

$$c_a = -\frac{\partial \Psi}{\partial \mu_a^c}, \quad \eta = -\frac{\partial \Psi}{\partial T}, \qquad -\nabla \phi = \frac{\partial \Psi}{\partial \boldsymbol{D}}, \quad \boldsymbol{S} = \frac{\partial \Psi}{\partial \boldsymbol{F}} \tag{3.69}$$

and the rest remain unchanged.

3.2.6.2. Interfacial constitutive equations

Similarly, the free energy density on the interface is given as $\varphi = E^{\mathscr{S}} - \eta^{\mathscr{S}} T$. By Equations (3.30), (3.43), (3.58) and (3.61), the inequality on the interface becomes in the form of

$$\begin{aligned} \overset{\square}{\varphi} \le -\eta^{\mathscr{S}} \overset{\square}{T} + \boldsymbol{S}^{\mathscr{S}} \cdot \left\langle \overset{\square}{\boldsymbol{F}} \right\rangle - \boldsymbol{d} \cdot \overset{\square}{\boldsymbol{m}} + \sum_a (\mu_a - \phi e z_a) \overset{\square}{c_a^{\mathscr{S}}} \\ + [\Phi] V - \sum_a (\mu_a - \phi e z_a)[c_a] V - (\boldsymbol{m} \cdot [\boldsymbol{F}^T \boldsymbol{S}] \boldsymbol{m} - \boldsymbol{m} \cdot Div_{\mathscr{S}} \boldsymbol{C}^{\mathscr{S}}) V \end{aligned} \tag{3.70}$$

where the local thermal equilibrium, $[T] = 0$, is imposed on the interface.

If φ is a function of $c_a^{\mathscr{S}}$, T, $\boldsymbol{m}$, and $\langle \boldsymbol{F} \rangle$, the constitutive equations on the interface is presented in the form of

$$\mu_a - \phi e z_a = \frac{\partial \varphi}{\partial c_a^{\mathscr{S}}}, \qquad s = -\frac{\partial \varphi}{\partial T}, \qquad \boldsymbol{d} = -\frac{\partial \varphi}{\partial \boldsymbol{m}}, \qquad \boldsymbol{S}^{\mathscr{S}} = \frac{\partial \varphi}{\partial \langle \boldsymbol{F} \rangle} \tag{3.71}$$

Similarly, by the Legendre transformation, the free energy density on the interface is given as $\psi = \varphi - \sum_a \frac{\partial \varphi}{\partial c_a^{\mathscr{S}}} c_a^{\mathscr{S}} = \varphi - \sum_a (\mu_a - \phi e z_a) c_a^{\mathscr{S}}$. By Equations (3.30), (3.43), (3.58), (3.60), (3.61) and (3.67), the inequality on the interface, Equation (3.70), is refined in the form of

$$\begin{aligned} \overset{\square}{\psi} - [\Psi] V \le -\eta^{\mathscr{S}} \overset{\square}{T} + \boldsymbol{S}^{\mathscr{S}} \cdot \left\langle \overset{\square}{\boldsymbol{F}} \right\rangle - \boldsymbol{d} \cdot \overset{\square}{\boldsymbol{m}} - \sum_a (\overset{\square}{\mu_a} - \overset{\square}{\phi} e z_a) c_a^{\mathscr{S}} \\ - (\boldsymbol{m} \cdot [\boldsymbol{F}^T \boldsymbol{S}] \boldsymbol{m} - \boldsymbol{m} \cdot Div_{\mathscr{S}} \boldsymbol{C}^{\mathscr{S}}) V \end{aligned} \tag{3.72}$$

If ψ is a function of $\boldsymbol{T}$, $\mu_a^c = \mu_a - \phi e z_a$, $\boldsymbol{m}$, and $\langle \boldsymbol{F} \rangle$, the constitutive equations on the interface is presented in the form of

$$\eta^{\mathscr{S}} = -\frac{\partial \psi}{\partial T}, \quad c_a^{\mathscr{S}} = -\frac{\partial \psi}{\partial \mu_a^c}, \quad \boldsymbol{d} = -\frac{\partial \psi}{\partial \boldsymbol{m}}, \qquad \boldsymbol{S}^{\mathscr{S}} = \frac{\partial \psi}{\partial \langle \boldsymbol{F} \rangle} \tag{3.73}$$

and the evolution equation in the form of

$$-[\Psi] + (\boldsymbol{m} \cdot [\boldsymbol{F}^T \boldsymbol{S}]\boldsymbol{m} - \boldsymbol{m} \cdot Div_{\mathscr{S}} \boldsymbol{C}^{\mathscr{S}}) = -mV \tag{3.74}$$

with the kinetic modulus $m = m(\boldsymbol{m}, \mu, \mathrm{V}, \langle \boldsymbol{F} \rangle) \geq 0$.

As well known, if the diffusion of molecules in each bulk phase is much faster than the interface evolution, the concentration of polymer is homogeneous in each phase during the phase transition. If the mobility is isotropic and homogeneous, i.e. $\boldsymbol{M}_a = M_a \boldsymbol{I}$, and no mass supply exists in each phase and on the Interface, the diffusion equations (3.29) and (3.30) reduce to

$$\nabla^2 \mu_a = 0 \tag{3.75}$$

$$\overset{\square}{c}_a^{\mathscr{S}} - c_a^{\mathscr{S}} KV - [c_a]V = [M_a \nabla \mu_a] \cdot \boldsymbol{m} \tag{3.76}$$

where the scalar mobility M_a is constant and $M_a = D_a c_a / (kT)$ with diffusion coefficient D_a of species a.

3.2.6.3. Reduced constitutive equations for a single-phase hydrogel

In the present model, a two-phase control volume $P(t)$ is considered, which migrates with time and is separated by the interface $\mathscr{S}(t)$ into two phases α and β, and the derivation of the constitutive equations is independent of the specific phase. Therefore, the constitutive equations in both bulk phases are formulated by Equations (3.69). In addition, Equations (3.73) are also included in the present model to account for the interfacial constitutive relations. When the system reduces into a single-phase hydrogel, namely when no interface exists, the interfacial constitutive equations (3.73) are ignored, and Equations (3.69) alone are enough to describe the bulk constitutive relations.

3.2.6.4. Advantages of the present constitutive equations over a published non-equilibrium model

As mentioned above, when the system reduces into a single-phase hydrogel, the constitutive equations reduces into Equations (3.69) accordingly, which are in fact the same form as those derived by a different approach, called the non-equilibrium thermodynamic theory (Hong, Zhao et al. 2008, Hong, Liu et al. 2009, Hong, Zhao et al. 2010). In other words, the non-equilibrium model proposed by Suo' group (Hong, Zhao et al. 2008, Hong, Liu et al. 2009, Hong, Zhao et al. 2010) is just a special case of the present model with respect to constitutive relations, when the present two-phase control volume reduces to a single-phase one, in which only the gel phase with constant crosslink density exists in the hydrogel system.

3.2.7. A novel formulation of the bulk free energy with the effect of crosslink density

In order to model the solution-gel phase transition of the physical hydrogel, the free energy is required. In this subsection, a novel free energy is developed to account for the effect of crosslink density ρ . As well known, the polymer chains of the physical hydrogel are crosslinked by weak physical bonds in general, such as van der Waals interaction and hydrogen bonds. As a result, the physical hydrogel is able to exhibit the phase transition between solid and liquid states, when the crosslinks are formed or broken, subject to environmental stimuli. Therefore, the crosslink density ρ has an important influence on the mechanical, thermal and chemical behavior of the hydrogel.

3.2.7.1. Elasticity

In the classical mechanics, usually an undeformed state is taken as a reference state. For modeling of the hydrogel, the dry state as the undeformed state is generally taken as a reference state (Hong, Zhao et al. 2008, Hong, Liu et al. 2009), in which there is no solution, and thus the elastic contribution to the free energy is formulated with respect to the dry state. It is noted that an isotropic distribution in a diamond lattice for the present crosslinks is assumed at the equilibrium state. As such, the functionality for each crosslink is equal to 4 (Rubinstein and Colby 2003), and the distance R_0 between the neighboring crosslinks at dry state is given as

$$R_0^3 = \frac{3\sqrt{3}}{8\rho_0} \tag{3.77}$$

where ρ_0 is the crosslink density at the dry state.

The entropy of stretching a polymer chain may be expressed below (Rubinstein and Colby 2003)

$$\Delta\eta_{elastic} = -\frac{1}{2}\frac{k}{Nb^2}(\lambda_x^2 + \lambda_y^2 + \lambda_z^2 - 3)R_0^2 \tag{3.78}$$

where λ_x, λ_y, λ_z are the principal stretches, b is the Kuhn length, and N is the average number of Kuhn monomers which are associated with each chain between two crosslinks.

The entropy density of the hydrogel is formulated, based on the affine network model (Rubinstein and Colby 2003),

$$\eta_{elastic} = \Delta\eta_{elastic} n = -\frac{3}{4}\frac{\rho}{\rho_0^{2/3}}\frac{k}{Nb^2}(\lambda_x^2 + \lambda_y^2 + \lambda_z^2 - 3) \tag{3.79}$$

in which n is the number density of the polymeric segments between the neighboring crosslinks at the current state, and $n = 2\rho$ with $\rho = \rho_0 / \det \boldsymbol{F}$ as the crosslink density at the current state.

By the affine model (Rubinstein and Colby 2003), the relative deformation of each network strand is the same as the macroscopic relative deformation imposed on the whole network (Rubinstein and Colby 2003). As such, it can be reasonably assumed that all the monomers are connected to the network. Therefore, the average number of Kuhn monomers in subchains N depends on the density of crosslinks ρ. If α represents the

number of monomers in a Kuhn monomer, the concentration of monomers c_m is thus associated with the average number N and the crosslink density ρ via

$$c_m = N \cdot \alpha \cdot n = 2N\alpha\rho \tag{3.80}$$

As such, the elastic energy is written in the scale form of

$$\Phi_{elastic} = -\eta_{elastic} T = \frac{3}{4} \frac{\rho^{1/3}}{(\det \boldsymbol{F})^{2/3}} \frac{kT}{Nb^2} (\lambda_x^2 + \lambda_y^2 + \lambda_z^2 - 3) \tag{3.81}$$

or in the tensor form of

$$\Phi_{elastic} = \frac{3}{4} \frac{\rho^{1/3}}{(\det \boldsymbol{F})^{2/3}} \frac{kT}{Nb^2} (F_{ij} F_{ij} - 3) \tag{3.82}$$

in which the entropy is considered only to make contribution into the elastic free energy (3.81) or (3.82).

3.2.7.2. Mixing

The energy of mixing between the polymer and solvent per lattice site may be written as follows, according to the Flory-Huggins solution theory (Flory and Rehner 1943, Flory and Rehner 1943, Flory 1953)

$$\Delta\Phi_{solvent} = kT \left\{ \frac{\vartheta_m}{N\alpha} \ln \vartheta_m + (1 - \vartheta_m) \ln(1 - \vartheta_m) + \chi \vartheta_m (1 - \vartheta_m) \right\} \tag{3.83}$$

in which ϑ_m is the volume fraction of polymer. χ is a dimensionless interaction parameter, and $\chi = A + B/T$ (Rubinstein and Colby 2003), where A and B are material dependent parameters. If the specific volume of a monomer unit is denoted by v and assumed as the same as that of the solvent and the mobile ions, we have $\vartheta_m = c_m v$, where c_m is the number concentrations of monomers in the bulk phases. Therefore, the free energy density of mixing between the polymer and solvent is given as follows.

$$\Phi_{solvent} = \frac{kT}{v}\left\{\frac{vc_m}{N\alpha}\ln(vc_m) + (1-vc_m)\ln(1-vc_m) + \chi vc_m(1-vc_m)\right\} \tag{3.84}$$

In addition, the mobile ions also contribute to the energy of mixing. If the concentrations of the mobile ions are low, their contribution to the free energy results from the entropy of mixing, namely (Hong, Zhao et al. 2010)

$$\Phi_{ion} = kT\sum_{a\neq m} c_a\left(\ln\frac{c_a}{vc_m c_a^0} - 1\right) \tag{3.85}$$

where c_a^0 is a reference concentration of species a when the chemical potential of the species is equal to zero.

Therefore, the energy of mixing of the system is in the form of

$$\begin{aligned}\Phi_{mixing} &= \Phi_{solvent} + \Phi_{ion} \\ &= \frac{kT}{v}\left\{\frac{vc_m}{N\alpha}\ln(vc_m) + (1-vc_m)\ln(1-vc_m) + \chi vc_m(1-vc_m)\right\} + kT\sum_{a\neq m} c_a\left(\ln\frac{c_a}{vc_m c_a^0} - 1\right)\end{aligned} \tag{3.86}$$

3.2.7.3. Polarization

If the hydrogel is an ideal dielectric, the energy of polarization is written in the form of (Zhao, Hong et al. 2007, Hong, Zhao et al. 2010)

$$\Phi_{pol} = D_i D_i / 2\varepsilon \tag{3.87}$$

3.2.7.4. Bonding

Meanwhile, the contribution coming from the breaking and forming of crosslinks due to the environmental stimuli is also considered to the free energy of the system. In order to characterize the crosslink, the same structure is assumed for all crosslinks via a generalized weak physical bond (An, Solis et al. 2010). As such, the energy of the generalized weak physical bonding may be written in the form as (An, Solis et al. 2010)

$$\Phi_{bonding} = -\rho E_a \tag{3.88}$$

where E_a is an activation energy required to break a crosslink.

3.2.7.5. Internal energy

If the specific heat capacity C_v is constant and independent of temperature, the contribution of internal energy to free energy is given as

$$\Phi_{internal} = C_v T(1 - \ln \frac{T}{T_M}) \tag{3.89}$$

where T_M is a reference temperature.

3.2.7.6. Total bulk free energy

In summary, the total free energy density Φ_{total} of the system is contributed by the elastic, mixing, polarization, bonding, and internal energies. Φ_{total} is thus obtained by Equations (3.82), (3.86), (3.87), (3.88) and (3.89) as

$$\begin{aligned}\Phi_{total} &= C_v T(1-\ln\frac{T}{T_M})+\frac{3}{4}\frac{\rho^{1/3}}{(\det \boldsymbol{F})^{2/3}}\frac{kT}{Nb^2}(F_{ij}F_{ij}-3)-\rho E_a+\frac{D_i D_i}{2\varepsilon}\\ &+\frac{kT}{v}\left\{\frac{vc_m}{N\alpha}\ln(vc_m)+(1-vc_m)\ln(1-vc_m)+\chi vc_m(1-vc_m)\right\}+kT\sum_{a\neq m}c_a(\ln\frac{c_a}{vc_m c_a^0}-1)\end{aligned} \tag{3.90}$$

As mentioned above, the dry state is taken as the reference state. If the hydrogel is a condensed matter, namely both the polymer and solvent molecules are incompressible, we have the incompressibility condition, given below (Hong, Zhao et al. 2008),

$$\frac{1}{vc_m}=\det \boldsymbol{F}\text{ , or }c_m=1/(v\det \boldsymbol{F}) \tag{3.91}$$

After the Legendre transformation, the free energy densities are reformed as $\Psi=\Phi-\sum_a\frac{\partial\Phi}{\partial c_a}c_a=\Phi-\sum_a(\mu_a-\varphi ez_a)c_a$.

By Equations (3.63) and (3.90), we have

$$\mu_a-\varphi ez_a=\frac{\partial\Phi}{\partial c_a}=kT\ln\frac{c_a}{vc_m c_a^0} \tag{3.92}$$

and consequently,

$$c_a = \nu c_m c_a^0 e^{(\mu_a - \phi e z_a)/kT}, \quad (a \neq m) \tag{3.93}$$

Based on Equations (3.29), (3.63), (3.64), (3.92), and the relation $\frac{\boldsymbol{M}_a kT}{c_a} = \boldsymbol{D}_a$, we may have the Nernst-Planck equation for the mass conservation, given as

$$\dot{c}_a = Div\left\{\boldsymbol{D}_a(\nabla c_a + \frac{ez_a c_a}{kT}\nabla\varphi)\right\} + r_a^b \tag{3.94}$$

Therefore, the free energy density Ψ of the whole system is formulated as the following form, according to Equation (3.80), Equation (3.90), the incompressibility condition (3.91), and Equation (3.93),

$$\begin{aligned}\Psi = {} & C_v T(1 - \ln\frac{T}{T_M}) + \frac{3}{2}\frac{(\rho^4 \det\boldsymbol{F})^{1/3} \nu kT}{b^2/\alpha}(F_{ij}F_{ij} - 3) - \rho E_a + \frac{D_i D_i}{2\varepsilon} \\ & + \frac{kT}{\nu}\left\{-2\rho\nu\ln(\det\boldsymbol{F}) + (1 - \frac{1}{\det\boldsymbol{F}})\ln(1 - \frac{1}{\det\boldsymbol{F}}) + \chi\frac{1}{\det\boldsymbol{F}}(1 - \frac{1}{\det\boldsymbol{F}})\right\} \\ & - \frac{\mu_m - \phi e z_m}{\nu\det\boldsymbol{F}} - kT\sum_{a\neq m}\frac{c_a^0}{\det\boldsymbol{F}} e^{(\mu_a - \phi e z_a)/kT}\end{aligned} \tag{3.95}$$

By the relation that $\mu_a^c = \mu_a - \phi e z_a$, Equation (3.95) may be rewritten as

$$\begin{aligned}\Psi = {} & C_v T(1 - \ln\frac{T}{T_M}) + \frac{3}{2}\frac{(\rho^4 \det\boldsymbol{F})^{1/3} \nu kT}{b^2/\alpha}(F_{ij}F_{ij} - 3) - \rho E_a + \frac{D_i D_i}{2\varepsilon} \\ & + \frac{kT}{\nu}\left\{-2\rho\nu\ln(\det\boldsymbol{F}) + (1 - \frac{1}{\det\boldsymbol{F}})\ln(1 - \frac{1}{\det\boldsymbol{F}}) + \chi\frac{1}{\det\boldsymbol{F}}(1 - \frac{1}{\det\boldsymbol{F}})\right\} \\ & - \frac{\mu_m^c}{\nu\det\boldsymbol{F}} - kT\sum_{a\neq m}\frac{c_a^0}{\det\boldsymbol{F}}\exp(\mu_a^c/kT)\end{aligned} \tag{3.96}$$

3.2.8. Surface tension

For simplicity, a constant free energy density on the interface is assumed in the present model, namely

$$\psi = \varphi - \sum_a \frac{\partial \varphi}{\partial c_a^{\mathscr{S}}} c_a^{\mathscr{S}} = \varphi - \sum_a (\mu_a - \phi e z_a) c_a^{\mathscr{S}} = \sigma = const \tag{3.97}$$

resulting in

$$\eta^{\mathscr{S}} = 0, \qquad c_a^{\mathscr{S}} = 0, \qquad \boldsymbol{d} = 0, \ \boldsymbol{S}^{\mathscr{S}} = 0 \tag{3.98}$$

Therefore, the configurational force on the interface is in the form of

$$\boldsymbol{C}^{\mathscr{S}} = \sigma \boldsymbol{P} \tag{3.99}$$

and thus

$$\boldsymbol{m} \cdot Div_{\mathscr{S}} \boldsymbol{C}^{\mathscr{S}} = \sigma K \tag{3.100}$$

with K the total curvature.

Consequently, the evolution equation (3.74) reduces to

$$-[\Psi] + \boldsymbol{m} \cdot [\boldsymbol{F}^T \boldsymbol{S}] \boldsymbol{m} - \sigma K = -mV \tag{3.101}$$

So far the formulation of the present model has been completed theoretically. It is composed of the force equilibrium equation (3.23) in the bulk phases and Equation (3.24) on the interface, the mass conservation equation (3.29) in the bulk phases and Equation

(3.30) on the interface, or their reduced form given by Equations (3.75) and (3.76), if the diffusion is much faster than the interface evolution and no mass supply exists, the energy conservation equation (3.42) in the bulk phases and Equation (3.43) on the interface, the Maxwell equations (3.53) and (3.55), and Equation (3.74) for the evolution of interface. By the second law of thermodynamics, the constitutive equations (3.69) are given in the bulk phases and Equations (3.73) on the interface, and the mas and heat flux are presented by Equation (3.64). The present model also includes the free energy density formulated by Equation (3.96) in the bulk phases and by Equation (3.97) on the interface. As mentioned above, this model couples the thermal, electrical, chemical and mechanical effects together, and it can perform the simulation of the interface kinetics of the physical hydrogel during the solution-gel phase transition.

3.3. Reduced one-dimensional model

In this section, the present model is reduced from a three-dimensional domain to a one-dimensional one for case study by simulation of evolving interface of a spherically symmetrically physical hydrogel during the solution-gel phase transition.

3.3.1. Force

For a spherically symmetrically evolving interface during solution-gel phase transition of physical hydrogel, the deformation in the one-dimensional domain is the displacement $y(r)$ in the radial direction. As a result, the stretch in the circumstantial direction is given as

$$\lambda_t = y / r \tag{3.102}$$

and the stretch in the radial direction is in the form of

$$\lambda_r = dy / dr \tag{3.103}$$

By Equations (3.69) and (3.96), the stress is given as

$$\begin{aligned}\boldsymbol{S} = \frac{\partial \Psi}{\partial \boldsymbol{F}} &= \frac{3}{2}\frac{\rho^{4/3} vkT}{b^2/\alpha}\left\{\frac{(\boldsymbol{F}_{ij}\boldsymbol{F}_{ij}-3)\boldsymbol{F}^{-T}(\det \boldsymbol{F})^{1/3}}{3} + 2\boldsymbol{F}(\det \boldsymbol{F})^{1/3}\right\} \\ &+ \frac{kT}{v}\left\{-2\rho v\boldsymbol{F}^{-T} + \frac{\boldsymbol{F}^{-T}}{\det \boldsymbol{F}}\ln(1-\frac{1}{\det \boldsymbol{F}}) + \frac{\boldsymbol{F}^{-T}}{\det \boldsymbol{F}} + \chi\frac{\boldsymbol{F}^{-T}}{\det \boldsymbol{F}}(\frac{2}{\det \boldsymbol{F}}-1)\right\} \\ &+ \frac{\mu_m^c \boldsymbol{F}^{-T}}{v\det \boldsymbol{F}} + kT\sum_{a\neq m}\frac{c_a^0 \boldsymbol{F}^{-T}}{\det \boldsymbol{F}}\exp(\mu_a^c / kT)\end{aligned} \tag{3.104}$$

in which the stress components are given in the radial and tangent directions respectively,

$$\begin{aligned}S_r &= \frac{3}{2}\frac{\rho^{4/3} vkT}{b^2/\alpha}\left\{\frac{(\lambda_r^2+2\lambda_t^2-3)(\lambda_r\lambda_t^2)^{1/3}}{3\lambda_r} + 2\lambda_r(\lambda_r\lambda_t^2)^{1/3}\right\} \\ &+ \frac{kT}{v}\left\{-\frac{2\rho v}{\lambda_r} + \frac{1}{\lambda_r^2\lambda_t^2}\ln(1-\frac{1}{\lambda_r\lambda_t^2}) + \frac{1}{\lambda_r^2\lambda_t^2} + \chi\frac{1}{\lambda_r^2\lambda_t^2}(\frac{2}{\lambda_r\lambda_t^2}-1)\right\} \\ &+ \frac{\mu_m^c}{v\lambda_r^2\lambda_t^2} + kT\sum_{a\neq m}\frac{c_a^0}{\lambda_r^2\lambda_t^2}\exp(\mu_a^c / kT)\end{aligned} \tag{3.105}$$

$$\begin{aligned}S_t &= \frac{3}{2}\frac{\rho^{4/3} vkT}{b^2/\alpha}\left\{\frac{(\lambda_r^2+2\lambda_t^2-3)(\lambda_r\lambda_t^2)^{1/3}}{3\lambda_t} + 2\lambda_t(\lambda_r\lambda_t^2)^{1/3}\right\} \\ &+ \frac{kT}{v}\left\{-\frac{2\rho v}{\lambda_t} + \frac{1}{\lambda_r\lambda_t^3}\ln(1-\frac{1}{\lambda_r\lambda_t^2}) + \frac{1}{\lambda_r\lambda_t^3} + \chi\frac{1}{\lambda_r\lambda_t^3}(\frac{2}{\lambda_r\lambda_t^2}-1)\right\} \\ &+ \frac{\mu_m^c}{v\lambda_r\lambda_t^3} + kT\sum_{a\neq m}\frac{c_a^0}{\lambda_r\lambda_t^3}\exp(\mu_a^c / kT)\end{aligned} \tag{3.106}$$

The force equilibrium thus requires

$$\frac{\partial S_r}{\partial r} + 2\frac{S_r - S_t}{r} = 0 \tag{3.107}$$

Specially, if the system is isotropic and homogeneous, $\lambda_r = \lambda_t = \lambda$ gives

$$\begin{aligned} S_r &= S_t = S \\ &= \frac{3}{2}\frac{\rho^{4/3} vkT}{b^2/\alpha}(3\lambda^2 - 1) + \frac{kT}{v}\left\{-\frac{2\rho v}{\lambda} + \frac{1}{\lambda^4}\ln(1-\frac{1}{\lambda^3}) + \frac{1}{\lambda^4} + \chi\frac{2-\lambda^3}{\lambda^7}\right\} \\ &+ \frac{\mu_m^c}{v\lambda^4} + kT\sum_{a\neq m}\frac{c_a^0}{\lambda^4}\exp(\mu_a^c/kT) \end{aligned} \tag{3.108}$$

The boundary condition for forces is given below, if the hydrogel is under the hydrostatic stress $P\boldsymbol{I}$,

$$S\,|_{r=R} = P \tag{3.109}$$

where R is the length of the one-dimensional domain, i.e., the radius of the spherical symmetrical system.

3.3.2. Temperature

By Equations (3.96) and the relation $\Phi = E - \eta T$, the bulk conservation of energy (3.42) reduce to the thermal conductivity equation as

$$C_v\dot{T} = K\nabla^2 T + q + \boldsymbol{S}\cdot\dot{\boldsymbol{F}} \tag{3.110}$$

which is automatically satisfied under constant temperature and zero heat supply.

By Equations (3.73), (3.97), and the relation $\varphi = E^{\mathscr{S}} - \eta^{\mathscr{S}} T$, the interfacial conservation of energy (3.43) reduces to

$$-E^{\mathscr{S}} KV - [E]V = -[\boldsymbol{h}] \cdot \boldsymbol{m} + q^{\mathscr{S}} - (\boldsymbol{m} \cdot [\boldsymbol{F}^T \boldsymbol{S}]\boldsymbol{m})V \tag{3.111}$$

By the above assumption for constant temperature and zero heat supply, we have $\boldsymbol{h} = \boldsymbol{0}$ and $q^{\mathscr{S}} = 0$. As a result Equation (3.111) may be further reduced to

$$[E - \lambda S] + \sigma K = 0 \tag{3.112}$$

which demonstrates the relation among the latent heat, the surface tension, and the total curvature at constant temperature.

3.3.3. Electrochemical potential

For evolving interface of the physical hydrogel, the mass conservation equations (3.75) and (3.76) reduce to the one-dimensional domain, given by

$$\frac{\partial}{\partial r}(r^2 \frac{\partial \mu_a}{\partial r}) = 0 \tag{3.113}$$

$$[c_a]V = -[M_a \frac{\partial \mu_a}{\partial r}] \tag{3.114}$$

The boundary condition due to the radial symmetry of μ_a is written as

$$\frac{\partial \mu_a}{\partial r}|_{r=0} = 0 \tag{3.115}$$

By Equations (3.113) and (3.115), the electrochemical potential is obtained in the form of

$$\mu_a = \begin{cases} u_a & 0 \le r \le w \\ U_a - \dfrac{w(U_a - u_a)}{R - w}\left(\dfrac{R}{r} - 1\right) & w \le r \le R \end{cases} \tag{3.116}$$

where U_a is the electrochemical potential of species a on the boundary, u_a is the electrochemical potential of species a on the interface, w is the coordinate of the interface in the radial direction, and thus $V = \dot{w}$. By Equations (3.114) and (3.116), the chemical potential on the interface is gotten in the form of

$$u_a = U_a + \frac{1}{M_a}[c_a]\dot{w}\frac{(R-w)w}{R} \tag{3.117}$$

3.3.4. Electric field

By the constitutive equation (3.69), and the bulk free energy density (3.96), and Equation (3.54), the electric potential ϕ, the scalar electric displacement D_r, and the scalar electric field $E_r = -\dfrac{\partial \phi}{\partial r}$ are associated via

$$D_r = \varepsilon E_r = -\varepsilon \frac{\partial \phi}{\partial r} \tag{3.118}$$

If only two species of ions of valences $+1$ and -1 are mobile in the gel and in the external solution, and no fixed charges are considered, the electrochemical potential of the two species are μ_+ and μ_-, respectively. As a result, Equations (3.53) and (3.55) thus reduce to

$$\dot{D}_r = -eM\left(\frac{\partial \mu_+}{\partial r} - \frac{\partial \mu_-}{\partial r}\right) \tag{3.119}$$

and

$$-\varepsilon \nabla^2 \phi = -\varepsilon \frac{\partial}{\partial r}\left(r^2 \frac{\partial \phi}{\partial r}\right) = Q = \sum_a e z_a c_a \tag{3.120}$$

respectively.

3.3.5. Crosslink density and the phase identification

At stable state, the crosslink density is determined by

$$\frac{\partial \Psi}{\partial \rho} = 0 \tag{3.121}$$

Therefore,

$$\rho^{1/3} = \frac{\frac{E_a}{kT} + 2\ln(\det \boldsymbol{F})}{2\frac{\nu\alpha}{b^2}(\det \boldsymbol{F})^{1/3}(\boldsymbol{F}_{ij}\boldsymbol{F}_{ij} - 3)} \tag{3.122}$$

If $\lambda_r = \lambda_t = \lambda$,

$$\rho^{1/3} = \frac{\frac{E_a}{6kT} + \ln \lambda}{\frac{\nu\alpha}{b^2}\lambda(\lambda^2 - 1)} \tag{3.123}$$

Inserting Equation (3.123) into Equation (3.108) gives

$$S\frac{v}{kT}=\frac{3}{2}\frac{b^6}{v^2\alpha^3}\frac{(3\lambda^2-1)}{\lambda^4(\lambda^2-1)^4}\left(\frac{E_a}{6kT}+\ln\lambda\right)^4-\frac{2b^6}{v^2\alpha^3}\frac{\left(\frac{E_a}{6kT}+\ln\lambda\right)^3}{\lambda^4(\lambda^2-1)^3}$$
$$+\frac{1}{\lambda^4}\ln\left(1-\frac{1}{\lambda^3}\right)+\frac{1}{\lambda^4}+\chi\frac{2-\lambda^3}{\lambda^7}+\frac{\mu_m^c}{kT\lambda^4}+\sum_{a\neq m}\frac{c_a^0 v}{\lambda^4}\exp(\mu_a^c/kT) \tag{3.124}$$

According to Equation (3.91), if the concentration c_a is homogenous in each phase, the stretch λ is also homogenous. As such, Equation (3.107) for force equilibrium reduces to

$$2kT\left\{\frac{\rho^{1/3}v}{b^2/\alpha}(3\lambda^2-1)-\frac{1}{\lambda}\right\}\frac{\partial\rho}{\partial r}+\frac{1}{v\lambda^4}\frac{\partial\mu_m^c}{\partial r}+\sum_{a\neq m}\frac{c_a^0}{\lambda^4}\exp(\mu_a^c/kT)\frac{\partial\mu_a^c}{\partial r}=0 \tag{3.125}$$

This equation (3.125) demonstrates the evolving relation between the crosslink density ρ and chemical potential μ_a^c in each phase during phase transition, with $\mu_a^c=\mu_a-\phi ez_a$.

3.3.6. Equilibrium states

At equilibrium state, there exists only one phase, and the derivatives with respect to time are zero. As a result, $\boldsymbol{j_a=0}$, $\boldsymbol{h=0}$, $V=0$, and ρ, c_a and λ are constants and determined entirely by the boundary conditions.

By Equations (3.109) and (3.124), the stretch may be determined via

$$S\frac{v}{kT}=P\frac{v}{kT}=\frac{3}{2}\frac{b^6}{v^2\alpha^3}\frac{(3\lambda^2-1)}{\lambda^4(\lambda^2-1)^4}\left(\frac{E_a}{6kT}+\ln\lambda\right)^4-\frac{2b^6}{v^2\alpha^3}\frac{\left(\frac{E_a}{6kT}+\ln\lambda\right)^3}{\lambda^4(\lambda^2-1)^3}$$
$$+\frac{1}{\lambda^4}\ln\left(1-\frac{1}{\lambda^3}\right)+\frac{1}{\lambda^4}+\chi\frac{2-\lambda^3}{\lambda^7}+\frac{U_m^c}{kT\lambda^4}+\sum_{a\neq m}\frac{c_a^0 v}{\lambda^4}\exp(U_a^c/kT) \tag{3.126}$$

where U_m^c and U_a^c are the chemical potentials of the monomer and species a on the boundary.

Consequently, by Equation (3.123), the crosslink density is given as

$$\rho^{1/3} = \frac{\frac{E_a}{6kT} + \ln\lambda}{\frac{v\alpha}{b^2}\lambda(\lambda^2 - 1)} \tag{3.127}$$

by Equations (3.69) and (3.96), c_m and c_a are thus given as

$$c_m = -\frac{\partial\Psi}{\partial\mu_m^c} = \frac{1}{v\det\boldsymbol{F}} = \frac{1}{v\lambda^3} \tag{3.128}$$

and

$$c_a = -\frac{\partial\Psi}{\partial\mu_a^c} = \frac{c_a^0}{\det\boldsymbol{F}}\exp(U_a^c/kT) = \frac{c_a^0}{\lambda^3}\exp(U_a^c/kT),\ (a \neq m) \tag{3.129}$$

respectively.

Additionally, the electric potential is also homogenous, namely

$$\phi = \phi|_{r=R} \tag{3.130}$$

As a result,

$$E_r = -\frac{\partial\phi}{\partial r} = 0\text{, and } D_r = \varepsilon E_r = 0 \tag{3.131}$$

3.3.7. Kinetic equation

By Equations (3.101), (3.108) and the condition $\lambda_r = \lambda_t = \lambda$, the evolution of the interface thus reduces to

$$-[\Psi]+[\lambda S]-\sigma K = -mV \tag{3.132}$$

So far the model has been reduced to one-dimensional domain, consisting of the reduced force equilibrium equation (3.125), the reduced electric displacement (3.118) and (3.119), and the reduced evolution equation (3.132), with the interfacial chemical potential (3.117). As consequence, the spherical symmetrical evolution of interface may be simulated numerically in one-dimensional domain for the physical hydrogel with solution-gel phase transition.

3.4. Numerical case studies and discussions

In this section, a MATLAB source code is developed, based on the reduced one-dimensional governing equations (3.107), (3.108), (3.110), (3.111), (3.116), (3.118), (3.119), and (3.132), and boundary conditions (3.109), (3.116), and (3.130), for simulation of spherical symmetrical evolution of interface of hydrogel with solution-gel phase transition. As case studies, the phase transitions of hydrogel are numerically simulated in water and in ionic solution respectively.

3.4.1. Phase transition of hydrogel in water

In this subsection, the phase transition of hydrogel in water is numerically simulated. When the hydrogel is in water, no ionic species exists, such that $z_a = 0$, $D_r = 0$, $\dot{D}_r = 0$, and $E_r = \frac{D_r}{\varepsilon} = -\frac{\partial \phi}{\partial r} = 0$. As a result, the relation $\mu_m^c = \mu_m - \phi e z_m$ reduces to $\mu_m^c = \mu_m$, and Equation (3.108) and (3.125) reduce to

$$\begin{aligned} S_r &= S_t = S \\ &= \frac{3}{2}\frac{\rho^{4/3} \nu kT}{b^2/\alpha}(3\lambda^2 - 1) + \frac{kT}{\nu}\left\{-\frac{2\rho\nu}{\lambda} + \frac{1}{\lambda^4}\ln(1-\frac{1}{\lambda^3}) + \frac{1}{\lambda^4} + \chi\frac{2-\lambda^3}{\lambda^7}\right\} + \frac{\mu_m}{\nu\lambda^4} \end{aligned} \quad (3.133)$$

and

$$2kT\left\{\frac{\rho^{1/3}\nu}{b^2/\alpha}(3\lambda^2 - 1) - \frac{1}{\lambda}\right\}\frac{\partial \rho}{\partial r} + \frac{1}{\nu\lambda^4}\frac{\partial \mu_m^c}{\partial r} = 0 \quad (3.134)$$

respectively.

By Equations (3.60) and (3.117), Equation (3.132) is rewritten in the form of

$$\dot{w} = \frac{-[\psi] + [\lambda S] - \sigma K + U[c]}{-m - \frac{1}{M}[c]^2 \frac{(R-w)w}{R}} \quad (3.135)$$

Based on Equations (3.116), (3.117), (3.133), (3.134), and (3.135), a MATLAB source code is developed for numerical simulation of phase transition of hydrogel in water. The inputs of parameters are given as follows. $E_a = 4\times10^{-23}\,\mathrm{J}$, $\alpha = 30$, $\nu = 10^{-28}\,\mathrm{m}^3$, a

constant room temperature $kT = 4\times10^{-21}\text{J}$, a constant interaction parameter $\chi = 1.1$, and the boundary conditions $P = 0$ and $U = 0$ for free swelling of the physical hydrogel.

In order to identify the phases of solution and gel in the stable state, a couple of the crosslink densities ρ subject to a stress S are required, where the smaller crosslink density corresponds to the solution phase, and the larger crosslink density to the gel phase. For this purpose, Fig. 3.2 is plotted by Equations (3.123), (3.124) and the boundary condition (3.109) for the relation between the crosslink density ρ and the stress S. It is observed from Fig. 3.2 that, for a given stress S, there always exist two values of the crosslink density ρ. In other words, of the two values of the crosslink density ρ, one corresponds to the solution phase and the other to the gel phase. It is also known from Fig. 3.2 that no numerical solution exists for the crosslink density ρ, if the stress S as a tension is very large (i.e. $S >> 0$). The peak value of the stress S corresponds to a critical state, where all the crosslinks are broken. On the other hand, if the stress S as a compression is very large (i.e. $S << 0$), namely when the system is subjected to large pressure ($P << 0$), a sole numerical solution exists and corresponds to a very large crosslink density ρ, indicating that large pressure results in the gel phase only. In addition, Fig. 3.3 is plotted by Equation (3.124) for the relation between the stretch λ and the stress S for free swelling. As discussed above, there exist the phases of solution and gel that are identified by the crosslink density ρ. The two phases corresponds to two different deformation states. This phenomenon is also verified by Fig. 3.3, where there always exist two values of the stretch λ accordingly for a given stress S.

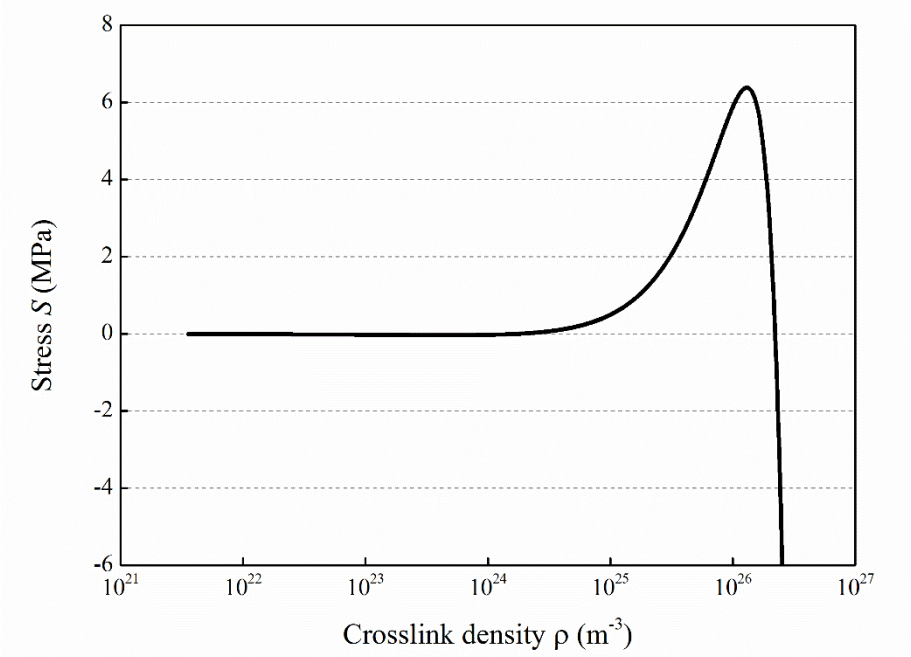

Fig. 3.2. Relation between the crosslink density ρ and stress S at a stable state

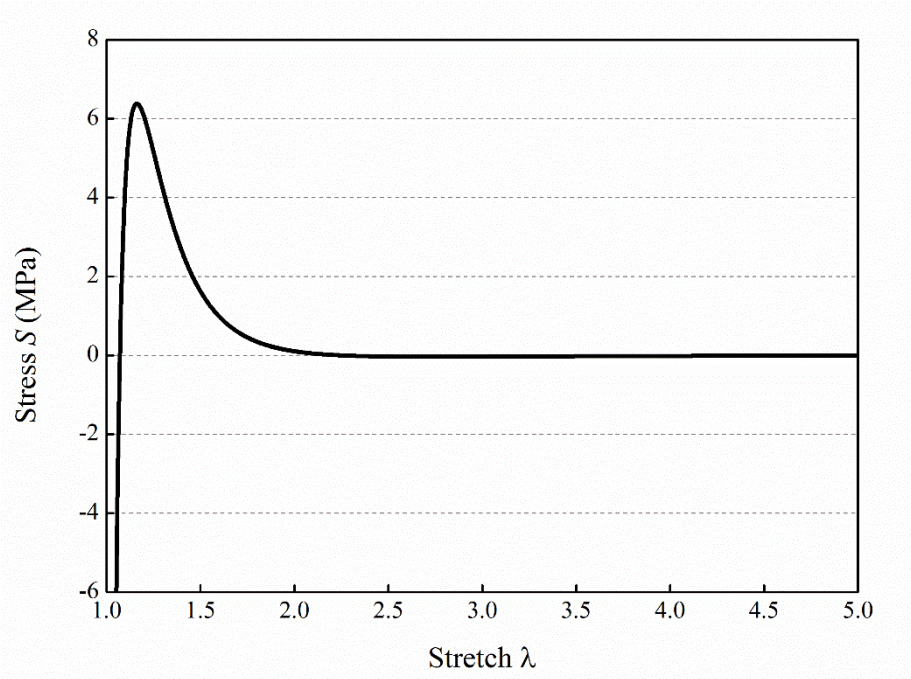

Fig. 3.3. Relation between the stretch λ and stress S at a stable state.

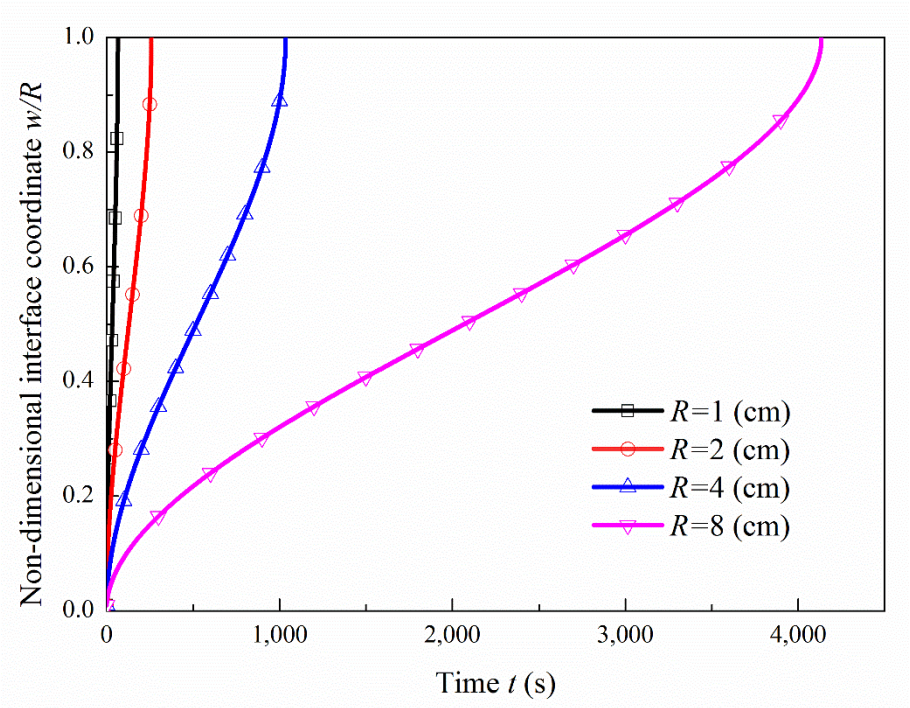

Fig. 3.4. Variation of non-dimensional interface coordinate w/R with time t for different domain sizes R.

Fig. 3.4 demonstrates the evolution of the interface during phase transition with different domain sizes $R = 1, 2, 4 \text{ and } 8\,\text{cm}$, where $m = 1000kT/v$, $\sigma = 10^{-5}kT/v$ and $M = 2.5\times10^{40}\,(\text{m}^3\cdot\text{s}/\text{Kg})$. In general, the phase transition from the solution to gel phase is triggered when a gel core is formed at $r = 0$ under certain environmental stimuli. Subsequently, the gel phase grows outward from the core to the boundary with the total curvature $K = -Div_{\mathcal{S}}\boldsymbol{m} = -2/(\lambda_\alpha s)$. It is found in Fig. 3.4 that the interface evolves from the center towards the boundary, since the gel phase with larger crosslink density is more favorable for the physical hydrogel subject to the boundary conditions $P = 0$ and $U = 0$, compared with the solution phase. It is also seen from Fig. 3.4 that the curve is steep at the beginning or when the interface approaches the boundary, indicating a fast phase transition near the center or the boundary.

Fig. 3.5 shows the effect of non-dimensional mobility $M^* = MvkT$ on the phase transition, where $m = 1000kT/v$, $R = 1\,\text{cm}$, and $\sigma = 0.001RkT/v$. It is observed that larger values of M^* result in the faster transition, which is consistent with the fact that the larger values of M^* result in the faster diffusion of polymer molecules.

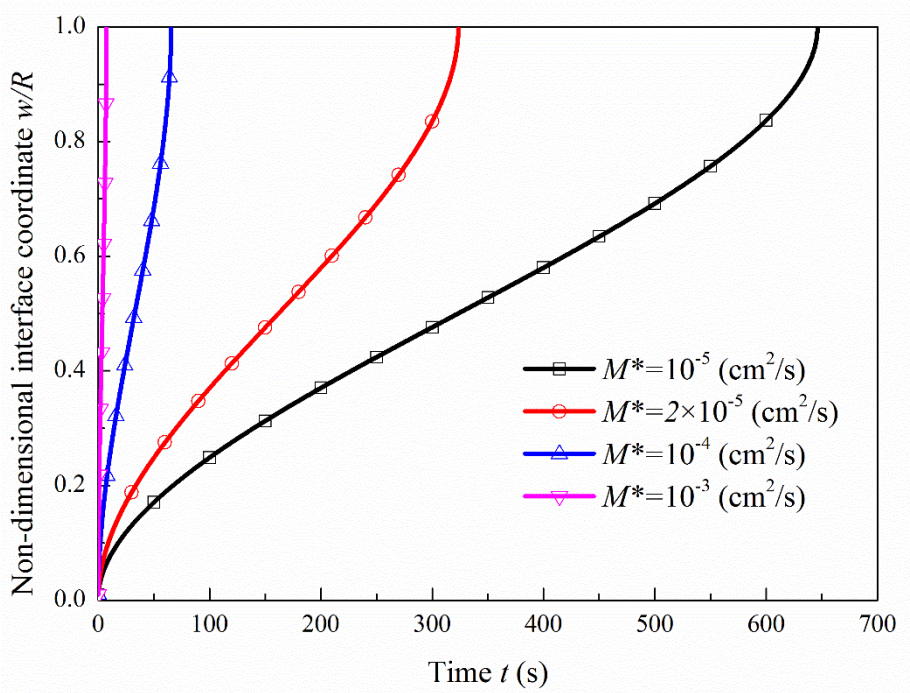

Fig. 3.5. Effect of the non-dimensional mobility $M^* = MvkT$ on the variation of the interface coordinate w with time t.

The influence of kinetic modulus m is also studied on the evolution of interface, as illustrated in Fig. 3.6, where $D = 10^{-4}\,\text{cm}^2/\text{s}$, $R = 1\,\text{cm}$, $\sigma = 0.01RkT/v$ and $m^* = mv/(kT)$. It is observed from Fig. 3.6 that, when m is very small, m has insignificant influence on the phase transition. If m becomes large, the phase transition takes a longer time.

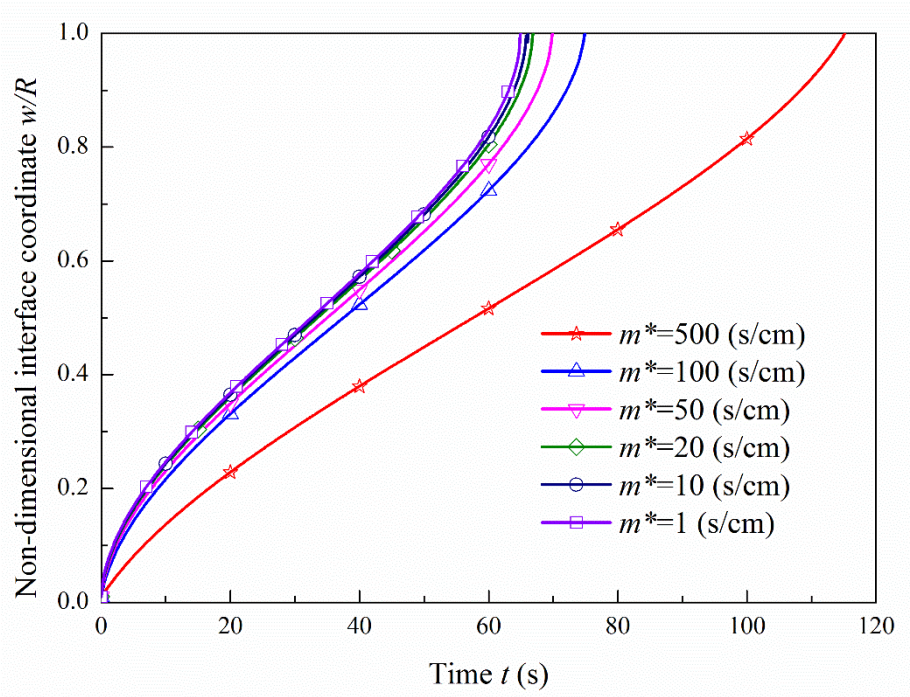

Fig. 3.6. Effect of the mobility $m^* = mv/kT$ on the variation of the interface coordinate w with time t.

As shown in Fig. 3.7, the surface tension σ has significant influence on the evolution of interface when $\sigma^* = \sigma v/(RkT)$ is large, where $m = 1000kT/v$, $D = 10^{-4}\,\mathrm{cm}^2/\mathrm{s}$, and $R = 1\,\mathrm{cm}$. It is demonstrated in Fig. 3.7 that the large surface tension slows the transition down, which is also a direct result of Equation (3.135).

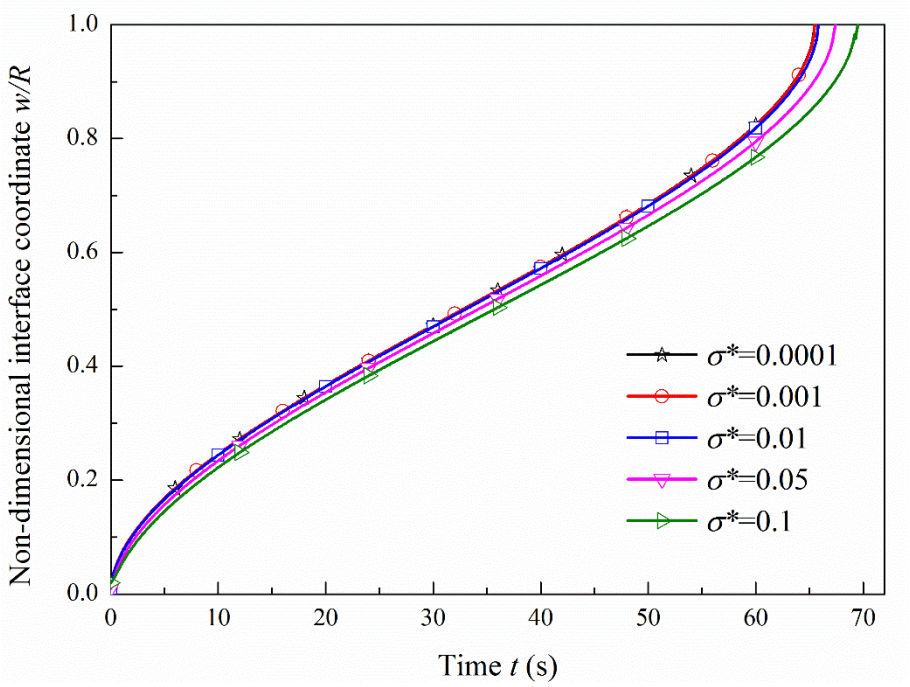

Fig. 3.7. Effect of the surface tension $\sigma^* = \sigma v / RkT$ on the variation of the interface coordinate w with time t.

3.4.2. Phase transition of hydrogel in ionic solution

In this subsection, the phase transition of hydrogel in ionic solution is numerically simulated. As mentioned above, the concentration of polymer is homogeneous in each phase during the phase transition, and determined by Equations (3.108), (3.109), and $u_a|_{r=R} = U_a$. Consequently, by Equations (3.93), (3.114), (3.116), the interfacial chemical potential u_a is obtained by solving the following equation

$$[\frac{c_a^0}{\det \boldsymbol{F}} e^{(u_a - \phi e z_a)/kT}]V = -M_a \frac{R(U_a - u_a)}{w(R-w)} \tag{3.136}$$

As a result, Equation (3.55) is reduced to

$$Div\boldsymbol{D} = Div(\varepsilon \boldsymbol{E}) = -\varepsilon \nabla^2 \phi = Q = \sum_a e z_a c_a = const \tag{3.137}$$

The electric potential is thus given as

$$\phi = \begin{cases} \phi_0 + \dfrac{Q_{out}}{\varepsilon} \ln R - \dfrac{w}{R} \cdot \dfrac{Q_{out}}{\varepsilon} \ln w & (0 \le r \le w) \\ \phi_0 + \dfrac{Q_{out}}{\varepsilon} \ln \dfrac{R}{r} + w\left(\dfrac{1}{r} - \dfrac{1}{R}\right) \dfrac{Q_{out}}{\varepsilon} \ln w & (w \le r \le R) \end{cases} \tag{3.138}$$

where Q_{out} is the total electric charge density in the outer phase, and is constant.

Based on Equations (3.136), (3.138), and Equations (3.108), (3.109), (3.116), (3.117), (3.125) and (3.132), a MATLAB source code is developed for numerical simulation of phase transition of hydrogel in ionic solution. The inputs of parameters are given as follows. $E_a = 4 \times 10^{-23}\text{J}$, $\alpha = 30$, $v = 10^{-28}\text{m}^3$, $\chi = 1.1$, $c_+^0 = c_-^0 = 10^{25}\text{m}^{-3}$, a constant room temperature $kT = 4 \times 10^{-21}\text{J}$, a constant non-dimensional kinetic modulus $m^* = mv/(kT) = 10^5$, and the boundary conditions $P = 0$, $U_a = 0$ and $\phi|_{r=R} = \phi_0 = 0.01kT/e$.

In order to demonstrate the evolution of the interface during the phase transition for different domain sizes, $R = 0.2\text{cm}$, $R = 0.4\text{cm}$, $R = 0.8\text{cm}$, and $R = 1\text{cm}$, Fig. 3.8 is plotted. It is found in Fig. 3.8 that the interface evolves from the center towards the boundary, indicating that the gel phase with larger crosslink density is more favorable for the physical hydrogel subject to the boundary conditions $P = 0$, $U_a = 0$ and $\phi|_{r=R} = \phi_0 = 0.01kT/e$, compared with the solution phase. It is also shown from Fig. 3.8

that the curve is steep at the beginning, indicating a fast phase transition when the interface is near the center.

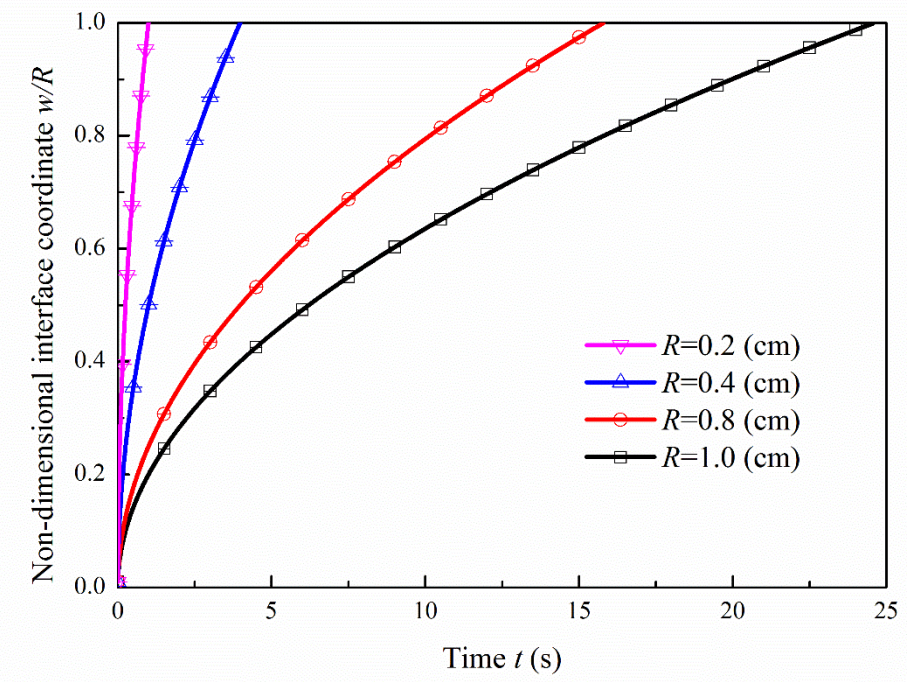

Fig. 3.8. Variation of non-dimensional interface coordinate w/R with time t for different domain sizes R.

Fig. 3.9 demonstrates the variation of interface electrochemical potential of monomers u_m with time t. It is found that the interface electrochemical potential u_m is smallest at the beginning, and increases when the gel phase grows outwards, and that the electrochemical potential u_m is always less than zero, the boundary condition. The profiles of the electrochemical potential of monomers μ_m are also plotted in Fig. 3.10 at different times $t = 0.1\,(\mathrm{s})$, $t = 1\,(\mathrm{s})$, $t = 5\,(\mathrm{s})$, $t = 10\,(\mathrm{s})$, $t = 15\,(\mathrm{s})$, $t = 20\,(\mathrm{s})$, and $t = t_f$, where t_f is the time cost for the evolution of interface to the boundary. It is found that the electrochemical potential μ_m is homogeneous in the gel phase ($r \le w$), and

varies with the coordinate in the solution phase ($r \geq w$), which is a direct result of Equation (3.116). Fig. 3.10 also shows that the electrochemical potential μ_m is homogeneous in the whole domain when the whole system is in the gel state, which also directly results from Equation (3.116).

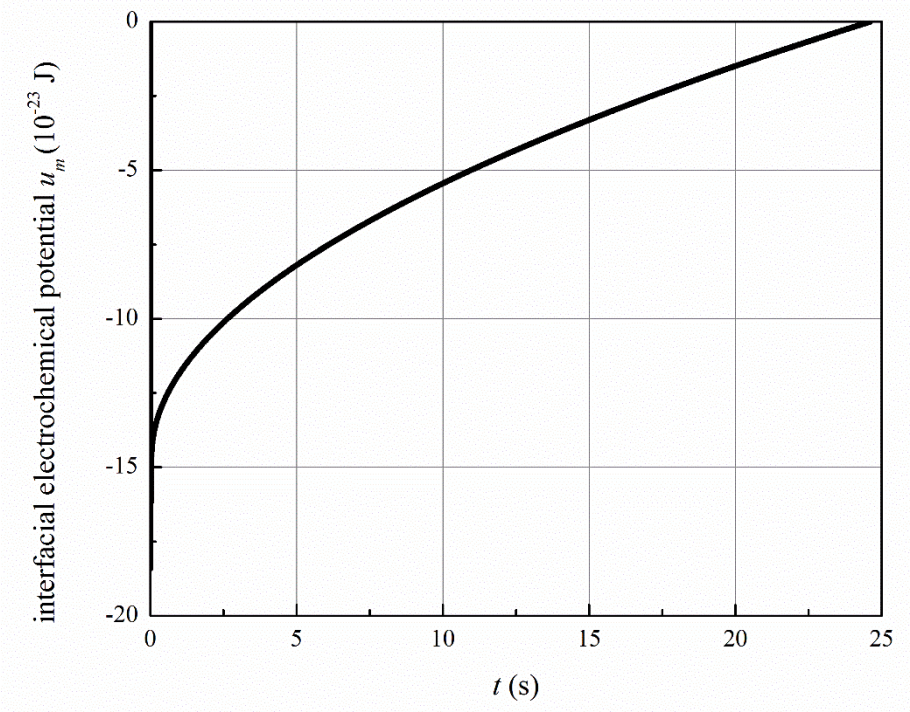

Fig. 3.9. Variation of interfacial electrochemical potential u_m with time t.

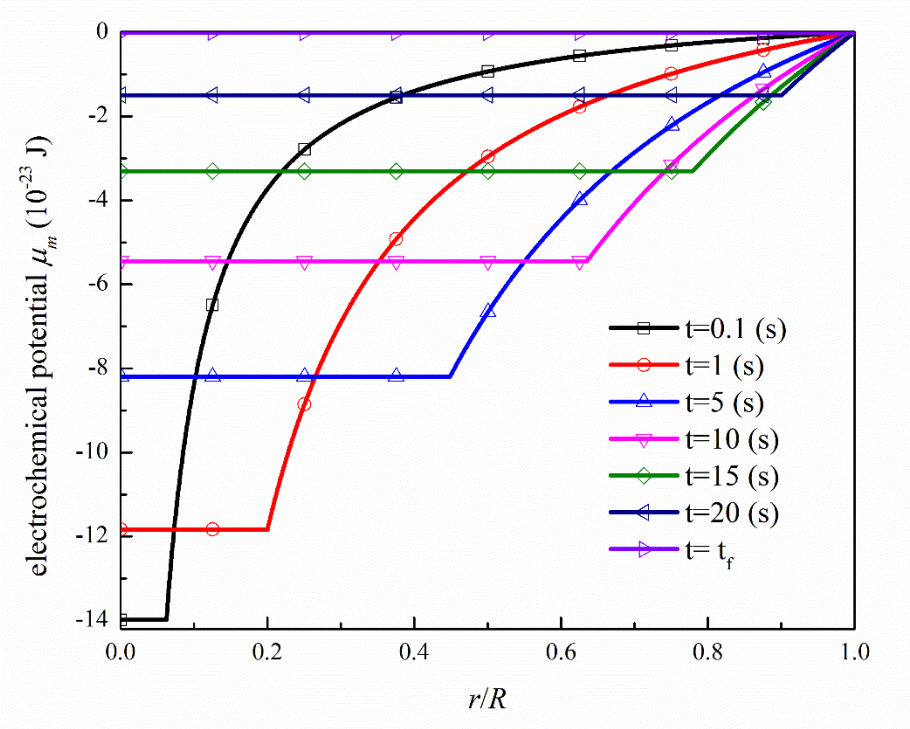

Fig. 3.10. Variation of the electrochemical potential μ_m with a non-dimensional coordinate r/R at different times.

The electrochemical potentials of the ionic species are also investigated, as shown in Fig. 3.11 and Fig. 3.12, which illustrate the variation of interface electrochemical potentials of ionic species u_+ and u_- with time t, respectively. It is shown that the interfacial electrochemical potentials increase when the interface evolves outwards, and reaches the boundary electrochemical potentials when the whole system transits into the gel phase. It is also found that the electrochemical potential of the cation u_+ is positive, while the electrochemical potential of the anion u_- is negative.

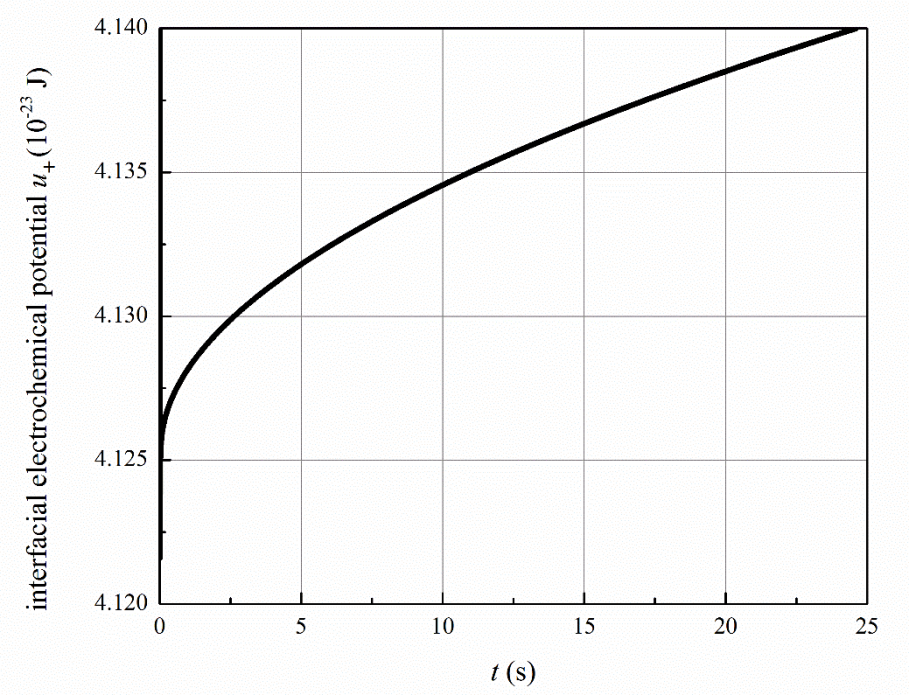

Fig. 3.11. Variation of interfacial electrochemical potential u_+ with time t.

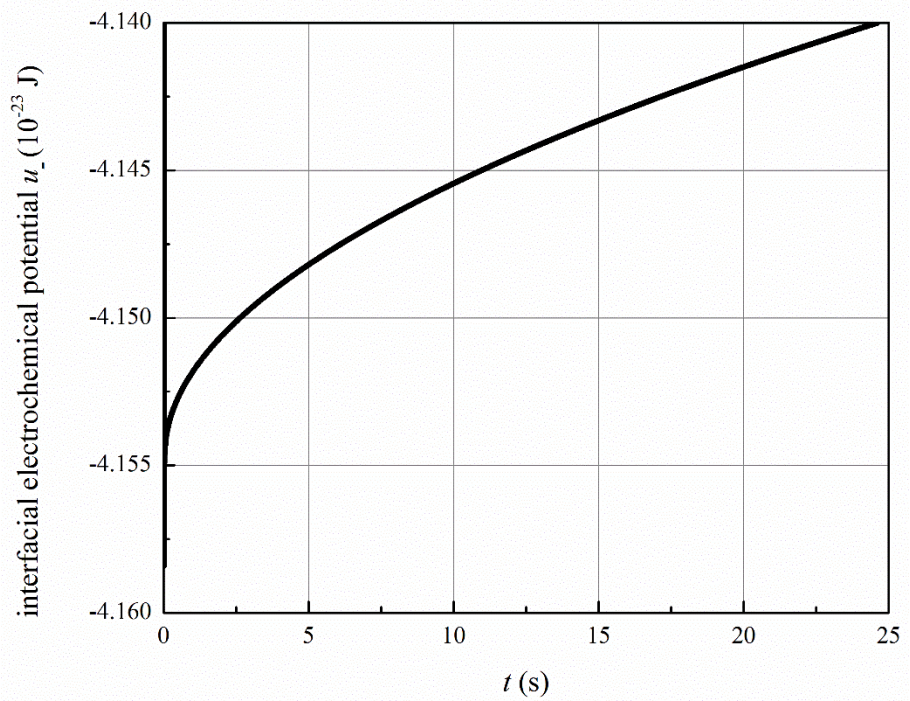

Fig. 3.12. Variation of interfacial electrochemical potential u_- with time t.

Additionally, the profiles of the electrochemical potential of the cations μ_+ at different times are plotted in Fig. 3.13, and the electrochemical potential of the anions μ_- at different times in Fig. 3.14. It is found that the electrochemical potentials are homogeneous in the gel phase ($r \le w$), and varies with the coordinate in the solution phase ($r \ge w$), which results directly from Equation (3.116).

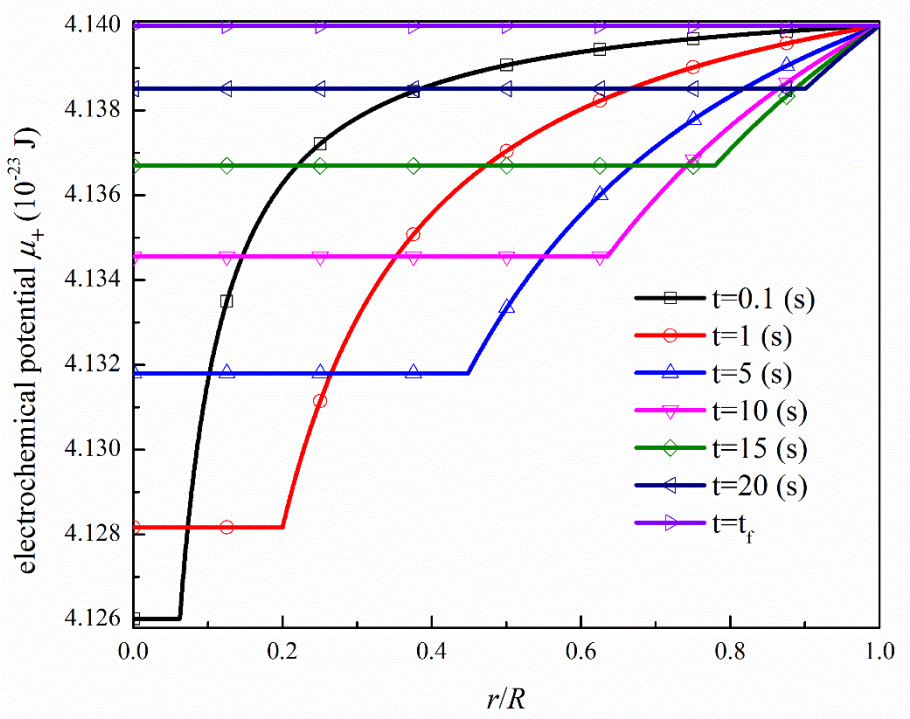

Fig. 3.13. Variation of the electrochemical potential μ_+ with a non-dimensional coordinate r/R at different times.

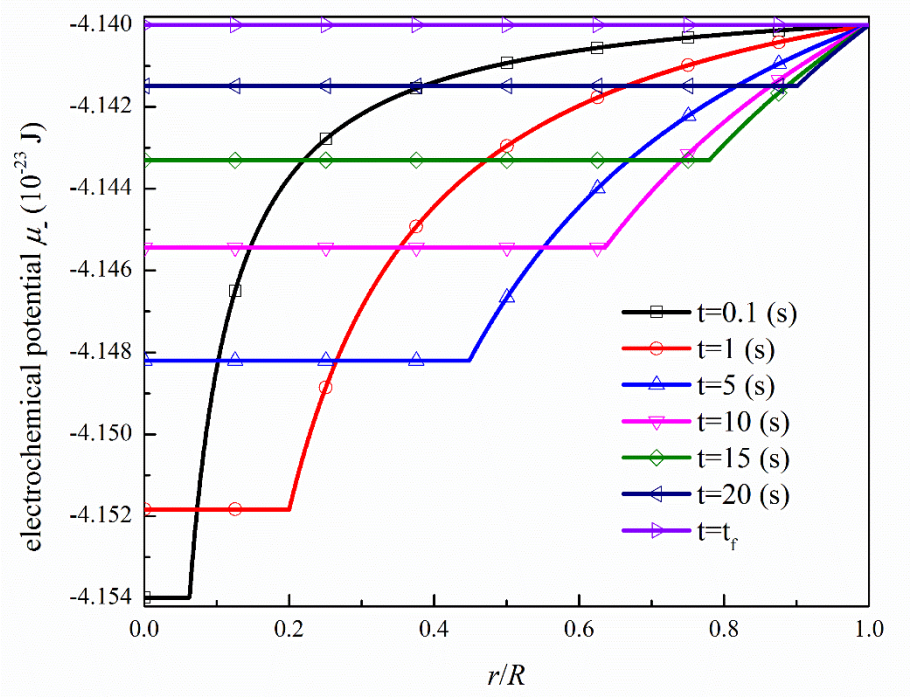

Fig. 3.14. Variation of the electrochemical potential μ_- with a non-dimensional coordinate r/R at different times.

3.5. Remarks

In this chapter, a multiphysics model has been developed for simulation of the interface evolution and characteristics for the physical hydrogel during solution-gel phase transition, which is based on a migrating control volume and couples the thermal, electrical, chemical and mechanical effects together. The present model includes the classical governing equations for mass and energy conservations, the force equilibrium equations for the two bulk phases and their interface, and additional equilibrium equations for a so-called configurational force imposed in the two bulk phases and on their interface for the effect of the solution-gel phase transition. Accordingly, the configurational heating and configurational mass supply are proposed for the change in entropy due to the migration of the control volume. Based on the second law of

thermodynamics, the constitutive equations are formulated, including an evolution equation for the interface.

A novel formulation of the free energy is proposed to characterize the solution-gel phase transition of the physical hydrogel, with consideration of the effects of crosslink density, in such a way that the solution phase is identified as a state where the crosslink density is very small, while the gel phase as the state where the crosslink density is very large. It can reduce to the non-equilibrium thermodynamic theory (Hong, Zhao et al. 2008, Hong, Liu et al. 2009, Hong, Zhao et al. 2010), if the interface is ignored when a single bulk phase exists only, i.e. no phase transition occurs. In other words, the theory proposed by Suo's group (Hong, Zhao et al. 2008, Hong, Liu et al. 2009, Hong, Zhao et al. 2010) is a special case of the present model.

For case studies, the spherical symmetrical solution-gel phase transition are numerically simulated respectively for analysis of the effect of diffusion coefficient in water and in ionic solution, surface tension and other parameters on the interface evolution and behavior during the solution-gel phase transition.

However, there are the following limitations in the presently developed model for simulation of the solution-gel phase transition of physical hydrogels with sharp interface/configurational forces.

- Since the model presented in this chapter is based on the sharp interface model, in which all the physical parameters suffer a sudden jump over the interface, the precise location of the interface is required in the whole time domain during the

numerical simulation. Although the present model is able to describe the interfacial evolution and surface properties, it is difficult to track the interfacial location for geometrically complex system.

- In the electric field, the present model considers only the limit of the concentrated solution, in which the fixed charges are negligible compared with the concentration of ions in the solution. However, in the limit of a dilute solution, the ions in the solution are fully compensated by the fixed charges. Therefore, the model needs to be further improved for the limit of a dilute solution.

Chapter 4. Development of a multiphysics model for hydrogel phase transition with diffuse interface

In Chapter 3, a multiphysics model is developed with the sharp interface/configurational forces, where all the physical parameters suffer a sudden jump over the interface. As a result, the precise location of the interface is required in the whole time domain during the numerical simulation. This is difficult to track for geometrically complex system. Therefore, a diffuse-interface model is developed in the present chapter to overcome the difficulty in tracking the interface. This chapter is organized as follows. A brief introduction is given in Section 4.1. After that, the three-dimensional model is formulated in Section 4.2, in which the crosslink density is employed as a novel thermodynamically-consistent order parameter, and a novel Ginzburg-Landau type of free energy is proposed. Section 4.3 presents the reduced one-dimensional model, and then the effects of the electrochemical potential, pressure and other boundary conditions on the phase transition are numerically analyzed in Section 4.4. Finally, the several conclusions are drawn in Section 4.4.2.

4.1. Introduction and assumptions

In this chapter, a thermo-electro-chemo-mechanical multiphysics model with the diffuse interface is developed for solution-gel phase transition of physical hydrogel, which couples the thermal, electrical, chemical and mechanical effects together. The present domain covers the gel and solution states that are considered as two distinct phases, and a diffuse interface between them, indicated by the density of crosslinks. As a result, the crosslink density is employed as a novel thermodynamically-consistent order parameter,

which is homogeneous in each distinct phase with smooth variation over the interface from one phase to another. Since all the parameters vary smoothly over the whole domain, the same constitutive equations are imposed on the two distinct phases as well as the interface. By the second law of thermodynamics, the constitutive equations are formulated. They include a novel Ginzburg-Landau type of free energy, which consists of the elastic, mixing, polarization and bonding contributions with the effect of crosslink density, as well as a gradient term of the crosslink density. The present governing equations account for the equilibrium of forces, the conservations of mass and energy, and an additional kinetic equation imposed for phase transition. As case studies, spherically symmetrical solution-gel phase transition of physical hydrogel is numerically simulated for analysis of the effect of electrochemical potential and pressure on the phase transition.

In order to develop the thermo-electro-chemo-mechanical multiphysics model with the diffuse interface for solution-gel phase transition of physical hydrogel, the assumptions are made below.

- The permittivity ε is constant.
- No heat supply exists.
- No chemical reaction occurs.
- No mass supply exists.
- The diffusion is much faster than the interface evolution.
- The mobility is isotropic and homogeneous, namely $\boldsymbol{M}_a = M_a \boldsymbol{I}$.

- The crosslinks are isotropically distributed in a diamond lattice at equilibrium state.
- All crosslinks are assumed in the same structure.
- The specific volume of a monomer unit is as the same as that of the solvent and the mobile ions.
- The specific heat capacity C_v is constant and independent of temperature.

4.2. Formulation of three-dimensional model

In this section, a three-dimensional diffuse interface model is developed, with the crosslink density as a novel thermodynamically-consistent order parameter.

4.2.1. Balance of force

According to nonlinear deformation theory (Gurtin 1981, Reddy 2007, Wang 2007), the deformation gradient can be defined as Equation (3.4), due to a material point at a place with coordinate $\boldsymbol{X} \in P$ moving to a new place $\boldsymbol{y} = \boldsymbol{y}(\boldsymbol{X}, t)$ at time t, namely $\boldsymbol{F} = \nabla \boldsymbol{y}$. The present force system consists of a deformation stress $\boldsymbol{S}$ and an external body force $\boldsymbol{b}$, such that the equilibrium of force and momentum is required by

$$\int_P \boldsymbol{S}\boldsymbol{n} da + \int_P \boldsymbol{b} dv = \boldsymbol{0} \tag{4.1}$$

and

$$\int_P \boldsymbol{y} \times \boldsymbol{S}\boldsymbol{n} da + \int_P \boldsymbol{y} \times \boldsymbol{b} dv = \boldsymbol{0} \tag{4.2}$$

By the divergence theorem, the local force is balanced by

$$Div\boldsymbol{S} + \boldsymbol{b} = \boldsymbol{0} \tag{4.3}$$

and

$$\boldsymbol{S}\boldsymbol{F}^T = \boldsymbol{F}\boldsymbol{S}^T \tag{4.4}$$

4.2.2. Conservation of mass

As mentioned above, due to the hydrogel being a mixture of polymeric network matrix and interstitial fluid, the conservation of mass is required by

$$\frac{d}{dt}\{\int_P c_a dv\} = -\int_{\partial P} \boldsymbol{j}_a \cdot \boldsymbol{n} da + \int_P r_a^b dv \tag{4.5}$$

where c_a is the number concentration of particles of species a, and $a = m$ for monomer, $\dot{j}_{\mathbb{I}}$ is the mass flux, and r_a^b is the external mass supply. As a result, the diffusion equation is in the form of

$$\dot{c}_a = -Div\boldsymbol{j}_a + r_a^b \tag{4.6}$$

4.2.3. Conservation of energy

In this subsection, the conservation of energy is formulated by the first law of thermodynamics. If the internal energy density is denoted as E, the total internal energy is expressed as

$$\int_P E dv \tag{4.7}$$

As required by the conservation of energy, the change of internal energy has to be equal to the sum of the heating and working, i.e.

$$\frac{d}{dt}\{\int_P E dv\} = -\int_P Div\boldsymbol{h} dv + \int_P q dv + W(P) \tag{4.8}$$

where q is the heat supply density, $\boldsymbol{h}$ the heat flux, and W the working in the form of

$$W = \int_P \boldsymbol{S}\boldsymbol{n} \cdot \dot{\boldsymbol{y}} da + \int_P \boldsymbol{b} \cdot \dot{\boldsymbol{y}} dv \tag{4.9}$$

where $\dot{\boldsymbol{y}}$ is the material velocity at each material point at time t.

By the divergence theorem and Equation (4.3), we have

$$W = \int_P \boldsymbol{S} \cdot \dot{\boldsymbol{F}} dv \tag{4.10}$$

As a result of Equation (4.8), the conservation of energy is given as

$$\dot{E} = -Div\boldsymbol{h} + q + \boldsymbol{S} \cdot \dot{\boldsymbol{F}} \tag{4.11}$$

4.2.4. Entropy subject to the second law of thermodynamics

In this subsection, the entropies subject to the second law of thermodynamics are formulated for the system.

4.2.4.1. Heating

The entropy change due to heating is given as

$$-\int_{\partial P}\frac{\boldsymbol{h}}{T}\cdot\boldsymbol{n}da+\int_{P}\frac{q}{T}dv \tag{4.12}$$

where T is the temperature.

By the divergence law, Equation (4.12) is rewritten as

$$-\int_{P}\frac{Div\boldsymbol{h}}{T}dv+\int_{P}\frac{\boldsymbol{h}\cdot\nabla T}{T^{2}}dv+\int_{P}\frac{q}{T}dv \tag{4.13}$$

4.2.4.2. Diffusion

The diffusion of particles into and out of P also contributes to the change in entropy, given as

$$\int_{\partial P}\frac{\mu_a\boldsymbol{j}_a}{T}\cdot\boldsymbol{n}da-\int_{P}\frac{\mu_a r_a^b}{T}dv \tag{4.14}$$

where μ_a is the electrochemical potential of species a, and $a=m$ for monomer.

By the divergence theorem, Equation (4.14) is written as

$$\int_{P}\frac{\mu_a Div\boldsymbol{j}_a}{T}dv+\int_{P}\frac{\boldsymbol{j}_a\cdot\nabla\mu_a}{T}dv-\int_{P}\frac{\mu_a\boldsymbol{j}_a\cdot\nabla T}{T^{2}}dv-\int_{P}\frac{\mu_a r_a^b}{T}dv \tag{4.15}$$

4.2.4.3. Electricity

Similarly, the electric field also contributes to the entropy change, given as

$$-\sum_a \left(\int_{\partial P} \frac{\phi e z_a \boldsymbol{j}_a}{T} \cdot \boldsymbol{n} da\right) + \sum_a \left(\int_P \frac{\phi e z_a r_a^b}{T} dv\right) \tag{4.16}$$

where e is the elementary charge, z_a is the valence of each species a, and $\phi = \phi(\boldsymbol{X}, t)$ is the electric potential relative to the ground.

By the divergence theorem, Equation (4.16) is written as

$$-\sum_a \left(\int_P \frac{e z_a \nabla\phi \cdot \boldsymbol{j}_a}{T} dv\right) - \sum_a \left(\int_P \frac{e z_a \phi Div \boldsymbol{j}_a}{T} dv\right) + \sum_a \left(\int_P \frac{e z_a \phi \nabla T \cdot \boldsymbol{j}_a}{T^2} dv\right) + \sum_a \left(\int_P \frac{\phi e z_a r_a^b}{T} dv\right)$$

(4.17)

Additionally, Equations (3.53) and (3.54) still hold for the present diffuse-interface model with neglecting magnetic effects (Wang, Wang et al. 1997), i.e.

$$\sum_a e z_a \boldsymbol{j}_a + \dot{\boldsymbol{D}} = 0 \tag{4.18}$$

where $\boldsymbol{D}$ is the electric displacement and is associated with the electric field $\boldsymbol{E} = -\nabla\phi$ via

$$\boldsymbol{D} = \varepsilon \boldsymbol{E} \tag{4.19}$$

where ε is the permittivity and is assumed to be constant in the whole system.

Therefore, Gauss' law is formulated as

$$Div\boldsymbol{D} = Div(\varepsilon \boldsymbol{E}) = Q = \sum_a ez_a c_a \tag{4.20}$$

where Q is the total electric charge density.

4.2.4.4. Application of the second law of thermodynamics

According to the second law of thermodynamics, the entropy of the whole system must not decrease i.e.

$$\begin{aligned}
&\frac{d}{dt}\{\int_P \eta dv\} \\
&\geq -\int_P \frac{Div\boldsymbol{h}}{T} dv + \int_P \frac{\boldsymbol{h}\cdot\nabla T}{T^2} dv + \int_P \frac{q}{T} dv \\
&\quad + \sum_a (\int_P \frac{\mu_a Div\boldsymbol{j}_a}{T} dv + \int_P \frac{\boldsymbol{j}_a\cdot\nabla\mu_a}{T} dv - \int_P \frac{\mu_a \boldsymbol{j}_a\cdot\nabla T}{T^2} dv - \int_P \frac{\mu_a r_a^b}{T} dv) \\
&\quad + \sum_a (-\int_P \frac{ez_a\nabla\phi\cdot\boldsymbol{j}_a}{T} dv - \int_P \frac{ez_a\phi Div\boldsymbol{j}_a}{T} dv + \int_P \frac{ez_a\phi\nabla T\cdot\boldsymbol{j}_a}{T^2} dv + \int_P \frac{\phi ez_a r_a^b}{T} dv)
\end{aligned} \tag{4.21}$$

As a result,

$$\begin{aligned}
T\dot{\eta} \geq & -Div\boldsymbol{h} + \frac{1}{T}\boldsymbol{h}\cdot\nabla T + q + \sum_a (\mu_a Div\boldsymbol{j}_a + \boldsymbol{j}_a\cdot\nabla\mu_a - \frac{1}{T}\mu_a\boldsymbol{j}_a\cdot\nabla T - \mu_a r_a^b) \\
& + \sum_a (-ez_a\nabla\phi\cdot\boldsymbol{j}_a - ez_a\phi Div\boldsymbol{j}_a + \frac{1}{T}ez_a\phi\nabla T\cdot\boldsymbol{j}_a + \phi ez_a r_a^b)
\end{aligned} \tag{4.22}$$

4.2.5. Constitutive equations

In this subsection, the constitutive equations are formulated based on the second law of thermodynamics.

According to thermodynamics, Helmholtz free energy density is given by $\Phi = E - \eta T$. By Equations (4.6), (4.11), (4.18), and (4.22), we have

$$\begin{aligned}\dot{\Phi} \le \boldsymbol{S}\cdot\dot{\boldsymbol{F}} - \eta\dot{T} - \nabla\phi\cdot\dot{\boldsymbol{D}} + \sum_a(\mu_a - ez_a\phi)\dot{c}_a - \frac{1}{T}\boldsymbol{h}\cdot\nabla T - \sum_a \boldsymbol{j}_a\cdot\nabla\mu_a \\ + \sum_a\left(\frac{\mu_a - \phi ez_a}{T}\boldsymbol{j}_a\cdot\nabla T\right)\end{aligned} \tag{4.23}$$

If $\Phi = \Phi(\boldsymbol{F}, c_a, T, \rho, \nabla\rho)$ is a function of the deformation gradient $\boldsymbol{F}$, number concentrations c_a, temperature T, crosslink density ρ and its gradient $\nabla\rho$, the constitutive equations are given as follows,

$$\mu_a - ez_a\phi = \frac{\partial\Phi}{\partial c_a}, \qquad \eta = -\frac{\partial\Phi}{\partial T}, \qquad -\nabla\phi = \frac{\partial\Phi}{\partial\boldsymbol{D}}, \quad \boldsymbol{S} = \frac{\partial\Phi}{\partial\boldsymbol{F}} \tag{4.24}$$

$$\boldsymbol{j}_a = -\boldsymbol{M}_a\nabla\mu_a, \qquad \boldsymbol{h} = -\boldsymbol{K}\nabla T \tag{4.25}$$

where $\boldsymbol{M}_a$ and $\boldsymbol{K}$ are the mobility and thermal conductivity, and both are positive-definite tensors.

Meanwhile, we also have the following two relations for an equilibrium state,

$$\frac{\partial\Phi}{\partial\rho} = 0 \text{ and } \frac{\partial\Phi}{\partial\nabla\rho} = 0 \tag{4.26}$$

In addition, a sufficient and necessary condition required by the second law of thermodynamics is imposed on the scalar thermal conductivity K, and scalar motility M_a as (Caginalp and Jones 1995)

$$KT - \frac{M_a}{4}(\mu_a - \phi e z_a)^2 \geq 0 \tag{4.27}$$

which is automatically satisfied when $\mu_a - \phi e z_a$ is sufficiently small.

If no mass supply exists, and when the molecules diffuse much faster than the phase transition with a constant mobility, i.e. $\boldsymbol{M}_a = M_a \boldsymbol{I}$ is very large, where the scalar mobility M_a is constant and associated with the diffusion coefficient D_a via $M_a = D_a/(kTv)$, the diffusion equation (4.6) reduces to

$$\nabla^2 \mu_a = 0 \tag{4.28}$$

Similarly, by the Legendre transformation, the free energy density is presented in the new form of $\Psi = \Phi - \sum_a \frac{\partial \Phi}{\partial c_a} c_a = \Phi - \sum_a (\mu_a - \phi e z_a) c_a$ (Gurtin and Voorhees 1993). Consequently, the inequality (4.27), is refined in the following form as

$$\begin{aligned} \dot{\Psi} \leq \boldsymbol{S} \cdot \dot{\boldsymbol{F}} - \eta \dot{T} - \sum_a (\dot{\mu}_a - \dot{\phi} e z_a) c_a - \nabla \phi \cdot \dot{\boldsymbol{D}} - \frac{1}{T} \boldsymbol{h} \cdot \nabla T - \sum_a (\boldsymbol{j}_a \cdot \nabla \mu_a) \\ + \sum_a \left(\frac{\mu_a - \phi e z_a}{T} \boldsymbol{j}_a \cdot \nabla T \right) \end{aligned} \tag{4.29}$$

If $\Psi = \Psi(\boldsymbol{F}, \mu_a^c, T, \rho, \nabla\rho)$ is a function of $\mu_a^c = \mu_a - \phi z_a$, T, $\boldsymbol{D}$ $\boldsymbol{F}$, ρ, and $\nabla\rho$, the constitutive equations (4.24) are refined as follows,

$$c_a = -\frac{\partial\Psi}{\partial\mu_a^c}, \quad \eta = -\frac{\partial\Psi}{\partial T}, \qquad -\nabla\phi = \frac{\partial\Psi}{\partial\boldsymbol{D}}, \quad \boldsymbol{S} = \frac{\partial\Psi}{\partial\boldsymbol{F}} \tag{4.30}$$

Equations (4.26) are refined as

$$\frac{\partial\Psi}{\partial\rho} = 0 \text{ and } \frac{\partial\Psi}{\partial\nabla\rho} = 0 \tag{4.31}$$

and the rest remain unchanged.

It is observed that the present constitutive equations (4.30) formulated by the second law of thermodynamics are in the same form as those deduced by Suo's group (Hong, Zhao et al. 2008, Hong, Liu et al. 2009, Hong, Zhao et al. 2010), and is a the same as the reduced constitutive equations derived in subsection 3.2.6 for a single-phase body. The identical constitutive equations (4.30) are imposed on the two distinct phases as well as the interface, since all the parameters vary smoothly over the whole domain.

4.2.6. Kinetic equation: Crosslink density as a thermodynamically consistent phase field parameter

Although there are several options for the order parameter, such as the volume fraction, or a simple numerical parameter, obviously the crosslink density ρ is a much more accurate parameter for characterizing the phases, compared with the other options, since the crosslink density ρ is directly associated with the elastic modulus. Definitely the

elastic modulus of the gel phase decreases as the crosslink density ρ lowers. If the crosslink density ρ lowers enough, or when certain amount of the crosslinks break, the hydrogel system transits into the solution phase, and then behave like a liquid. Therefore, the crosslink density ρ is a better candidate for the order parameter to characterize the system states and thus identify whether the gel/solution phase or interface occurs, for simulation of the solution-gel phase transition.

In addition, the number of the order parameters has to be determined according to the number of phases (Steinbach, Pezzolla et al. 1996, Tiaden, Nestler et al. 1998, Steinbach, Zhang et al. 2012). As well known, for the two-phase transition problem between the present gel and solution phases, only one order parameter can be required (Kobayashi 1993, McFadden, Wheeler et al. 1993, Kobayashi 1994, Hong and Wang 2013). In brief, taking the crosslink density ρ as the order parameter is one of the novelties in the present work, since the crosslink density ρ is a simple and crucial parameter without requirement of extra computational cost, especially it has significant advantage over other parameters such as the volume fraction.

It is found from Equations (4.26) and (4.31) that the derivatives of the free energy density with respect to ρ and $\nabla\rho$ have to be zero at an equilibrium state. However, when the system experiences a phase transition, the kinetics is governed by an Allen-Cahn equation regarding an order parameter and its gradient (Allen and Cahn 1979), which is defined as the crosslink density ρ. This novel thermodynamically-consistent order parameter is homogeneous in each distinct phase with smooth variation over the interface from one phase to another. Therefore, the kinetic equation is given as

$$\tau\dot{\rho} = -\frac{\delta\Psi}{\delta\rho} \tag{4.32}$$

where τ is constant and associated with the rate of relaxation to equilibrium.

4.2.7. Double-well free energy identified by crosslink density

In this subsection, a novel Ginzburg-Landau type of free energy is formulated and is shown in a double-well profile. As mentioned above in Subsection 3.2.7, the bulk free energy density is given by Equation (3.96). Additionally, in the present model, the interface also contributes to the free energy, and the interfacial energy Ψ_i is generally represented through the gradient term of the order parameter (Cahn and Hilliard 1958, Cahn 1961, Wheeler, Boettinger et al. 1992, Kobayashi 1993, McFadden, Wheeler et al. 1993, Wheeler, Boettinger et al. 1993). In the present formulation, as mentioned above, the crosslink density ρ is taken as the order parameter, such that the interfacial contribution to the free energy is given as

$$\Psi_i = \frac{\xi^2 kT}{2}(\nabla\rho)^2 \tag{4.33}$$

where $\xi > 0$ is a constant coefficient of the crosslink density gradient.

In summary, the total free energy density Ψ of the present diffuse-interface model is thus obtained by Equations (3.96) and (4.33) as

$$\Psi = \frac{\xi^2 kT}{2}(\nabla\rho)^2 + C_v T(1-\ln\frac{T}{T_M}) + \frac{3}{2}\frac{(\rho^4 \det \boldsymbol{F})^{1/3} \nu kT}{b^2/\alpha}(F_{ij}F_{ij}-3) - \rho E_a + \frac{D_i D_i}{2\varepsilon}$$
$$+ \frac{kT}{\nu}[-2\rho\nu\ln(\det \boldsymbol{F}) + (1-\frac{1}{\det \boldsymbol{F}})\ln(1-\frac{1}{\det \boldsymbol{F}}) + \chi\frac{1}{\det \boldsymbol{F}}(1-\frac{1}{\det \boldsymbol{F}})] \quad (4.34)$$
$$- \frac{\mu_m^c}{\nu \det \boldsymbol{F}} - kT\sum_{a\neq m}\frac{c_a^0}{\det \boldsymbol{F}}\exp(\mu_a^c/kT)$$

In particular, for a spherically symmetrical phase transition, the radial displacement $y(r)$ is only the deformation in a one-dimensional domain, such that the circumstantial stretch is given as

$$\lambda_t = y/r \quad (4.35)$$

and the radial stretch is in the form of

$$\lambda_r = dy/dr \quad (4.36)$$

Specially, if the system is isotropic and homogeneous, $\lambda_r = \lambda_t = \lambda$, and no ionic species exists, the free energy density (4.34) may be reformulated in a scalar form as

$$\Psi = \frac{\xi^2 kT}{2}(\nabla\rho)^2 + C_v T(1-\ln\frac{T}{T_M}) + \frac{9}{2}\frac{(\rho^4\lambda^3)^{1/3}\alpha\nu kT}{b^2}(\lambda^2-1)$$
$$+ \frac{kT}{\nu}\left\{-6\rho\nu\ln\lambda + (1-\frac{1}{\lambda^3})\ln(1-\frac{1}{\lambda^3}) + \chi\frac{1}{\lambda^3}(1-\frac{1}{\lambda^3})\right\} - \rho E_a - \frac{\mu_m}{\nu\lambda^3} \quad (4.37)$$

At equilibrium state, the crosslink density becomes homogeneous. Therefore, $\nabla\rho = 0$, and the crosslink density of the hydrogel determined by Equation (4.32) is given as

$$\frac{\partial\Psi}{\partial\rho} = 0 \quad (4.38)$$

As a consequence,

$$\rho^{1/3} = \frac{\frac{E_a}{6kT} + \ln\lambda}{\frac{\nu\alpha}{b^2}\lambda(\lambda^2 - 1)} \tag{4.39}$$

By Substituting Equation (4.39) into Equation (4.37), the free energy density at equilibrium state is given as

$$\begin{aligned}\Psi = {} & C_v T(1 - \ln\frac{T}{T_M}) + \frac{9}{2}\frac{\lambda\alpha\nu kT}{b^2}(\lambda^2 - 1)\left[\frac{(E_a + 6kT\ln\lambda)b^2}{6\alpha\nu kT\lambda(\lambda^2 - 1)}\right]^4 \\ & + \frac{kT}{\nu}\left\{-6\nu\ln\lambda\left[\frac{(E_a + 6kT\ln\lambda)b^2}{6\alpha\nu kT\lambda(\lambda^2 - 1)}\right]^3 + (1 - \frac{1}{\lambda^3})\ln(1 - \frac{1}{\lambda^3}) + \chi\frac{1}{\lambda^3}(1 - \frac{1}{\lambda^3})\right\} \\ & - E_a\left[\frac{(E_a + 6kT\ln\lambda)b^2}{6\alpha\nu kT\lambda(\lambda^2 - 1)}\right]^3 - \frac{\mu}{\nu\lambda^3}\end{aligned} \tag{4.40}$$

where $\mu_m = \mu$.

In order to illustrate the variation of the free energy density Ψ with the crosslink density $\rho^{1/3}$, Fig. 4.1 is plotted according to Equations (4.39) and (4.40) for $\mu^* = 0$, $\mu^* = -10$ and $\mu^* = -50$, where $\mu^* = \mu/(kT)$. The inputs of parameters include $\nu = 10^{-28}(\mathrm{m}^3)$, $b/\sqrt{\alpha} = \sqrt[3]{30\nu}(\mathrm{m})$, a constant room temperature $kT = 4\times10^{-21}(\mathrm{J})$, $E_a = 0.006kT(\mathrm{J})$, and a constant interaction parameter $\chi = 1.1$. It is shown that the free energy density Ψ becomes smaller when μ^* decreases. It is also demonstrated that Ψ is in a double-well profile, of which one lies between $\rho^{1/3} = 0(\mathrm{m}^{-1})$ and $\rho^{1/3} = 5\times10^{9}(\mathrm{m}^{-1})$, and the other near $\rho^{1/3} = 1.5\times10^{10}(\mathrm{m}^{-1})$. As mentioned above, there exist the solution and gel phases

and the interface between them, which are identified by the crosslink density ρ. In other words, of the two wells within the free energy density Ψ, the one with the smaller crosslink density ρ corresponds to the solution phase, and the other with the larger ρ to the gel phase. This phenomenon is also verified by Fig. 4.1.

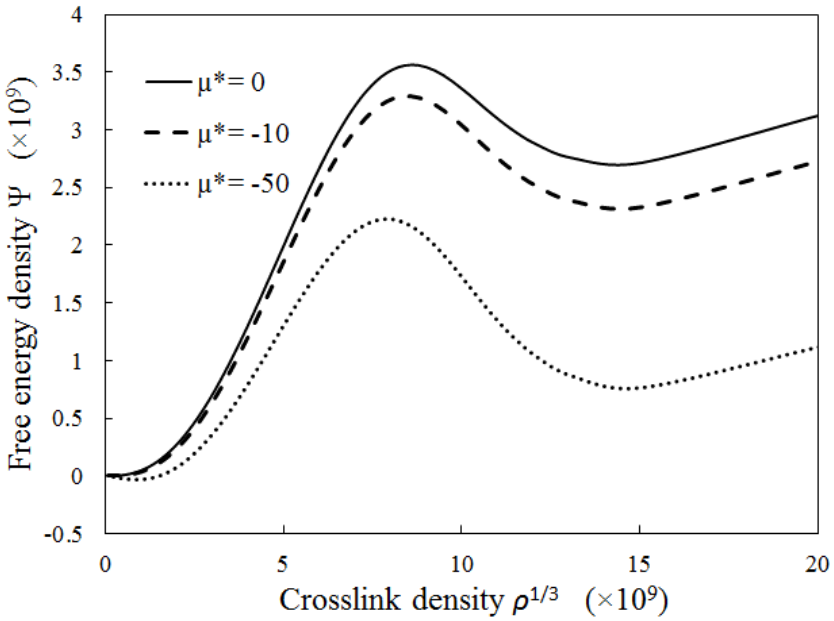

Fig. 4.1. Profile of the free-energy Ψ for a spherically symmetric homogeneous system on the variation of crosslink density ρ at different chemical potentials $\mu*$.

So far the formulation of the present model has been completed. It consists of the force equilibrium equations (4.3) and (4.4), the mass conservation equation (4.6), or its reduced form given by Equation (4.28) if the molecules diffuse much faster than the phase transition and no mass supply exists, the energy conservation equation (4.11), the Maxwell equations (4.18) and (4.20), and the kinetic equation (4.32). By the second law of thermodynamics, the constitutive equations (4.30) are given, and the mas and heat flux are presented by Equations (4.25). The present model also includes the free energy

density formulated by Equation (4.34). This model provides a platform for simulation of the phase transition of the physical hydrogel between the solution and gel phases.

4.3. Reduced one-dimensional model

In order to investigate the effect of pressure P, electrochemical potential μ_a and other boundary conditions on the phase transition of physical hydrogel between solution and gel phases, an one-dimensional reduction is performed on the present model.

4.3.1. Force

As mentioned above, during a spherically symmetrical phase transition, the deformation $y(r)$ exists in radial direction only, such that the radial and circumstantial stretches are given by Equations (4.35) and (4.36). As a result, by Equations (4.30) and (4.34), the stress $\boldsymbol{S}$ is explicitly given as

$$\begin{aligned}\boldsymbol{S} = \frac{\partial \Psi}{\partial \boldsymbol{F}} = \frac{3}{2}\frac{\rho^{4/3} \nu k T}{b^2/\alpha}\left\{\frac{(\boldsymbol{F}_{ij}\boldsymbol{F}_{ij}-3)\boldsymbol{F}^{-T}(\det \boldsymbol{F})^{1/3}}{3} + 2\boldsymbol{F}(\det \boldsymbol{F})^{1/3}\right\} \\ + \frac{kT}{\nu}\left\{-2\rho\nu\boldsymbol{F}^{-T} + \frac{\boldsymbol{F}^{-T}}{\det \boldsymbol{F}}\ln(1-\frac{1}{\det \boldsymbol{F}}) + \frac{\boldsymbol{F}^{-T}}{\det \boldsymbol{F}} + \chi\frac{\boldsymbol{F}^{-T}}{\det \boldsymbol{F}}(\frac{2}{\det \boldsymbol{F}}-1)\right\} \\ + \frac{\mu_m^c \boldsymbol{F}^{-T}}{\nu \det \boldsymbol{F}} + kT\sum_{a\neq m}\frac{c_a^0 \boldsymbol{F}^{-T}}{\det \boldsymbol{F}}\exp(\mu_a^c/kT)\end{aligned} \quad (4.41)$$

in which the radial and tangent components are given respectively as,

$$S_r = \frac{3}{2}\frac{\rho^{4/3}\nu kT}{b^2/\alpha}\left\{\frac{(\lambda_r^2+2\lambda_t^2-3)(\lambda_r\lambda_t^2)^{1/3}}{3\lambda_r}+2\lambda_r(\lambda_r\lambda_t^2)^{1/3}\right\}$$
$$+\frac{kT}{\nu}\left\{-\frac{2\rho\nu}{\lambda_r}+\frac{1}{\lambda_r^2\lambda_t^2}\ln(1-\frac{1}{\lambda_r\lambda_t^2})+\frac{1}{\lambda_r^2\lambda_t^2}+\chi\frac{1}{\lambda_r^2\lambda_t^2}(\frac{2}{\lambda_r\lambda_t^2}-1)\right\} \quad (4.42)$$
$$+\frac{\mu_m^c}{\nu\lambda_r^2\lambda_t^2}+kT\sum_{a\neq m}\frac{c_a^0}{\lambda_r^2\lambda_t^2}\exp(\mu_a^c/kT)$$

$$S_t = \frac{3}{2}\frac{\rho^{4/3}\nu kT}{b^2/\alpha}\left\{\frac{(\lambda_r^2+2\lambda_t^2-3)(\lambda_r\lambda_t^2)^{1/3}}{3\lambda_t}+2\lambda_t(\lambda_r\lambda_t^2)^{1/3}\right\}$$
$$+\frac{kT}{\nu}\left\{-\frac{2\rho\nu}{\lambda_t}+\frac{1}{\lambda_r\lambda_t^3}\ln(1-\frac{1}{\lambda_r\lambda_t^2})+\frac{1}{\lambda_r\lambda_t^3}+\chi\frac{1}{\lambda_r\lambda_t^3}(\frac{2}{\lambda_r\lambda_t^2}-1)\right\} \quad (4.43)$$
$$+\frac{\mu_m^c}{\nu\lambda_r\lambda_t^3}+kT\sum_{a\neq m}\frac{c_a^0}{\lambda_r\lambda_t^3}\exp(\mu_a^c/kT)$$

The force equilibrium thus reduces to

$$\frac{\partial S_r}{\partial r}+2\frac{S_r-S_t}{r}=0 \quad (4.44)$$

In particular, for an isotropic and homogeneous system, namely $\lambda_r=\lambda_t=\lambda$,

$$S_r=S_t=S=\frac{3}{2}\frac{\rho^{4/3}\alpha\nu kT}{b^2}(3\lambda^2-1)+\frac{kT}{\nu}\left\{-\frac{2\rho\nu}{\lambda}+\frac{1}{\lambda^4}\ln(1-\frac{1}{\lambda^3})+\frac{1}{\lambda^4}+\chi\frac{2-\lambda^3}{\lambda^7}\right\} \quad (4.45)$$
$$+\frac{\mu_m^c}{\nu\lambda^4}+kT\sum_{a\neq m}\frac{c_a^0}{\lambda^4}\exp(\mu_a^c/kT)$$

and

$$\frac{\partial S_r}{\partial r}=0 \quad (4.46)$$

If the hydrogel is under the hydrostatic stress $P\boldsymbol{I}$, the boundary condition is imposed as

$$S\,|_{r=R} = P \tag{4.47}$$

where R is the radius of the spherical symmetrical system, i.e. the dimension of the one-dimensional domain.

4.3.2. Temperature

By Equations (4.34) and the relation $\Phi = E - \eta T$, the conservation of energy (4.11) reduces to the thermal conductivity equation as

$$C_v \dot{T} = K\nabla^2 T + q + \boldsymbol{S}\cdot\dot{\boldsymbol{F}} \tag{4.48}$$

which is automatically satisfied under constant temperature and zero heat supply.

4.3.3. Electrochemical potential

For the one-dimensional phase transition of the physical hydrogel, the mass conservation equation (4.28) is reduced, given by

$$\frac{\partial}{\partial r}(r^2 \frac{\partial \mu_a}{\partial r}) = 0 \tag{4.49}$$

The radial symmetry of μ_a requires

$$\frac{\partial \mu_a}{\partial r}|_{r=0} = 0 \tag{4.50}$$

The boundary condition on the border of the domain is given as

$$\mu_a|_{r=R} = U_a \tag{4.51}$$

where U_a is the electrochemical potential on the boundary.

Based on the symmetry condition (4.50), and the boundary condition (4.51), Equation (4.49) may be solved analytically, depending on the interface position. For simplicity, we take the homogeneous polymeric electrochemical potential for the system in the whole domain, namely,

$$\mu_m = U_m \tag{4.52}$$

As a result, $\dot{c}_m = 0$, and by the incompressibility condition (3.91), $\dot{\boldsymbol{F}} = 0$.

4.3.4. Electric field

By the constitutive equation (4.30), and the free energy density (4.34), and Equation (4.19), the electric potential ϕ, the scalar electric displacement D_r, and the scalar electric field $E_r = -\dfrac{\partial \phi}{\partial r}$ are associated via

$$D_r = \varepsilon E_r = -\varepsilon \frac{\partial \phi}{\partial r} \tag{4.53}$$

If only two species of ions of valences $+1$ and -1 are mobile in the gel and in the external solution, and no fixed charges are considered, the electrochemical potential of

the two species are μ_+ and μ_-, respectively. Consequently, Equation (4.18) and (4.22) reduce to

$$\dot{D}_r = -eM\left(\frac{\partial \mu_+}{\partial r} - \frac{\partial \mu_-}{\partial r}\right) \tag{4.54}$$

and

$$-\varepsilon \nabla^2 \phi = -\varepsilon \frac{\partial}{\partial r}\left(r^2 \frac{\partial \phi}{\partial r}\right) = Q = \sum_a e z_a c_a \tag{4.55}$$

The electric boundary condition is given as

$$\phi|_{r=R} = \phi_0 \tag{4.56}$$

where ϕ_0 is the electric potential on the boundary.

4.3.5. Kinetic equation

In the one-dimensional domain, the kinetic Equation (4.32) is reduced to

$$\tau \dot{\rho} = -\frac{\delta \Psi}{\delta \rho} = \xi^2 kT \nabla^2 \rho - 6\frac{\rho^{1/3} \alpha v k T}{b^2} \lambda(\lambda^2 - 1) + 6kT \ln \lambda + E_a \tag{4.57}$$

So far the reduction of the present model into one-dimensional domain has been completed. It consists of the reduced force equilibrium equation (4.44), the reduced Maxwell equation (4.55), and the reduced kinetic equation (4.57) with the homogeneous electrochemical potential (4.52). In the following subsection, the phase transition for the

physical hydrogel is numerically simulated in the spherically symmetrical domain, for investigation of the influence of the pressure P, the electrochemical potential μ_a and other boundary conditions on the phase transition between solution and gel phases.

4.4. Numerical case studies and discussions

In this section, a MATLAB source code is developed based on the reduced one-dimensional governing equations (4.46), (4.48), (4.49), (4.55), and (4.57), and boundary conditions (4.47) and (4.51), for simulation of spherical symmetrical evolution of interface of hydrogel with solution-gel phase transition. As case studies, the phase transitions of hydrogel are numerically simulated in water and in ionic solution respectively.

4.4.1. Phase transition of hydrogel in water

In this subsection, the phase transition of hydrogel in water is numerically simulated. When the hydrogel is in water, no ionic species exists, such that $z_a = 0$, $D_r = 0$, $\dot{D}_r = 0$, and $E_r = \frac{D_r}{\varepsilon} = -\frac{\partial \phi}{\partial r} = 0$. As a result, the relation $\mu_m^c = \mu_m - \phi e z_m$ reduces to $\mu_m^c = \mu_m = \mu$, and Equation (4.44) and (4.45) reduce to

$$S_r = S_t = S = \frac{3}{2}\frac{\rho^{4/3} vkT}{b^2/\alpha}(3\lambda^2 - 1) + \frac{kT}{v}\left\{-\frac{2\rho v}{\lambda} + \frac{1}{\lambda^4}\ln(1 - \frac{1}{\lambda^3}) + \frac{1}{\lambda^4} + \chi\frac{2-\lambda^3}{\lambda^7}\right\} + \frac{\mu}{v\lambda^4} \quad (4.58)$$

and

$$\frac{\partial\lambda}{\partial r}\left\{9\frac{\rho^{4/3}vkT}{b^2/\alpha}\lambda+\frac{kT}{v}\left[\frac{2\rho v}{\lambda^2}-\frac{4}{\lambda^5}\ln(1-\frac{1}{\lambda^3})+\frac{3}{\lambda^5(\lambda^3-1)}-\frac{4}{\lambda^5}+\chi(-\frac{14}{\lambda^8}+\frac{4}{\lambda^5})\right]-\frac{4\mu}{v\lambda^5}\right\} \quad (4.59)$$
$$+\frac{\partial\rho}{\partial r}\left\{2\frac{\rho^{1/3}vkT}{b^2/\alpha}(3\lambda^2-1)-\frac{2kT}{\lambda}\right\}=0$$

respectively.

In the present case study for numerical simulation of the spherically symmetrical phase transition of physical hydrogel in water, the inputs of parameters are required, as given by $v=10^{-28}(\mathrm{m}^3)$, $\alpha=30$, a constant room temperature $kT=4\times10^{-21}(\mathrm{J})$, $E_a=0.06kT$, $\tau=0.5\times10^{-13}(\mathrm{s})$, and a constant interaction parameter $\chi=1.1$. As discussed above, the values of crosslink density ρ for the two phases are calculated via the boundary conditions (4.47) and (4.52), and the crosslink density ρ varies smoothly over the interface. As well known, for solving a nonlinear system, an initial estimate is generally required for numerical iteration process. Furthermore, it is commonly understood that the actual profile of the interface should only have negligible effect on the numerical simulation (Steinbach, Zhang et al. 2012). Therefore, a gel core associated with an initial linear interface profile with finite width is assigned as initial estimates for numerical solution of the present nonlinear system (Cahn and Hilliard 1958, Langer and Sekerka 1975).

In order to simulate the solution-gel phase transition of physical hydrogel in the spherically symmetric domain, a MATLAB source code is developed, based on the governing equations (4.59) (4.52) and (4.57), and the boundary conditions (4.47) and (4.51).

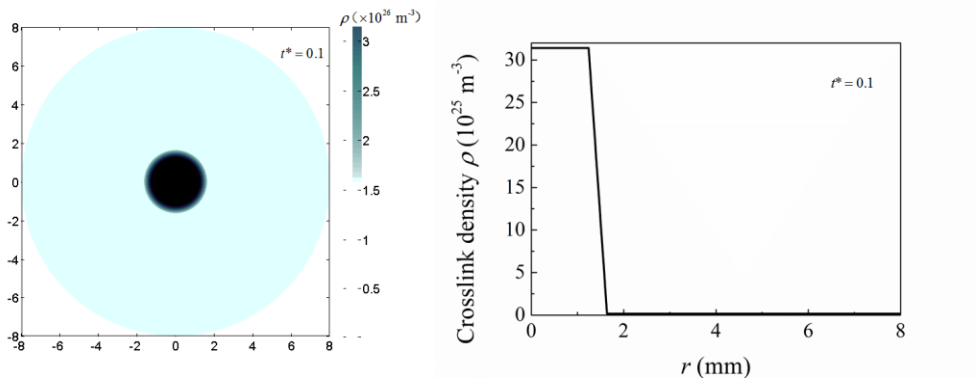
ρ (×10^26 m^-3)
t* = 0.1
Crosslink density ρ (10^25 m^-3)
r (mm)

(a)

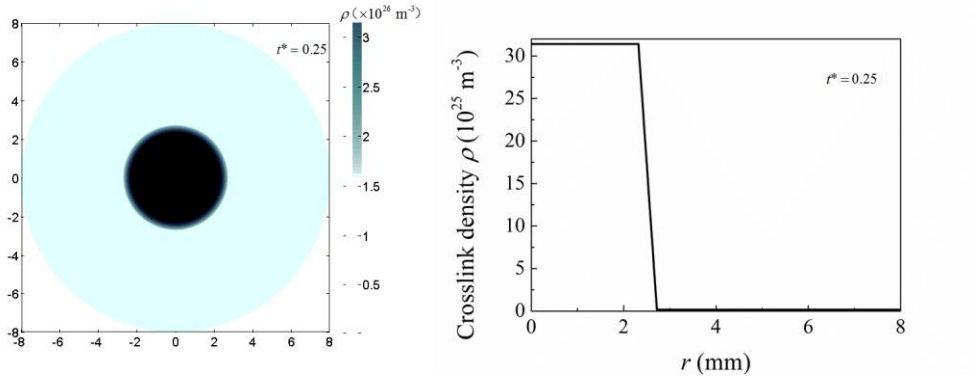
ρ (×10^26 m^-3)
t* = 0.25
Crosslink density ρ (10^25 m^-3)
r (mm)

(b)

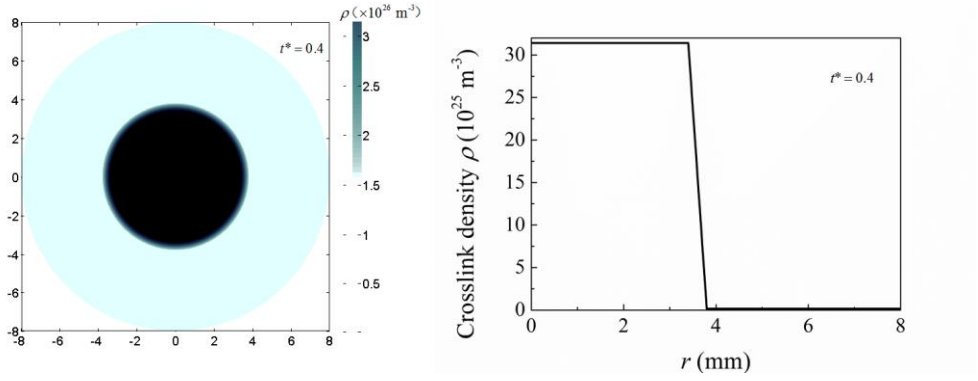
ρ (×10^26 m^-3)
t* = 0.4
Crosslink density ρ (10^25 m^-3)
r (mm)

(c)

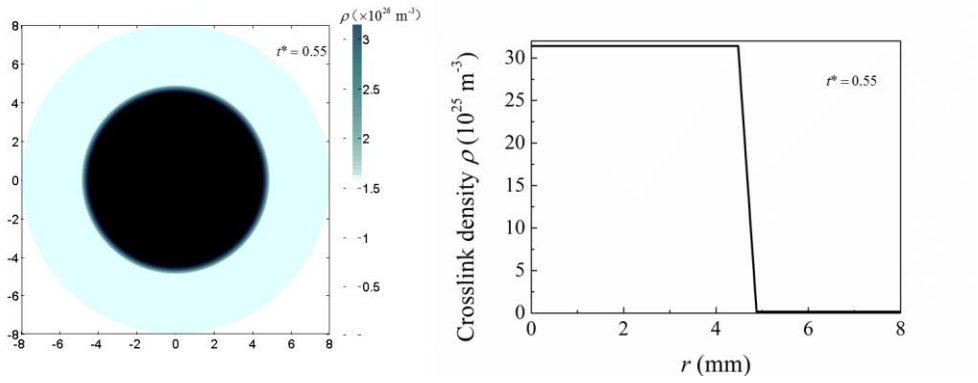
ρ (×10^26 m^-3)
t* = 0.55
Crosslink density ρ (10^25 m^-3)
r (mm)

(d)

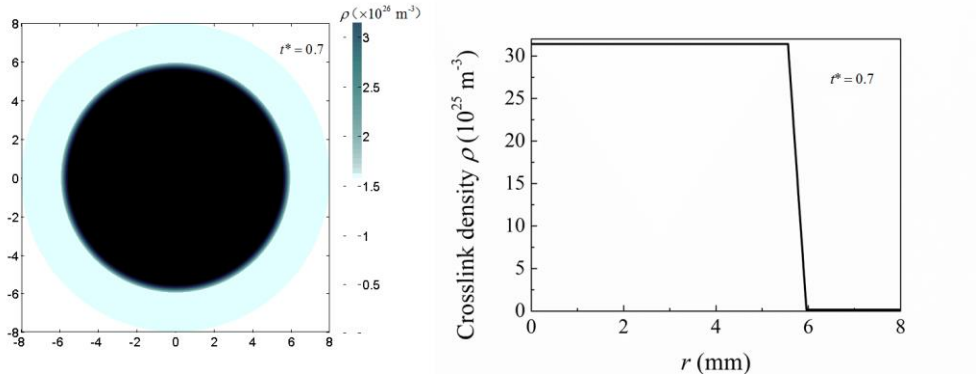
ρ (×10^26 m^-3)
t* = 0.7
Crosslink density ρ (10^25 m^-3)
r (mm)

(e)

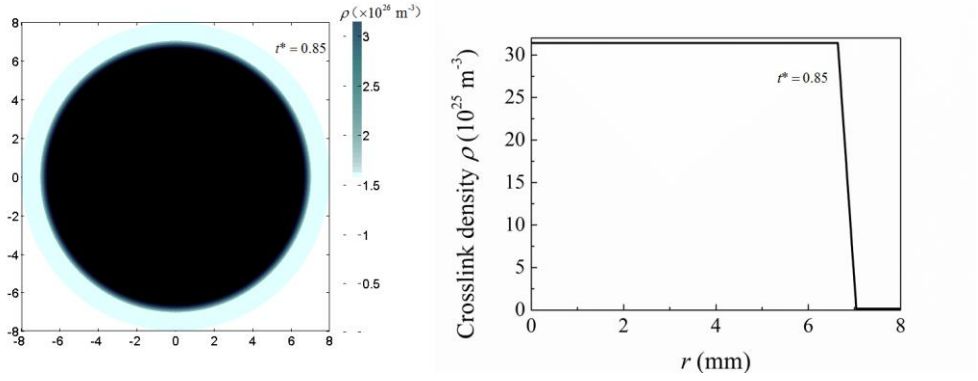
ρ (×10^26 m^-3)
t* = 0.85
Crosslink density ρ (10^25 m^-3)
r (mm)

(f)

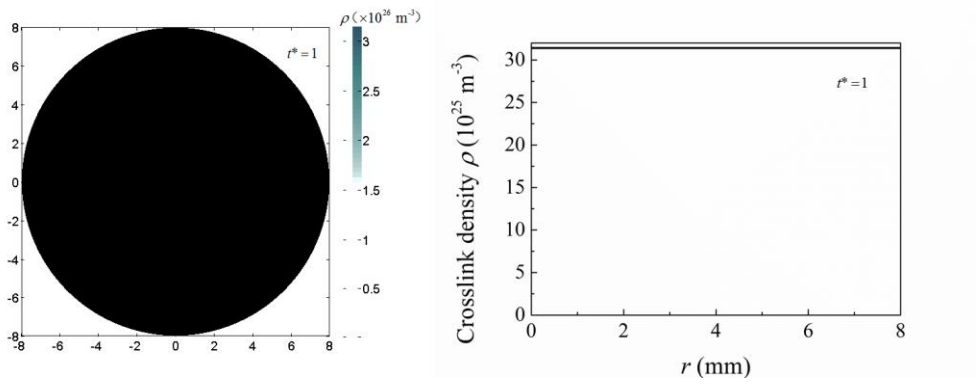

(g)

Fig. 4.2. Several snapshots of the evolution progress of the crosslink density ρ associated with the corresponding crosslink density profile at different non-dimensional times: $t^* = 0.1$ (a), $t^* = 0.25$ (b), $t^* = 0.4$ (c), $t^* = 0.55$ (d), $t^* = 0.7$ (e), $t^* = 0.85$ (f), and $t^* = 1$ (g).

In order to investigate the interface evolution of physical hydrogel with time, the several snapshots of the numerically simulated region are captured at different non-dimensional times $t^* = t / t_T$ associated with the corresponding profiles of the crosslink density ρ, as illustrated in Fig. 4.2, where $\xi = 1(\mathrm{m/J^{1/2}})$, $R = 8\,(\mathrm{mm})$, $\mu^* = \mu/(kT) = 0$, $P = 0\,(\mathrm{Pa})$, and t_T is the total time to fulfill phase transition. According to Equations (4.47) and (4.51), the crosslink density subject to the present boundary condition is given as $\rho_{gel} = 3.1416 \times 10^{26}\,(\mathrm{m^{-3}})$ in the gel phase, and $\rho_{solution} = 1.5749 \times 10^{24}\,(\mathrm{m^{-3}})$ in the solution phase. It is observed from Fig. 4.2 that the phase transition occurs over an interface region. As mentioned above, the crosslink density ρ is associated with the phase of the physical hydrogel, in such a way that the crosslink density ρ increases when the physical hydrogel transits from solution phase into gel one. It is demonstrated in Fig. 4.2 that the crosslink density ρ increases in the region where phase transition occurs, i.e. over the interface, from solution phase into gel one, when the gel phase

propagates outwards. This phenomenon results directly from the phase transition from solution phase into gel one, when the crosslink density ρ increases. It is seen from Fig. 4.2 that the crosslink density is distributed homogeneously in each phase and varies smoothly over the interface, and that the interface evolves outwards with finite width. It is also demonstrated by Fig. 4.2 that, when the interface reaches the boundary at time $t = t_T$, the whole domain is occupied by the gel phase with homogeneously distributed crosslink density $\rho_{gel} = 3.1416 \times 10^{26}$ (m^{-3}).

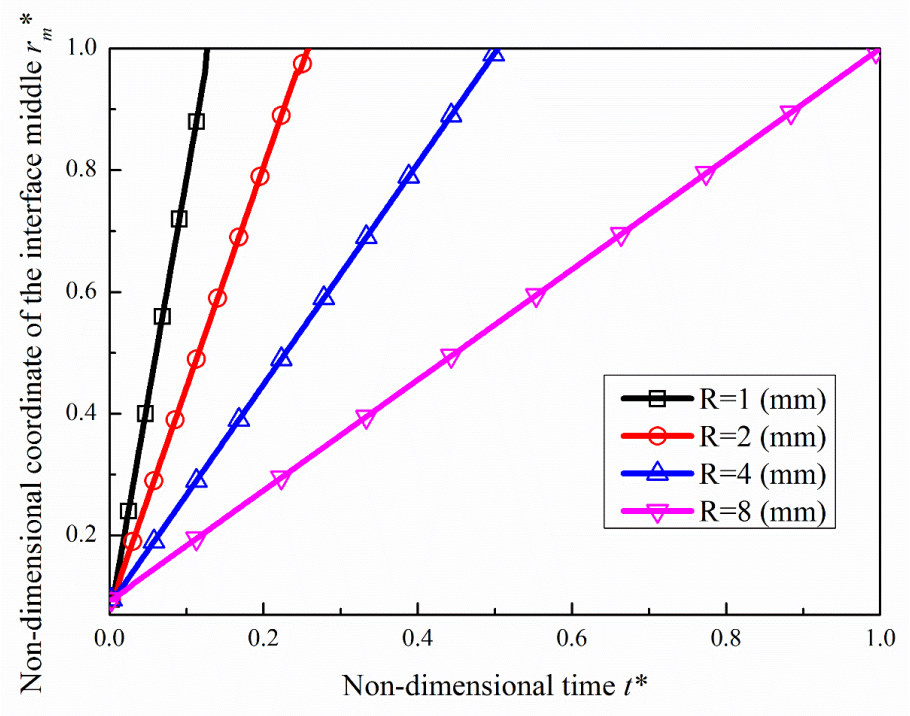

Fig. 4.3. Variation of the non-dimensional coordinate of the interface middle r_m^* with a non-dimensional time t^* for the different domain sizes R.

In order to study the rate of the phase transition, Fig. 4.3 is plotted for variation of the non-dimensional coordinate of the interface middle r_m^* with the non-dimensional time t^*

subject to different domain sizes $R = 1,\ 2,\ 4,\ \text{and}\ 8\,(\text{mm})$, where $\xi = 1(\text{m}/\text{J}^{1/2})$, $\mu^* = \mu/(kT) = 0$, and $P = 0\,(\text{Pa})$. Since the interface evolves with finite width and the actual profile of the interface has negligible effect (Steinbach, Zhang et al. 2012), the non-dimensional coordinate of the interface middle r_m^* is workable to denote the position of the interface. It is found in Fig. 4.3 that the interface evolves from the center towards the boundary, since the gel phase with larger crosslink density is more favorable for the physical hydrogel subject to the boundary conditions $P = 0$ and $U = 0$, compared with the solution phase. It is seen from Fig. 4.3 that the interface evolves almost linearly outwards, i.e. a phase transition with quasi-constant velocity. It is also observed from Fig. 4.3 that the total time to fulfill the phase transition is almost linearly proportional to the domain size. In other words, the domain size has insignificant influence on the evolution velocity.

4.4.2. Phase transition of hydrogel in ionic solution

In this subsection, the phase transition of hydrogel in ionic solution is numerically simulated, in the limit of the concentrated solution. When the concentration of ions in the external solution is much higher than the fixed charges, the fixed charges only have negligible effect. As a result, the hydrogel behaves the same as the neutral hydrogel gel, and the electroneutrality requires that the number of the ions is equal to the number of the anions, namely $c_+ = c_-$ (Hong, Zhao et al. 2010). Based on the governing equations (4.45), (4.46), (4.49), (4.55), and (4.57), and the boundary conditions (4.47), (4.50), (4.51), (4.56), a MATLAB source code is developed for numerical simulation of phase transition of hydrogel in ionic solution with diffuse interface. The inputs of parameters

are given as follows. $E_a = 4\times10^{-23}\mathrm{J}$, $\alpha = 30$, $\nu = 10^{-28}\mathrm{m}^3$, $\chi = 1.1$, $c_+^0 = c_-^0 = 10^{15}\mathrm{m}^{-3}$, $\chi = 1.1$, $\tau = 0.5\times10^{-13}\,(\mathrm{s})$, $\xi = 1(\mathrm{m/J}^{1/2})$, a constant room temperature $kT = 4\times10^{-21}\mathrm{J}$, and the boundary conditions $P = 0$, $\phi_0 = 0.01kT/e$, $U_m = 0$, $U_+ = -\phi_0 e$, $U_- = \phi_0 e$.

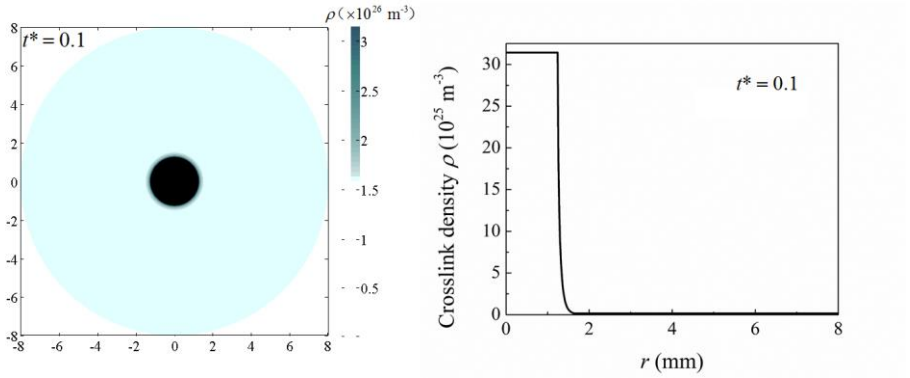

(a)

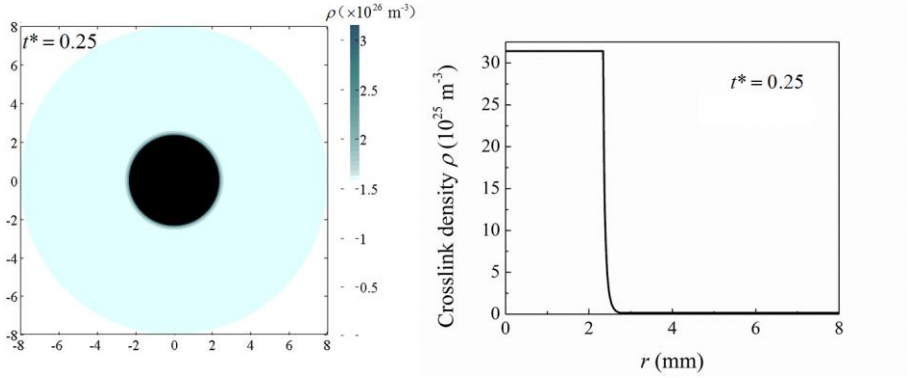

(b)

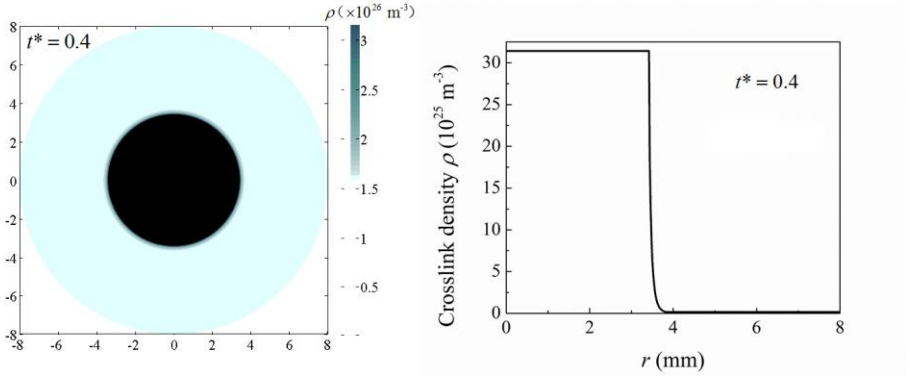

(c)

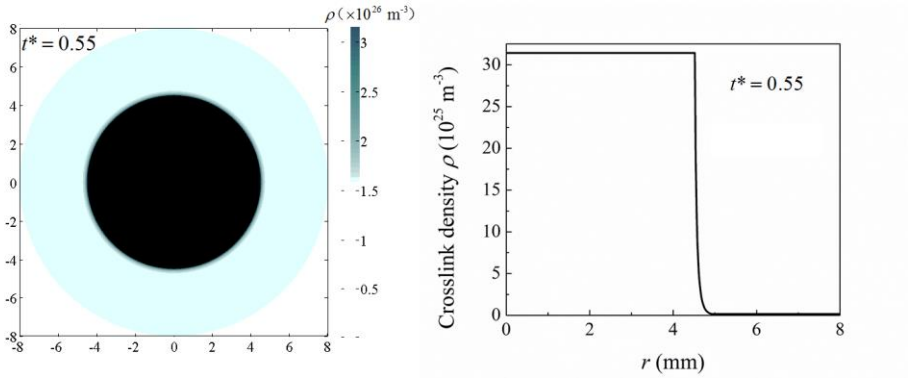
ρ (×10^26 m^-3)
t* = 0.55
Crosslink density ρ (10^25 m^-3)
t* = 0.55
r (mm)

(d)

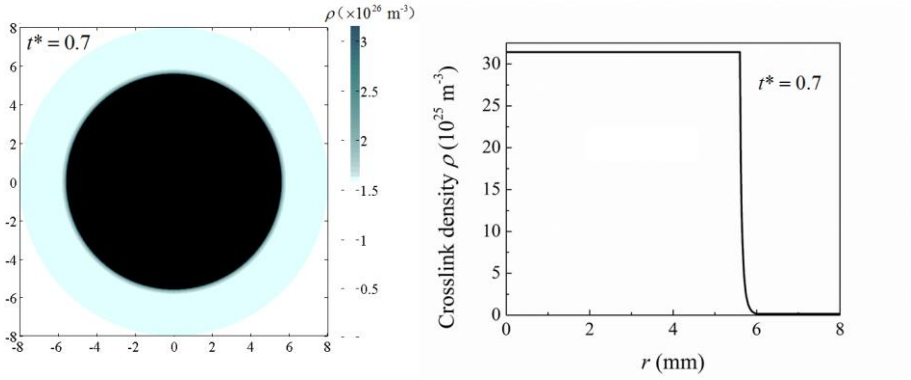
ρ (×10^26 m^-3)
t* = 0.7
Crosslink density ρ (10^25 m^-3)
t* = 0.7
r (mm)

(e)

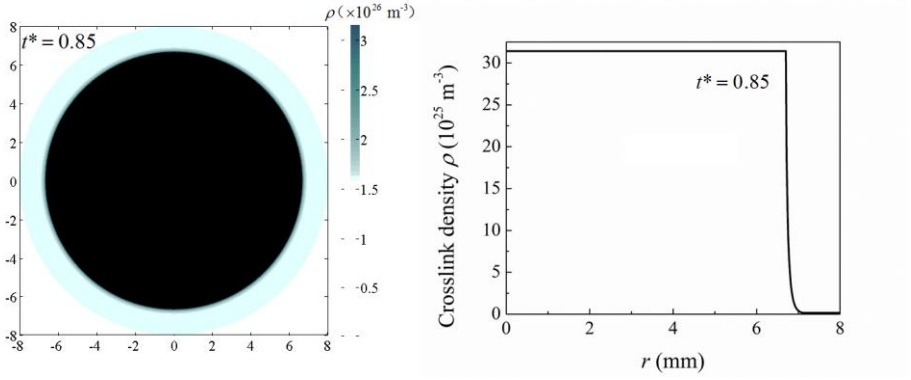
ρ (×10^26 m^-3)
t* = 0.85
Crosslink density ρ (10^25 m^-3)
t* = 0.85
r (mm)

(f)

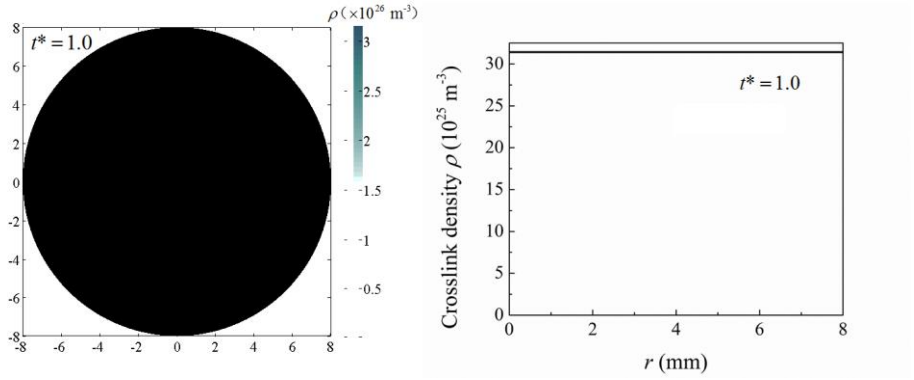

(g)

Fig. 4.4. Several snapshots of the evolution progress of the crosslink density ρ associated with the corresponding crosslink density profile at different non-dimensional times: $t^* = 0.1$ (a), $t^* = 0.25$ (b), $t^* = 0.4$ (c), $t^* = 0.55$ (d), $t^* = 0.7$ (e), $t^* = 0.85$ (f), and $t^* = 1$ (g).

Fig. 4.4 shows the several snapshots of the numerically simulated region captured at different non-dimensional times $t^* = t / t_T$ associated with the corresponding profiles of the crosslink density, where $\xi = 1(\mathrm{m/J^{1/2}})$, $R = 8\,(\mathrm{mm})$, and t_T is the total time to fulfill phase transition. It is observed from Fig. 4.4 that the phase transition from solution into gel occurs over an interface region. As mentioned above, the crosslink density ρ is associated with the phase of the physical hydrogel, in such a way that the crosslink density ρ increases significantly when the physical hydrogel transits from solution phase into gel one. It is demonstrated in Fig. 4.4 that the crosslink density ρ increases in the region where phase transition occurs, i.e. over the interface, when the gel phase propagates outwards. This phenomenon is a direct result of the phase transition from solution phase into gel one. As demonstrated Fig. 4.4, the crosslink density is distributed homogeneously in each phase and varies smoothly over the interface. It is also seen from Fig. 4.4 that, when the interface reaches the boundary at $t^* = 1$, the whole domain is occupied by the gel phase with homogeneously distributed crosslink density.

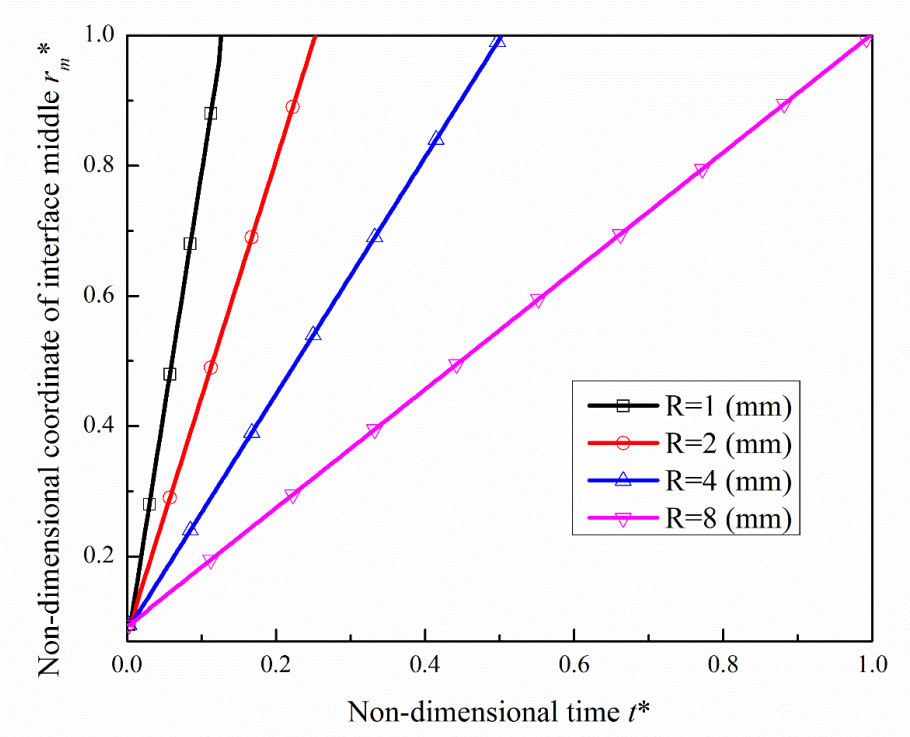

Fig. 4.5. Variation of the non-dimensional coordinate of the interface middle r_m^* with a non-dimensional time t^* for the different domain sizes R.

Since the interface evolves with finite width and the actual profile of the interface has negligible effect (Steinbach, Zhang et al. 2012), the non-dimensional coordinate of the interface middle r_m^* is workable to denote the position of the interface. Therefore, Fig. 4.5 is plotted to investigate the rate of the phase transition, which shows the variation of the non-dimensional coordinate of the interface middle r_m^* with the non-dimensional time t^* subject to different domain sizes $R = 1,\ 2,\ 4,$ and $8\,(\text{mm})$. It is found in Fig. 4.5 that the interface evolves almost linearly from the center towards the boundary, since the gel phase with larger crosslink density is more favorable for the physical hydrogel subject to the present boundary conditions, compared with the solution phase. It is also observed from Fig. 4.5 that the total time to fulfill the phase transition is almost linearly

proportional to the domain size. These results reveal that the gel phase propagates outwards with a quasi-constant velocity. In other words, the domain size has insignificant influence on the evolution velocity.

In order to study the polymeric chemical potential during the phase transition, Fig. 4.6 is plotted to show the variation of the non-dimensional polymeric chemical potential μ_m^{c*} with a non-dimensional coordinate r/R at different non-dimensional times, where $\mu_m^{c*} = \mu_m^c / kT$. It is shown in Fig. 4.6 that the non-dimensional polymeric chemical potential μ_m^{c*} is also homogeneous in each phase and varies smoothly over the interface, which is similar to the profiles of the crosslink density ρ. This phenomenon reveals that the crosslink density ρ, and consequently the phase, may have significant effect on the polymeric chemical potential μ_m^{c*}. It is also demonstrated in Fig. 4.6 that the value of the non-dimensional polymeric chemical potential μ_m^{c*} in the solution phase is equal to the boundary value, and that the value of the non-dimensional polymeric chemical potential μ_m^{c*} in the gel phase increases with time. When the whole domain is occupied by the gel phase with homogeneously distributed crosslink density at $t^*=1$, the non-dimensional polymeric chemical potential μ_m^{c*} is also homogeneous in the whole domain, and equal to the boundary value U_m^{c*}.

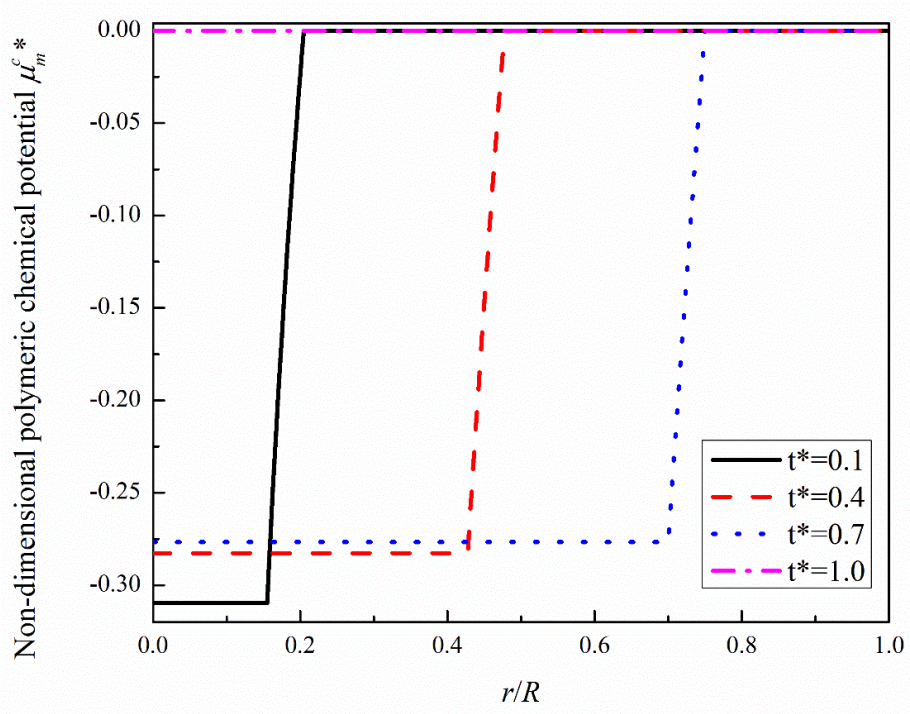

Fig. 4.6. Variation of the non-dimensional polymeric chemical potential μ_m^{c*} with a non-dimensional coordinate r/R at different non-dimensional times.

The ionic chemical potential is also numerically studied. As mentioned, in the limit of the concentrated solution, the number of the ions is equal to the number of the anions. As a result, according to (3.39), the chemical potential of the ions is the same as the anions. Therefore, Fig. 4.7 plots the variation of the non-dimensional ionic chemical potential μ_{ion}^{c*} with a non-dimensional coordinate r/R at different non-dimensional times, where $\mu_m^{c*} = \mu_m^c / kT$. It is shown in Fig. 4.7 that the non-dimensional ionic chemical potential μ_{ion}^{c*} is homogeneous in each phase and varies smoothly over the interface, which is also similar to the crosslink density ρ. It is also demonstrated in Fig. 4.7 that the non-dimensional polymeric chemical potential μ_{ion}^{c*} is also homogeneous in the whole domain, and equal to the boundary value U_{ion}^{c*} when $t^*=1$.

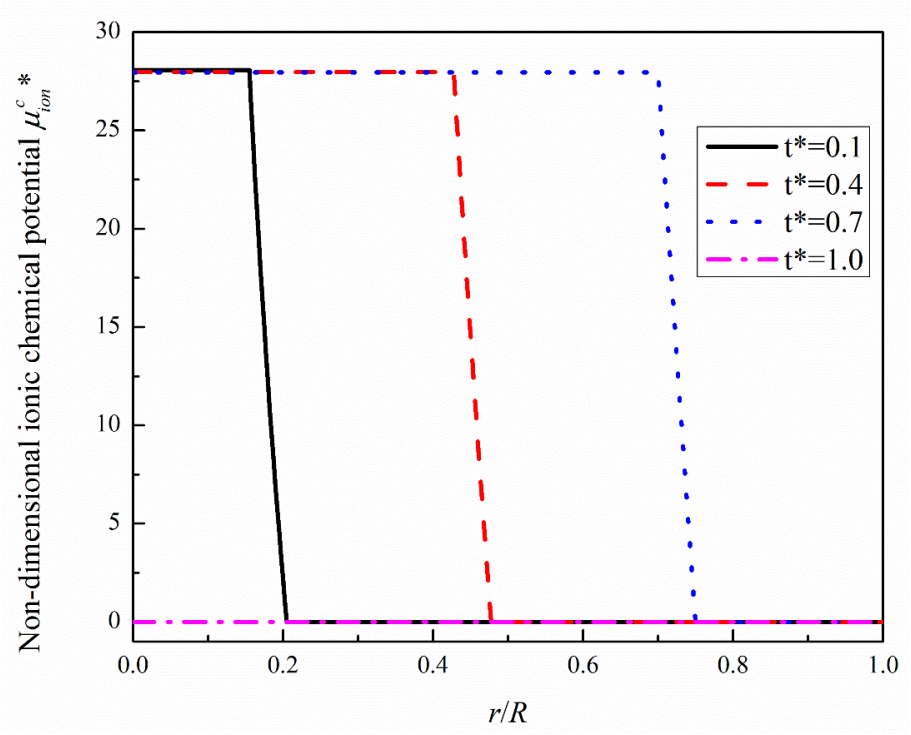

Fig. 4.7. Variation of the non-dimensional ionic chemical potential μ_{ion}^{c*} with a non-dimensional coordinate r/R at different non-dimensional times.

4.5. Remarks

In this chapter, a diffuse-interface based model has been developed for simulation of solution-gel phase transition for the physical hydrogel. The present domain includes the gel and solution phases, as well as a diffuse interface between them. They are indicated by the density of crosslinks in such a way that the solution phase is identified as the state when the crosslink density is small, while the gel as the state if the crosslink density becomes large. Therefore, a novel thermodynamically-consistent order parameter is defined as the crosslink density ρ, which is homogeneous in each distinct phase and varies smoothly over the interface from one phase to another. Since all the parameters are continuous over the whole domain, the same constitutive equations are imposed in the

two distinct phases as well as over the interface, by taking the free energy Ψ as a function of the deformation gradient $\boldsymbol{F}$, chemical potential μ_a^c, temperature T, crosslink density ρ and its gradient $\nabla\rho$. In this model, the constitutive equations formulated by the second law of thermodynamics result in the same form as those derived by a different approach, called the non-equilibrium thermodynamic theory (Hong, Zhao et al. 2008, Hong, Liu et al. 2009). A novel Ginzburg-Landau type of free energy Ψ is also included to account for the effect of crosslink density ρ on the elastic and mixing contributions to the free energy Ψ, as well as the interface effect by including a gradient term $\xi^2 kT(\nabla\rho)^2/2$ of the crosslink density. The governing equations account for the equilibrium of forces, the conservations of mass and energy, and an additional equation imposed for kinetics of phase transition. As case studies, spherically symmetrical solution-gel phase transition are numerically simulated respectively for analysis of the phase transition in water and in ionic solution, as well as the evolution of the chemical potentials, crosslink density and other parameters during the phase transition.

However, there are following limitations in the presently developed model for the solution-gel phase transition of physical hydrogel with the diffuse interface.

- In the numerical implementation, the present model considers only one-dimensional spherical symmetric phase transition. Therefore, the numerical implementation needs to be improved for higher-dimensional phase transition in complicated geometric domains.

- In the electric field, only the limit of the concentrated solution is considered in the present model, in which the fixed charges are negligible compared with the concentration of ions in the solution. However, in the limit of a dilute solution, the fixed charges play a very important role to compensate the ions in the solution. Therefore, the model needs to be further improved to solve the problems in both concentrated and dilute solutions.

Chapter 5. Conclusions and future work

This chapter summarizes the achievements of the research work presented in this thesis and provides recommendations for future work.

5.1. Conclusions

The achievements in this thesis are categorized as follows.

- *Theoretical development of a thermo-electro-chemo-mechanical model for simulation of the solution-gel phase transition, in which the solution and gel states are considered as two distinct phases, with both sharp and diffuse interface approaches.*

As the first contribution mentioned above, the thermo-electro-chemo-mechanical model has been developed theoretically for simulation of the solution-gel phase transition, with both sharp and diffuse interface approaches. The presently developed model couples the effects of thermal, electrical, chemical and mechanical fields together. Therefore, the governing equations consist of the equilibrium of forces, the conservations of mass and energy, and an additional kinetic equation imposed for phase transition. The present domain covers the gel and solution states that are considered as two distinct phases, and an interface between them. They are indicated by the density of crosslinks in such a way that the solution phase is identified as the state when the crosslink density is small, while the gel as the state if the crosslink density becomes large. The interface is treated by two different methods, the sharp interface/configurational forces and the diffuse interface approaches.

- *Comparison between the present constitutive equations with those derived by a different approach, called the non-equilibrium thermodynamic theory.*

The second contribution extracted from the present thesis is comparison between the present constitutive equations with those derived by a different approach, called the non-equilibrium thermodynamic theory. Based on the second law of thermodynamics, the present constitutive equations are formulated, in the bulk phases and over the interface. If the interface is ignored when only a single bulk phase exists, i.e. no phase transition occurs, the system reduces into a single-phase hydrogel. Consequently, the present constitutive equations reduce into the bulk constitutive equations accordingly, which are in fact the same form as those derived by a different approach, called the non-equilibrium thermodynamic theory (Hong, Zhao et al. 2008, Hong, Liu et al. 2009, Hong, Zhao et al. 2010). In other words, the non-equilibrium model proposed by Suo's group (Hong, Zhao et al. 2008, Hong, Liu et al. 2009, Hong, Zhao et al. 2010) is just a special case of the present model with respect to constitutive relations, when the present two-phase control volume reduces to a single-phase one, in which only the gel phase with constant crosslink density exists in the hydrogel system.

- *Proposal of a novel free energy density, in which the gel and solution states are indicated by the density of crosslinks, in such a way that the solution phase is identified as a state when the crosslink density is small, while the gel is identified as another state with the large crosslink density.*

A novel free energy is proposed as the third contribution, which accounts for the effects of crosslink density. The presently proposed free energy density is composed of the

elastic, mixing, internal, binding, polarization and interface contributions, and is in a double-well profile, of which one corresponds to the gel phase, and the other to the solution phase. In other words, of the two wells within the free energy density Ψ, the one with the smaller crosslink density ρ corresponds to the solution phase, and the other with the larger ρ to the gel phase.

- *Analysis for the behavior of the bulk phases and the evolution of their interface for phase transition between the solution and gel states by the presently developed multiphysics model.*

The last contribution from the present thesis is the analysis for the behavior of the bulk phases and the evolution of their interface for phase transition between the solution and gel states by the presently developed multiphysics model. The presently developed model has been reduced from a three-dimensional domain to a one-dimensional one, for case study by simulation of evolving interface of a spherically symmetrically physical hydrogel during the solution-gel phase transition. Based on the reduced one-dimensional governing equations and boundary conditions, a MATLAB source code is developed. And then the evolution of interface for spherical symmetrical hydrogel with solution-gel phase transition in water and in ionic solution is numerically simulated, and the effect of chemical potential, pressure, surface tension and other parameters on the phase transition is analyzed.

In conclusion, the four contributions mentioned above constitute the entire thesis. It is believed that the present research work is significant in science for further understanding

of fundamental mechanism of phase transition and key material properties of physical hydrogels.

5.2. Future work

Based on the research results presented in this thesis, some potential studies for future work related to physical hydrogel phase transition modeling are recommended below.

- In the electric field, the present model considers only the limit of the concentrated solution, in which the fixed charges are negligible compared with the concentration of ions in the solution. However, in the limit of a dilute solution, the ions in the solution are fully compensated by the fixed charges. Therefore, it is recommended to investigate the influence of concentration of the fixed charges in the limit of a dilute solution.

- The present thesis has theoretically developed a general model for simulation for solution-gel phase transition of physical hydrogel in ionic solution. However, the effects of the specified ionic species, such as H^+ and OH^-, need to be investigated further. Therefore, it is recommended to study the influence of the various specified ionic species, such as H^+, on the phase transition of physical hydrogels.

- In the theoretical development of models, the interface is treated with two different methods, the sharp interface/configurational forces and the diffuse interface approaches. It would be interesting to compare the two models via

asymptotic analysis. It is expected that the diffuse interface model would reduce to the sharp interface when the interface width approaches zero.

- In the numerical implementation, the present thesis considers only one-dimensional spherical symmetric phase transition. However, higher-dimensional phase transition in complicated geometric domains is worth investigating. Therefore, it is recommended to analyze the influence of the surface tension, interfacial curvature and other parameters on the phase transition of physical hydrogel in a complicated geometric domain.

- The present work has theoretically developed a thermo-electro-chemo-mechanical model for solution-gel phase transition of physical hydrogel, and numerically simulated one-dimensional spherical symmetric phase transition. Therefore, it is definitely a worthwhile work to conduct experiments under the guide of the present numerical simulations, and in turn to validate the present numerical results by the experimental observations.

References

Abeyaratne, R. and J. K. Knowles (1993). "A continuum model of a thermoelastic solid capable of undergoing phase transitions." Journal of the Mechanics and Physics of Solids **41**(3): 541-571.

Allen, S. M. and J. W. Cahn (1979). "Microscopic theory for antiphase boundary motion and its application to antiphase domain coarsening." Acta Metallurgica **27**(6): 1085-1095.

An, Y., F. J. Solis and H. Jiang (2010). "A thermodynamic model of physical gels." Journal of the Mechanics and Physics of Solids **58**(12): 2083-2099.

Angenent, S. and M. E. Gurtin (1989). "Multiphase thermomechanics with interfacial structure 2. evolution of an isothermal interface." Archive for Rational Mechanics and Analysis **108**(4): 323-391.

Biancamaria, B. (2007). "Hydrogels for tissue engineering and delivery of tissue-inducing substances." Journal of Pharmaceutical Sciences **96**(9): 2197-2223.

Caginalp, G. and J. Jones (1995). "A Derivation and Analysis of Phase Field Models of Thermal Alloys." Annals of Physics **237**(1): 66-107.

Caginalp, G. and W. Xie (1993). "Phase-field and sharp-interface alloy models." Physical Review E **48**(3): 1897-1909.

Cahn, J. W. (1961). "On spinodal decomposition." Acta Metallurgica **9**(9): 795-801.

Cahn, J. W. and J. E. Hilliard (1958). "Free Energy of a Nonuniform System. I. Interfacial Free Energy." The Journal of Chemical Physics **28**(2): 258.

Cai, S., K. Bertoldi, H. Wang and Z. Suo (2010). "Osmotic collapse of a void in an elastomer: breathing, buckling and creasing." Soft Matter **6**(22): 5770.

Cai, S. and Z. Suo (2011). "Mechanics and chemical thermodynamics of phase transition in temperature-sensitive hydrogels." Journal of the Mechanics and Physics of Solids **59**(11): 2259-2278.

Chester, S. A. and L. Anand (2010). "A coupled theory of fluid permeation and large deformations for elastomeric materials." Journal of the Mechanics and Physics of Solids **58**(11): 1879-1906.

Chester, S. A. and L. Anand (2011). "A thermo-mechanically coupled theory for fluid permeation in elastomeric materials: Application to thermally responsive gels." Journal of the Mechanics and Physics of Solids **59**(10): 1978-2006.

Deng, H. and T. Pence (2010). "Equilibrium States of Mechanically Loaded Saturated and Unsaturated Polymer Gels." Journal of Elasticity **99**(1): 39-73.

Deng, H. and T. J. Pence (2010). "Shear induced loss of saturation in a fluid infused swollen hyperelastic cylinder." International Journal of Engineering Science **48**(6): 624-646.

Dolbow, J., E. Fried and H. Ji (2004). "Chemically induced swelling of hydrogels." Journal of the Mechanics and Physics of Solids **52**(1): 51-84.

Dolbow, J., E. Fried and H. Ji (2005). "A numerical strategy for investigating the kinetic response of stimulus-responsive hydrogels." Computer Methods in Applied Mechanics and Engineering **194**(42-44): 4447-4480.

Duda, F. P., A. C. Souza and E. Fried (2010). "A theory for species migration in a finitely strained solid with application to polymer network swelling." Journal of the Mechanics and Physics of Solids **58**(4): 515-529.

Emmerich, H. (2011). The Diffuse Interface Approach in Materials Science: Thermodynamic Concepts and Applications of Phase-Field Models, Springer Publishing Company, Incorporated.

English, A. E., T. Tanaka and E. R. Edelman (1996). "Polyelectrolyte hydrogel instabilities in ionic solutions." The Journal of Chemical Physics **105**(23): 10606-10613.

English, A. E., T. Tanaka and E. R. Edelman (1997). "Equilibrium and non-equilibrium phase transitions in copolymer polyelectrolyte hydrogels." The Journal of Chemical Physics **107**(5): 1645-1654.

Ericksen, J. L. (1975). "Equilibrium of bars." Journal of Elasticity **5**(3-4): 191-201.

Eshelby, J. D. (1951). "The Force on an Elastic Singularity." Philosophical Transactions of the Royal Society of London. Series A, Mathematical and Physical Sciences **244**(877): 87-112.

Eshelby, J. D. (1956). The Continuum Theory of Lattice Defects. Solid State Physics. S. Frederick and T. David, Academic Press. **Volume 3:** 79-144.

Flory, P. J. (1953). Principles of polymer chemistry, Ithaca : Cornell University Press.

Flory, P. J. and J. Rehner (1943). "Statistical mechanics of cross-linked polymer networks I. rubberlike elasticity." The Journal of Chemical Physics **11**(11): 512.

Flory, P. J. and J. Rehner (1943). "Statistical mechanics of cross-linked polymer networks II. swelling." The Journal of Chemical Physics **11**(11): 521.

Gurtin, M. (1995). "The nature of configurational forces." Archive for Rational Mechanics and Analysis **131**(1): 67-100.

Gurtin, M. E. (1981). An introduction to continuum mechanics, New York : Academic Press.

Gurtin, M. E. (1988). "Multiphase thermomechanics with interfacial structure 1. heat-conduction and the capillary balance law." Archive for Rational Mechanics and Analysis **104**(3): 195-221.

Gurtin, M. E. (2000). Configurational forces as basic concepts of continuum physics, New York : Springer.

Gurtin, M. E. and P. W. Voorhees (1993). "The Continuum Mechanics of Coherent Two-Phase Elastic Solids with Mass Transport." Proceedings of the Royal Society of London. Series A: Mathematical and Physical Sciences **440**(1909): 323-343.

Hoare, T. R. and D. S. Kohane (2008). "Hydrogels in drug delivery: Progress and challenges." Polymer **49**(8): 1993-2007.

Hoffman, A. S. (2002). "Hydrogels for biomedical applications." Advanced Drug Delivery Reviews **54**(1): 3-12.

Hong, W., Z. Liu and Z. Suo (2009). "Inhomogeneous swelling of a gel in equilibrium with a solvent and mechanical load." International Journal of Solids and Structures **46**(17): 3282-3289.

Hong, W. and X. Wang (2013). "A phase-field model for systems with coupled large deformation and mass transport." Journal of the Mechanics and Physics of Solids **61**(6): 1281-1294.

Hong, W., X. Zhao and Z. Suo (2009). "Formation of creases on the surfaces of elastomers and gels." Applied Physics Letters **95**(11): 111901.

Hong, W., X. Zhao and Z. Suo (2010). "Large deformation and electrochemistry of polyelectrolyte gels." Journal of the Mechanics and Physics of Solids **58**(4): 558-577.

Hong, W., X. Zhao, J. Zhou and Z. Suo (2008). "A theory of coupled diffusion and large deformation in polymeric gels." Journal of the Mechanics and Physics of Solids **56**(5): 1779-1793.

Hou, Q., P. A. De Bank and K. M. Shakesheff (2004). "Injectable scaffolds for tissue regeneration." Journal of Materials Chemistry **14**(13): 1915-1923.

Huang, Y., H. Yu and C. Xiao (2007). "pH-sensitive cationic guar gum/poly (acrylic acid) polyelectrolyte hydrogels: Swelling and in vitro drug release." Carbohydrate Polymers **69**(4): 774-783.

Ji, H., H. Mourad, E. Fried and J. Dolbow (2006). "Kinetics of thermally induced swelling of hydrogels." International Journal of Solids and Structures **43**(7-8): 1878-1907.

Jones, A. and D. Vaughan (2005). "Hydrogel dressings in the management of a variety of wound types: A review." Journal of Orthopaedic Nursing **9**(Supplement 1): S1-S11.

Kamath, K. R. and K. Park (1993). "Biodegradable hydrogels in drug delivery." Advanced Drug Delivery Reviews **11**(1–2): 59-84.

Kim, S. G., W. T. Kim and T. Suzuki (1999). "Phase-field model for binary alloys." Physical Review E **60**(6): 7186-7197.

Kim, S. W., Y. H. Bae and T. Okano (1992). "Hydrogels: Swelling, Drug Loading, and Release." Pharmaceutical Research **9**(3): 283-290.

Kobayashi, R. (1993). "Modeling and numerical simulations of dendritic crystal growth." Physica D: Nonlinear Phenomena **63**(3–4): 410-423.

Kobayashi, R. (1994). "A Numerical Approach to Three-Dimensional Dendritic Solidification." Experimental Mathematics **3**(1): 59-81.

Lai, F. and H. Li (2011). "Transient modeling of the reversible response of the hydrogel to the change in the ionic strength of solutions." Mechanics of Materials **43**(6): 287-298.

Lai, F., H. Li and R. Luo (2010). "Chemo-electro-mechanical modeling of ionic-strength-sensitive hydrogel: Influence of Young's modulus." International Journal of Solids and Structures **47**(22-23): 3141-3149.

Lam, K. Y., H. Li, T. Y. Ng and R. Luo (2006). "Modeling and simulation of the deformation of multi-state hydrogels subjected to electrical stimuli." Engineering Analysis with Boundary Elements **30**(11): 1011-1017.

Langer, J. S. and R. F. Sekerka (1975). "Theory of departure from local equilibrium at the interface of a two-phase diffusion couple." Acta Metallurgica **23**(10): 1225-1237.

Langer, R. and J. Vacanti (1993). "Tissue engineering." Science **260**(5110): 920-926.

Lee, B. H., B. West, R. McLemore, C. Pauken and B. L. Vernon (2006). "In-Situ Injectable Physically and Chemically Gelling NIPAAm-Based Copolymer System for Embolization." Biomacromolecules **7**(6): 2059-2064.

Lee, K. Y. and D. J. Mooney (2001). "Hydrogels for Tissue Engineering." Chemical Reviews **101**(7): 1869-1880.

Levitas, V. I. and K. Samani (2011). "Size and mechanics effects in surface-induced melting of nanoparticles." Nature Communications **2**: 284.

Li, H., R. Luo, E. Birgersson and K. Y. Lam (2007). "Modeling of multiphase smart hydrogels responding to pH and electric voltage coupled stimuli." Journal of Applied Physics **101**(11): 114905.

Li, H., R. Luo, E. Birgersson and K. Y. Lam (2009). "A chemo-electro-mechanical model for simulation of responsive deformation of glucose-sensitive hydrogels with the effect of enzyme catalysis." Journal of the Mechanics and Physics of Solids **57**(2): 369-382.

Li, H., R. Luo and K. Y. Lam (2007). "Modeling of ionic transport in electric-stimulus-responsive hydrogels." Journal of Membrane Science **289**(1-2): 284-296.

Li, H., X. Wang, G. Yan, K. Y. Lam, S. Cheng, T. Zou and R. Zhuo (2005). "A novel multiphysic model for simulation of swelling equilibrium of ionized thermal-stimulus responsive hydrogels." Chemical Physics **309**(2-3): 201-208.

Li, Y. J., E. H., C. R. T., R. M. T. and F. K. E. Healy (2006). "Hydrogels as artificial matrices for human embryonic stem cell self-renewal." Journal of Biomedical Materials Research Part A **79A**(1): 1-5.

McFadden, G. B., A. A. Wheeler, R. J. Braun and S. R. Coriell (1993). "Phase-field models for anisotropic interfaces." Physical Review E **48**(3): 2016-2024.

Onuki, A. and S. Puri (1999). "Spinodal decomposition in gels." Physical Review E Statistical Physics Plasmas Fluids & Related Interdisciplinary Topics **59**(2): R1331-R1334.

Osada, Y. and J. Gong (1993). "Stimuli-responsive polymer gels and their application to chemomechanical systems." Progress in polymer science **18**(2): 187-226.

Otake, K., H. Inomata, M. Konno and S. Saito (1989). "A new model for the thermally induced volume phase transition of gels." The Journal of Chemical Physics **91**(2): 1345-1350.

Peppas, N. A. (1987). Hydrogels in Medicine and Pharmacy: Properties and applications, CRC Press.

Peppas, N. A., P. Bures, W. Leobandung and H. Ichikawa (2000). "Hydrogels in pharmaceutical formulations." European Journal of Pharmaceutics and Biopharmaceutics **50**(1): 27-46.

Putz, A. V. and T. Burghelea (2009). "The solid–fluid transition in a yield stress shear thinning physical gel." Rheologica Acta **48**(6): 673-689.

Qiu, Y. and K. Park (2001). "Environment-sensitive hydrogels for drug delivery." Advanced Drug Delivery Reviews **53**(3): 321-339.

Reddy, J. N. (2007). An Introduction to Continuum Mechanics, Cambridge : Cambridge University Press.

Rubinstein, M. and R. H. Colby (2003). Polymer physics, Oxford ; New York : Oxford University Press.

Sawa, Y., E. Tatsumi, A. Funakubo, T. Horiuchi, K. Iwasaki, A. Kishida, T. Masuzawa, K. Matsuda, M. Nishimura, T. Nishimura, Y. Tomizawa, T. Yamaoka and H. Watanabe (2008). "Journal of Artificial Organs 2007: the year in review." Journal of Artificial Organs **11**(1): 4-11.

Sekimoto, K. and K. Kawasaki (1989). "Elastic instabilities and phase coexistence of gels." Physica A Statistical Mechanics & Its Applications **154**(3): 384-420.

Sekimoto, K., N. Suematsu and K. Kawasaki (1989). "Spongelike domain structure in a two-dimensional model gel undergoing volume-phase transition." Physical Review A **39**(9): 4912-4914.

Snyders, R., K. I. Shingel, O. Zabeida, C. Roberge, M.-P. Faure, L. M. Jolanta and E. Klemberg-Sapieha (2007). "Mechanical and microstructural properties of hybrid poly(ethylene glycol)-soy protein hydrogels for wound dressing applications." Journal of Biomedical Materials Research Part A **83A**(1): 88-97.

Steinbach, I., F. Pezzolla, B. Nestler, M. Seeßelberg, R. Prieler, G. J. Schmitz and J. L. L. Rezende (1996). "A phase field concept for multiphase systems." Physica D: Nonlinear Phenomena **94**(3): 135-147.

Steinbach, I., L. Zhang and M. Plapp (2012). "Phase-field model with finite interface dissipation." Acta Materialia **60**(6-7): 2689-2701.

Studenovská, H., M. Šlouf and F. Rypáček (2008). "Poly(HEMA) hydrogels with controlled pore architecture for tissue regeneration applications." Journal of Materials Science: Materials in Medicine **19**(2): 615-621.

Tanaka, T. (1979). "Phase transitions in gels and a single polymer." Polymer **20**(11): 1404-1412.

Tanaka, T. (1981). "Gels." Scientific American **244**(1): 124-136, 138.

Tiaden, J., B. Nestler, H. J. Diepers and I. Steinbach (1998). "The multiphase-field model with an integrated concept for modelling solute diffusion." Physica D: Nonlinear Phenomena **115**(1-2): 73-86.

Wang, X. (2007). "Modeling the nonlinear large deformation kinetics of volume phase transition for the neutral thermosensitive hydrogels." The Journal of Chemical Physics **127**(17): 174705.

Wang, X., X.-B. Wang and P. R. C. Gascoyne (1997). "General expressions for dielectrophoretic force and electrorotational torque derived using the Maxwell stress tensor method." Journal of Electrostatics **39**(4): 277-295.

Wheeler, A., W. Boettinger and G. McFadden (1993). "Phase-field model of solute trapping during solidification." Physical Review E **47**(3): 1893-1909.

Wheeler, A. A., W. J. Boettinger and G. B. McFadden (1992). "Phase-field model for isothermal phase transitions in binary alloys." Physical Review A **45**(10): 7424-7439.

Wu, M. S. and H. O. K. Kirchner (2010). "Nonlinear elasticity modeling of biogels." Journal of the Mechanics and Physics of Solids **58**(3): 300-310.

Wu, M. S. and H. O. K. Kirchner (2011). "Second-order elastic solutions for spherical gels subjected to spherically symmetric dilatation." Mechanics of Materials **43**(11): 721-729.

Yoo, H.-J. and H.-D. Kim (2008). "Synthesis and properties of waterborne polyurethane hydrogels for wound healing dressings." Journal of Biomedical Materials Research Part B: Applied Biomaterials **85B**(2): 326-333.

Zhao, X., W. Hong and Z. Suo (2007). "Electromechanical hysteresis and coexistent states in dielectric elastomers." Physical Review B **76**(13): 134113.

Zhao, X., W. Hong and Z. Suo (2008). "Inhomogeneous and anisotropic equilibrium state of a swollen hydrogel containing a hard core." Applied Physics Letters **92**(5): 051904.

Zhao, X., W. Hong and Z. Suo (2008). "Stretching and polarizing a dielectric gel immersed in a solvent." International Journal of Solids and Structures **45**(14-15): 4021-4031.

Zhao, X. and Z. Suo (2008). "Electrostriction in elastic dielectrics undergoing large deformation." Journal of Applied Physics **104**(12): 123530.